

國立交通大學

電信工程學系碩士班

碩士論文

以外來資訊轉換圖設計調變器映射規則於

位元交錯調變碼之迭代解碼系統



EXIT-Chart Based Labeling Design for

Bit-interleaved Coded Modulation

with Iterative Decoding

指導教授：沈文和 博士

研究生：王楚硯

中華民國九十六年七月

以外來資訊轉換圖設計調變器映射規則於
位元交錯調變碼之迭代解碼系統

**EXIT-Chart Based Labeling Design for
Bit-interleaved Coded Modulation
with Iterative Decoding**

研究生：王楚硯

Student：Chu-Yan Wang

指導教授：沈文和 博士

Advisor：Dr. Wern-Ho Sheen

國立交通大學

電信工程學系碩士班



Submitted to Department of Communication Engineering

College of Electrical and Computer Engineering

National Chiao Tung University

in Partial Fulfillment of the Requirements

for the Degree of

Master of Science

in Communication Engineering

July 2007

Hsinchu, Taiwan, Republic of China

中華民國九十六年七月

以外來資訊轉換圖設計調變器映射規則於 位元交錯調變碼之迭代解碼系統

研究生：王楚硯

指導教授：沈文和 博士

國立交通大學

電信工程學系碩士班



本論文利用外來資訊轉換圖 (Extrinsic Information Transfer Chart, EXIT-Chart) 聯合設計調變器映射規則 (Labeling) 與外部編碼器以增進位元交錯調變碼之迭代解碼系統 (Bit-Interleaved Coded Modulation with Iterative Decoding, BICM-ID) 的性能。針對均勻的調變星座，我們提出一個有系統的調變星座映射規則的設計方法以得到一組具有好的外來資訊轉換圖特性的映射規則；對每一種外部編碼器皆可以從中選擇出一個最理想的映射規則，使解調器和解碼器的轉換特性曲線能相交在外來資訊轉換圖上越遠的位置而且讓區線間的通道能夠打開以達到理想的錯誤率。我們還擴展此映射規則設計方法到多維度的調變星座上，多維度調變星座將一群位元映射到一組以一維度星座調變的符號使系統的設計上具有更高的彈性與潛在性能的提升。經由模擬結果證實我們的設計比傳統的設計提供了卓越的訊雜比增益。

EXIT-Chart Based Labeling Design for Bit-interleaved Coded Modulation with Iterative Decoding

Student: Chu-Yan Wang

Advisor: Dr. Wern-Ho Sheen

**Department of Communication Engineering
National Chiao Tung University**



In this thesis, constellation labeling is jointly designed with the outer code by using an EXIT-chart based analysis to improve the performance of bit-interleaved coded modulation with iterative decoding (BICM-ID). A systematic design method is proposed to obtain a set of labelings with good EXIT-chart characteristics for the regular one-dimensional (complex) modulation. Given an outer code, the best matched labeling can be employed to improve the BER performance. Furthermore, the method is extended to the multi-dimensional modulation case, where a group of bits are mapped to a vector of one-dimensional complex symbols. This general mapping strategy allows for more flexibility and potential performance improvements. Verified by the simulation results, our design provides a significant SNR gain over the conventional ones.

誌謝

首先要感謝我的指導教授 沈文和博士細心教導做研究的方法，不斷鼓勵學生精益求精；老師嚴謹認真的求學態度一直是我們的最好的榜樣，讓我從研究過程得到很多，對以後也有很大的幫助。感謝 王忠炫博士的教誨，老師不時的提醒及激發學生的想法都讓學生受益匪淺。老師們每次 meeting 的建議都是學生研究最大動力來源，使得這篇論文可以順利完成。

這篇論文主要是接著益彰學長的論文再加以改良，感謝學長之前辛苦的找出這一個可以發揮的題目，讓我可以專心地想辦法解決問題；謝謝王老師、倉緯學長幫忙寫 ISIT 的論文使能順利發表。也感謝這兩年來在實驗室所有的同學，正欣學長、志成學長、宜康學長、香君學姊、鑫賢學長、順吉學長、東融學長、昱帆學長、聖文學長、宸睿學長、相榮學長、文傑、友亮、小白、哲群、承瑋、政揚、宜勳，感謝大家在各方面的幫助、照應，讓研究生活不單調。感謝在交大六年來所有的師長、朋友，讓我增廣見聞。

最後要特別感謝我的爸媽的支持與照顧，爸媽辛苦的工作使我得以專心完成學業，我一定會再更努力以報答我的家人。

民國九十六年七月

研究生王楚硯謹識於交通大學

Contents

摘要.....	i
Abstract.....	ii
誌謝.....	iii
Contents	iv
List of Tables.....	vi
List of Figures	vii
Abbreviations.....	x
Chapter 1 Introduction	1
1-1 Thesis Contributions.....	4
1-2 Thesis Organization.....	5
Chapter 2 System Model.....	6
2-1 Transmitter.....	7
2-2 Channel model.....	8
2-3 Receiver.....	9
2-3-1 Demapper.....	9
2-3-2 Decoder.....	11
Chapter 3 Exit-Chart Based Analysis.....	12
3-1 Transfer Characteristics of Demapper.....	12
3-2 Transfer Characteristics of Decoder.....	16
3-3 Design Guideline Based on EXIT-chart.....	17
Chapter 4 One-dimensional Labeling Design.....	21
4-1 Design criteria.....	21
4-1-1 Without A Priori Information.....	22
4-1-2 Ideal A Priori Information.....	24
4-1-2-1 AWGN Channels.....	24
4-1-2-2 Rayleigh Fading Channels.....	26
4-2 Design Method.....	28
4-3 Proposed Labelings.....	31
4-3-1 8-PSK.....	31
4-3-2 16-QAM.....	33
4-3-3 64-QAM.....	35
4-4 Simulation Results.....	37
Chapter 5 Multi-dimensional Labeling Design.....	47
5-1 Design Criteria.....	48

5-1-1 Multi-dimensional Mapping over Spatial Domain.....	48
5-1-1-1 Without A Priori Information.....	48
5-1-1-2 Ideal A Priori Information.....	50
5-1-2 Multi-dimensional Mapping over Time Domain	52
5-1-2-1 Without A Priori Information.....	52
5-1-2-2 Ideal A Priori Information.....	52
5-2 Design Method	56
5-3 Proposed Labelings.....	57
5-3-1 Multi-dimensional Mapping over Spatial Domain.....	57
5-3-1-1 $N \times$ BPSK.....	59
5-3-1-2 $N \times$ QPSK.....	62
5-3-1-3 $N \times$ 8-PSK	64
5-3-1-4 $N \times$ 16-QAM	65
5-3-2 Multi-dimensional Mapping over Time Domain	66
5-3-2-1 $N \times$ BPSK.....	67
5-3-2-2 $N \times$ QPSK.....	72
5-3-2-3 $N \times$ 8-PSK	75
5-3-2-4 $N \times$ 16-QAM.....	77
5-4 Simulation Results.....	79
5-4-1 Multi-dimensional Mapping over Spatial Domain.....	79
5-4-2 Multi-dimensional Mapping over Time Domain	87
Chapter 6 Conclusions	96
Reference	97

List of Tables

Table 4-1 Candidate set for 8-PSK	31
Table 4-2 Candidate set for 16-QAM	33
Table 4-3 Candidate set for 64-QAM	35
Table 5-1 Summary of design criteria.....	56
Table 5-2 Candidate set for 2xBPSK	59
Table 5-3 Candidate set for 3xBPSK	60
Table 5-4 Candidate set for 4xBPSK	61
Table 5-5 Candidate set for 2xQPSK	62
Table 5-6 Candidate set for 3xQPSK	63
Table 5-7 Candidate set for 2x8-PSK	64
Table 5-8 Candidate set for 2x16-QAM	65
Table 5-9 Candidate set for 2xBPSK	67
Table 5-10 Candidate set for 3xBPSK	69
Table 5-11 Candidate set for 4xBPSK	70
Table 5-12 Candidate set for 2xQPSK	72
Table 5-13 Candidate set for 3xQPSK	73
Table 5-14 Candidate set for 2x8-PSK	75
Table 5-15 Candidate set for 2x16-QAM	77

List of Figures

Fig. 1-1 Block diagram of BICM systems	2
Fig. 1-2 Block diagram of BICM-ID systems	2
Fig. 2-1 System model	6
Fig. 3-1 Demapper transfer curve of Gray labeling for 16QAM in AWGN channel ..	15
Fig. 3-2 Demapper transfer curve of Anti-Gray labeling for 16QAM in AWGN channel	15
Fig. 3-3 Decoder transfer curves of turbo code and convolutional codes	17
Fig. 3-4 An example of the EXIT-chart for BICM-ID at $E_b / N_0 = 4\text{dB}$ in AWGN channel	18
Fig. 3-5 Observation I for labeling design.	19
Fig. 3-6 Observation II for labeling design	20
Fig. 4-1 Two mappings of 8-PSK constellation: (a) Gray and (b) Set-partitioning.....	25
Fig. 4-2 Labelings for 8-PSK in Table 4-1 at (a) $E_b / N_0 = 3\text{dB}$ in AWGN channel.....	32
Fig. 4-3 Labelings for 16-QAM in Table 4-2 at (a) $E_b / N_0 = 3.5\text{dB}$ in AWGN channel	34
Fig. 4-4 Labelings for 64-QAM in Table 4-3 at (a) at $E_b / N_0 = 6\text{dB}$ in AWGN channel	36
Fig. 4-5 (a) EXIT-chart at $E_b / N_0 = 2.6\text{dB}$ and (b) performance plots of the BICM-ID system with 8-PSK and (5, 7) convolutional code in AWGN channel	38
Fig. 4-6 (a) EXIT-chart at $E_b / N_0 = 3\text{dB}$ and (b) performance plots of the BICM-ID system with 8-PSK and (133, 171) convolutional code in AWGN channel	39
Fig. 4-7 (a) EXIT-chart at $E_b / N_0 = 4.8\text{dB}$ and (b) performance plots of the BICM-ID system with 8-PSK and (133, 171) convolutional code in Rayleigh channel	40
Fig. 4-8 (a) EXIT-chart at $E_b / N_0 = 3.5\text{dB}$ and (b) performance plots of the BICM-ID system with 16-QAM and (5, 7) convolutional code in AWGN channel	41
Fig. 4-9 (a) EXIT-chart at $E_b / N_0 = 4\text{dB}$ and (b) performance plots of the BICM-ID system with 16-QAM and (133, 171) convolutional code in AWGN channel	42
Fig. 4-10 (a) EXIT-chart at $E_b / N_0 = 5.2\text{dB}$ and (b) performance plots of the BICM-ID system with 16-QAM and (133, 171) convolutional code in Rayleigh channel.....	43
Fig. 4-11 (a) EXIT-chart at $E_b / N_0 = 6\text{dB}$ and (b) performance plots of the BICM-ID system with 64-QAM and (5, 7) convolutional code in AWGN channel	44
Fig. 4-12 (a) EXIT-chart at $E_b / N_0 = 6\text{dB}$ and (b) performance plots of the BICM-ID system with 64-QAM and (133, 171) convolutional code in AWGN channel	45
Fig. 4-13 (a) EXIT-chart at $E_b / N_0 = 8\text{dB}$ and (b) performance plots of the BICM-ID	

system with 64-QAM and (133, 171) convolutional code in Rayleigh channel.....	46
Fig. 5-1 Equivalent and convenient model of the multi-dimensional mapper over spatial domain	58
Fig. 5-2 Constituent two-dimensional mappers: (a) BPSK (b) QPSK (c) 8-PSK (d) 16-QAM and (e) 64-QAM.....	58
Fig. 5-3 Labelings for 2xBPSK in Table 5-2 at $E_b / N_0 = 2\text{dB}$ in 2x2 fast Rayleigh fading channel.....	59
Fig. 5-4 Labelings for 3xBPSK in Table 5-3 at $E_b / N_0 = 2\text{dB}$ in 3x3 fast Rayleigh fading channel.....	60
Fig. 5-5 Labelings for 4xBPSK in Table 5-4 at $E_b / N_0 = 2\text{dB}$ in 4x4 fast Rayleigh fading channel.....	61
Fig. 5-6 Labelings for 2xQPSK in Table 5-5 at $E_b / N_0 = 3\text{dB}$ in 2x2 fast Rayleigh fading channel.....	62
Fig. 5-7 Labelings for 3xQPSK in Table 5-6 at $E_b / N_0 = 3\text{dB}$ in 3x3 fast Rayleigh fading channel.....	63
Fig. 5-8 Labelings for 2x8-PSK in Table 5-7 at $E_b / N_0 = 5\text{dB}$ in 2x2 fast Rayleigh fading channel.....	64
Fig. 5-9 Labelings for 2x16-QAM in Table 5-8 at $E_b / N_0 = 6\text{dB}$ in 2x2 fast Rayleigh fading channel.....	66
Fig. 5-10 Equivalent and convenient model of the multi-dimensional mapper over time domain	67
Fig. 5-11 Labelings for 2xBPSK in Table 5-9 at (a) at $E_b / N_0 = 1\text{dB}$ in AWGN channel and (b) $E_b / N_0 = 3\text{dB}$ in block Rayleigh fading channel	68
Fig. 5-12 Labelings for 3xBPSK in Table 5-10 at (a) at $E_b / N_0 = 1\text{dB}$ in AWGN channel and (b) $E_b / N_0 = 3\text{dB}$ in block Rayleigh fading channel	70
Fig. 5-13 Labelings for 4xBPSK in Table 5-11 at (a) $E_b / N_0 = 1\text{dB}$ in AWGN channel and (b) $E_b / N_0 = 3\text{dB}$ in block Rayleigh fading channel.....	71
Fig. 5-14 Labelings for 2xQPSK in Table 5-12 at (a) $E_b / N_0 = 1\text{dB}$ in AWGN channel and (b) $E_b / N_0 = 3\text{dB}$ in block Rayleigh fading channel.....	73
Fig. 5-15 Labelings for 3xQPSK in Table 5-13 at (a) $E_b / N_0 = 1\text{dB}$ in AWGN channel and (b) $E_b / N_0 = 3\text{dB}$ in block Rayleigh fading channel.....	74
Fig. 5-16 Labelings for 2x8-PSK in Table 5-14 at (a) $E_b / N_0 = 3\text{dB}$ in AWGN channel and (b) $E_b / N_0 = 5\text{dB}$ in block Rayleigh fading channel.....	76
Fig. 5-17 Labelings for 2x8-PSK in Table 5-15 at (a) $E_b / N_0 = 3.5\text{dB}$ in AWGN channel and (b) $E_b / N_0 = 6\text{dB}$ in block Rayleigh fading channel.....	78
Fig. 5-18 (a) EXIT-chart at $E_b / N_0 = 2\text{dB}$ and (b) performance plots of the BICM-ID system with (5, 7) convolutional code in 2x2 fast Rayleigh fading channel.....	80
Fig. 5-19 (a) EXIT-chart at $E_b / N_0 = 2\text{dB}$ and (b) performance plots of the BICM-ID	

system with (5, 7) convolutional code in 3x3 fast Rayleigh fading channel.....	81
Fig. 5-20 (a) EXIT-chart at $E_b / N_0 = 2$ dB and (b) performance plots of the BICM-ID system with (5, 7) convolutional code in 4x4 fast Rayleigh fading channel.....	82
Fig. 5-21 (a) EXIT-chart at $E_b / N_0 = 3$ dB and (b) performance plots of the BICM-ID system with (5, 7) convolutional code in 2x2 fast Rayleigh fading channel.....	83
Fig. 5-22 (a) EXIT-chart at $E_b / N_0 = 3$ dB and (b) performance plots of the BICM-ID system with (5, 7) convolutional code in 3x3 fast Rayleigh fading channel.....	84
Fig. 5-23 (a) EXIT-chart at $E_b / N_0 = 5$ dB and (b) performance plots of the BICM-ID system with (5, 7) convolutional code in 2x2 fast Rayleigh fading channel.....	85
Fig. 5-24 (a) EXIT-chart at $E_b / N_0 = 6$ dB and (b) performance plots of the BICM-ID system with (5, 7) convolutional code in 2x2 fast Rayleigh fading channel.....	86
Fig. 5-25 (a) EXIT-chart at $E_b / N_0 = 1$ dB and (b) performance plots of the BICM-ID system with (5, 7) convolutional code in 1x1 AWGN channel	88
Fig. 5-26 (a) EXIT-chart at $E_b / N_0 = 3$ dB and (b) performance plots of the BICM-ID system with (5, 7) convolutional code in 1x1 block Rayleigh fading channel.....	89
Fig. 5-27 (a) EXIT-chart at $E_b / N_0 = 1$ dB and (b) performance plots of the BICM-ID system with (5, 7) convolutional code in 1x1 AWGN channel	90
Fig. 5-28 (a) EXIT-chart at $E_b / N_0 = 3$ dB and (b) performance plots of the BICM-ID system with (5, 7) convolutional code in 1x1 block Rayleigh fading channel.....	91
Fig. 5-29 (a) EXIT-chart at $E_b / N_0 = 2.6$ dB and (b) performance plots of the BICM-ID system with (5, 7) convolutional code in 1x1 AWGN channel	92
Fig. 5-30 (a) EXIT-chart at $E_b / N_0 = 5$ dB and (b) performance plots of the BICM-ID system with	93
Fig. 5-31 (a) EXIT-chart at $E_b / N_0 = 3.5$ dB and (b) performance plots of the BICM-ID system with (5, 7) convolutional code in 1x1 AWGN channel	94
Fig. 5-32 (a) EXIT-chart at $E_b / N_0 = 6$ dB and (b) performance plots of the BICM-ID system with	95

Abbreviations

APP	A Posteriori Probability
AWGN	Additive White Gaussian Noise
BER	Bit Error Rate
BICM	Bit-Interleaved Coded Modulation
BICM-ID	Bit-Interleaved Coded Modulation with Iterative Decoding
BI-STCM-ID	Bit-Interleaved Space-Time Coded Modulation with Iterative Decoding
BPSK	Binary Phase Shift Keying
BSA	Binary Switching Algorithm
CSI	Channel State Information
dB	Decibel
EFF	Error-free Feedback
FED	Free Squared Euclidean Distance
EXIT	Extrinsic Information Transfer
LLR	Log-Likelihood Ratio
MAP	Maximum A Posteriori Probability
MIMO	Multi-Input Multi-Output
ML	Maximum Likelihood
PEP	Pairwise Error Probability
PSK	Phase-shift Keying
QAM	Quadrature Amplitude Modulation
QAP	Quadratic Assignment Problem
QPSK	Quadrature Phase Shift Keying
SISO	Single-Input Single-Output
SNR	Signal-to-Noise Ratio
TCM	Trellis-Coded Modulation

Chapter 1

Introduction

Coded-modulation is a bandwidth-efficient scheme for data transmission on a bandwidth-limited channel. With joint design of coding and modulation, coded-modulation imposes no extra system bandwidth while achieves a coding gain comparable to the traditional coded system. Trellis-Coded Modulation (TCM) [1], proposed by Ungerboeck, is a form of coded modulation designed for additive white Gaussian (AWGN) channels, where the minimum free Euclidean distance (FED) of the coded symbol sequences determines the asymptotic BER performance. In [1], with a set-partitioning principle, TCM was designed with the largest FED by maximizing the intra-subset minimum Euclidean distance. Nevertheless, when transmitting over fading channels, the TCM performance will be degraded because in this case diversity order rather than the minimum FED becomes the primary factor that determines the BER performance [2].

An approach to improve the performance coded-modulation systems in fading channels is to use bit-interleaved coded modulation (BICM) [3], [4]. BICM is a serial concatenation of a conventional channel code (called the outer code) and a mapper (called the inner code) with a bit-wise interleaver inserted between them, as shown in Fig. 1.1. The bit-wise interleaver can break the fading correlations and increase the diversity order to the minimum Hamming distance of the code at the expense of reducing the minimum FED [3]. Therefore, the performance of BICM outperforms TCM in fading channels but performs less favorably in AWGN channels. In [3], Zehavi suggested a suboptimal decoding method that separates demodulation and

decoding as two steps because joint demodulation and decoding is too complicated to implement, and in [4], Caire laid a theoretic foundation on BICM, provided tools for evaluating its performance and gave design guidelines.

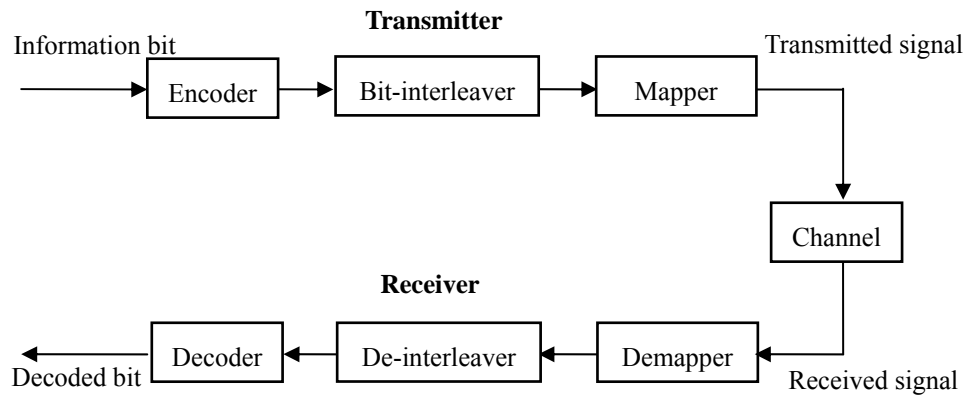


Fig. 1-1 Block diagram of BICM systems

Motivated by the serial concatenated structure of BICM, BICM with iterative decoding (BICM-ID) was proposed in [5], [6], [7] to improve the performance. The block diagram of a typical BICM-ID is shown in Fig. 1-2. Iterative decoding iteratively exchanges information between demapper and decoder. Through iterative decoding and with a proper labeling, the minimum inter-signal Euclidean distance of BICM is increased while the desired Hamming distance is preserved [6]. Therefore, BICM-ID can provide excellent performance in both AWGN and fading channels.

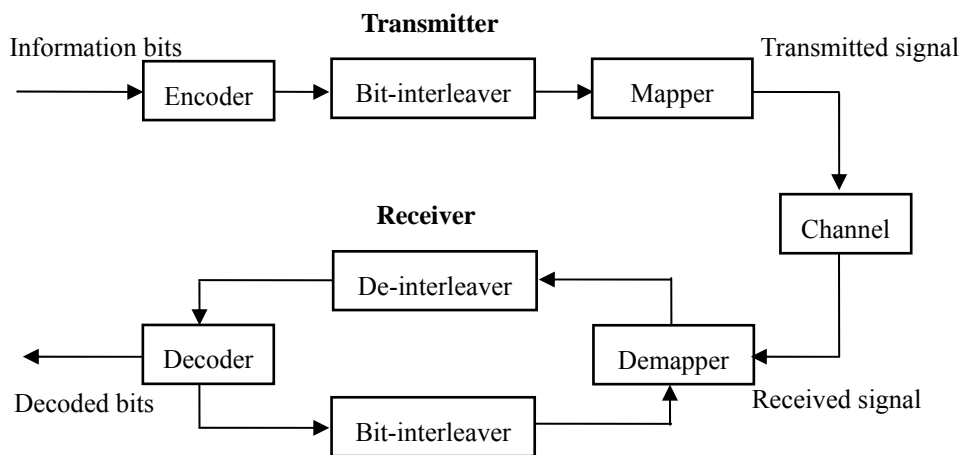


Fig. 1-2 Block diagram of BICM-ID systems

It was shown in [4], [6], [7] that constellation labeling is crucial to the performance of BICM and BICM-ID systems. In [4], Gray labeling was proved to provide the best performance for BICM. In [6]-[7], different labelings were shown to have different influences on the bit error rate (BER) performance of BICM-ID. To find the optimal labeling for BICM-ID, the BER bounds of BICM [4] were extended in [6]-[7] with the assumption of error free feedback (EFF) to provide insight into the design of labeling. Their results suggest that the minimum Euclidean distance between any pairs of modulated symbols which have only one distinct bit on their labels should be maximized to minimize the BER upper bound at high signal-to-noise ratio (SNR). Beside, labeling design based on the extrinsic information transfer (EXIT) chart [8]-[10] indicates that under EFF assumption, the larger mutual information of demapper outputs is, the better asymptotic performance can be achieved.

Based on these criteria, many one-dimensional labelings for regular complex constellations (e.g., phase-shift keying (PSK) and quadrature amplitude modulation (QAM)) have been introduced. In [6]-[7], the authors use random computer search to choose a labeling that has reasonable first round performance and large iterative decoding gain to achieve low BER through several iterations. In [11], a general design algorithm based on binary switching algorithm (BSA) was proposed to find optimum labelings which can achieve the best asymptotic performance. The labeling optimization problem in [12] is solved by applying the generic solutions to the quadratic assignment problem (QAP) to achieve the largest asymptotic coding gain.

BICM-ID can also take advantage of multi-dimensional modulation schemes, which map a sequence of coded bits into a vector of symbols to form a multi-dimensional signal, to make labeling design more flexible and achieve better performance. Previous researches in [13]-[16] and [17]-[18] consider

multi-dimensional modulation in single-input single-output (SISO) systems (i.e., the multi-dimensional signal is transmitted over consecutive time slots) and multi-input multi-output (MIMO) systems (i.e., the multi-dimensional signal is transmitted over distinct antennas), respectively. Labeling designs in [15]-[18] are based on the distance criteria derived from the BER bounds to achieve best asymptotic performance. In [13]-[14], the authors use the EXIT-chart to design the labelings that are high at two end points of its demapper transfer curve to achieve good trade-off between the waterfall region and the BER floor.

1-1 Thesis Contributions

In terms of the EXIT-chart, given an outer code, a good labeling should be designed to form a tunnel between the transfer curve of demapper and decoder at SNR as low as possible to guarantee a low open tunnel threshold for BICM-ID. The demapper curve should also intersect the decoder curve at a point with mutual information as large as possible to avoid the undesired error floor at high SNR. However, labelings obtained in the previous works are designed separately from the outer code. The expected optimal performance hence can not always be achieved as different outer codes are employed. In most of the cases, those labelings perform well only at high SNR while unacceptable BER degradation is observed in the low SNR region. Given an outer code, we are to design the labeling to achieve the acceptable BER performance in the low SNR region.

In this thesis, therefore, constellation labeling is jointly designed with the outer code by an EXIT-chart based analysis. For an outer code, we observe that the demapper transfer curve of a good labeling should match to the decoder transfer curve and be high at its two end points to avoid early crossing with the decoder curve at low SNR and to achieve low BER after several iterations. In addition, we also observe that for different outer codes, the best labeling is different from code to code. Stimulated the above observations, a systematic methodology of labeling design is proposed for both one-dimensional and multi-dimensional modulation schemes which can easily obtain a set of labelings (called the candidate set) with good EXIT-chart characteristics. Given an outer code, we can then choose a labeling from the candidate set which is most matched to the outer code. Verified by the simulation results, our design can provide remarkable SNR gain over the conventional ones.

1-2 Thesis Organization



The rest of this thesis is organized as follows. In chapter 2, we describe the system model of BICM-ID. A brief review of the EXIT-chart based analysis as well as the basic guidelines of labeling design are given in chapter 3. A systematic design methodology for one-dimensional labeling is presented in chapter 4. The design methodology is extended in chapter 5 for multi-dimensional labeling. Simulation results are provided in chapter 4 and chapter 5 for one-dimensional and multi-dimensional designs, respectively, to verify the superiority of our design. Finally, a summary is drawn in chapter 6 to conclude this work.

Chapter 2

System Model

As mentioned in chapter 1, both one-dimensional and multi-dimensional constellations can be used in BICM-ID. This thesis is to provide a systematic labeling design for both one-dimensional and multi-dimensional complex constellations. The general system model with N_T transmit antennas and N_R receive antennas is shown in Fig. 2-1. When employing multi-dimensional constellation, the mapper maps a sequence of coded bits to form a signal in multi-dimensional space. The multi-dimensional signal can be sent via distinct transmit antennas at a time or via single transmit antenna over consecutive time slots.

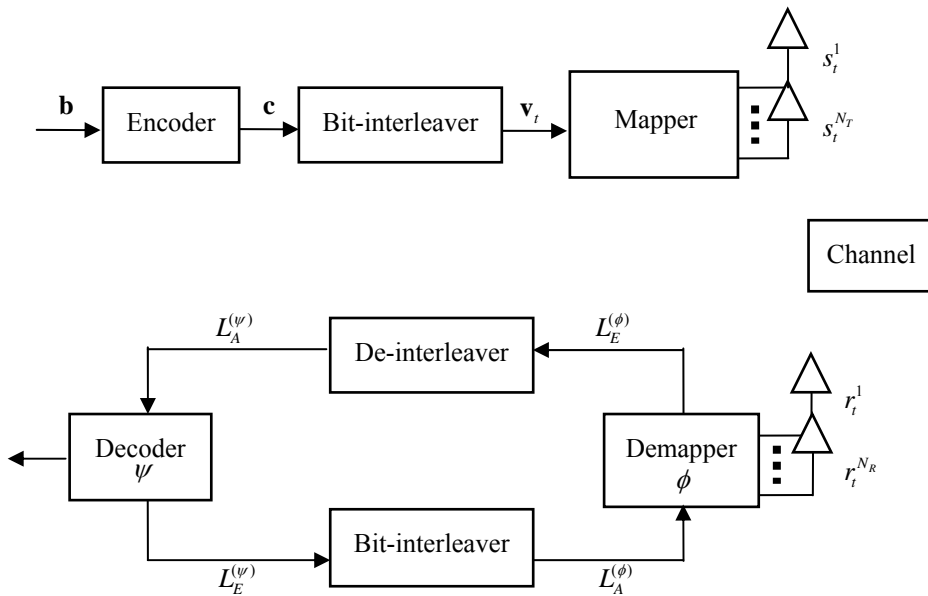


Fig. 2-1 System model

When employing one-dimensional constellation and reducing the number of transmit antenna and receive antenna to one, the model is reduced to a conventional BICM-ID system. The detailed system model is to be introduced in this chapter.

2-1 Transmitter

When a N -dimensional constellation is considered, a sequence of information bits \mathbf{b} are encoded to \mathbf{c} and then interleaved and grouped into blocks of mN coded bits; the t -th block is denoted $\mathbf{v}_t = (v_t[0], \dots, v_t[mN])$. Then, \mathbf{v}_t is mapped to a vector of symbols $\mathbf{s}_t = (s_t^1, \dots, s_t^N)$, where each element of \mathbf{s}_t is in a one-dimensional complex constellation with $M = 2^m$ signal points. The signal \mathbf{s}_t is in a N -dimensional constellation χ which has M^N signal points $\mathbf{x}_0, \mathbf{x}_1, \dots, \mathbf{x}_{M^N-1}$ and is equipped with a labeling μ which assigns \mathbf{x}_i a unique label $\mu(\mathbf{x}_i)$ with $0 \leq \mu(\mathbf{x}_i) < M^N$. By setting $N = N_T$, the N -dimensional signal \mathbf{s}_t is sent via N_T transmit antennas at a time and received by N_R antennas. If $N_T = 1$ and $N_R = 1$, the N -dimensional signal \mathbf{s}_t is transmitted in a SISO channel over N consecutive time slots. Furthermore, when employing one-dimensional constellation and setting $N_T = 1, N_R = 1$, the model is reduced to a conventional BICM-ID system and the transmitter parameters described above can also be applied in this case by setting $N = 1$. Therefore, we will discuss the most general system model employing multi-dimensional modulation with N_T transmit antennas and N_R receive antennas in the following.

2-2 Channel model

Assume the N -dimensional signal \mathbf{s}_t is transmitted via N_T antennas over a flat fading channel \mathbf{H} , where $N = N_T$. Each element of the $N_R \times N_T$ matrix \mathbf{H} is assumed to be zero-mean i.i.d. complex Gaussian distributed with variance $1/2$ per dimension. Let $\mathbf{r}_t = (r_t^1, \dots, r_t^{N_R})$ represent the received signal corresponding to \mathbf{s}_t and \mathbf{r}_t is given by

$$\mathbf{r}_t = \mathbf{H}\mathbf{s}_t + \mathbf{n}_t \quad (2-1)$$

where \mathbf{n}_t is a vector of noise with zero mean and variance $N_0/2$ per dimension. On the other hand, if \mathbf{s}_t is transmitted via single antenna over N consecutive time slots over a flat fading channel and received by single antenna, the received signal corresponding to \mathbf{s}_t is denoted $\mathbf{r}_t = (r_t^1, \dots, r_t^N)$ and r_t^p is given by

$$r_t^p = \alpha_t^p s_t^p + n_t^p \quad (2-2)$$

where α_t^p denotes the channel gain, n_t^p stands for the noise with zero mean and variance $N_0/2$ per dimension and $1 \leq p \leq N$. If setting fading coefficients equal to 1, it becomes an AWGN channel. Moreover, when employing one-dimensional constellation and setting $N_T = 1$, $N_R = 1$, the model is reduced to a conventional BICM-ID system. The system model is given by

$$r_t = \alpha_t s_t + n_t \quad (2-3)$$

Also, assume channel state information (CSI) is available at the receiver.

2-3 Receiver

The demapper ϕ takes \mathbf{r}_t 's and the *a priori* input $L_A^{(\phi)}(v_t[i])$'s (i.e., the log-likelihood ratio (LLR) of $v_t[i]$'s fed back from the decoder ψ) and then compute the extrinsic output by [12]

$$\begin{aligned}
 L_E^{(\phi)}(v_t[i]) &= \ln \frac{\Pr(v_t[i]=1 | \mathbf{r}_t)}{\Pr(v_t[i]=0 | \mathbf{r}_t)} - L_A^{(\phi)}(v_t[i]) \\
 &= \ln \frac{\sum_{\mathbf{s}_t \in \chi_b^i} \exp \left\{ -\frac{\|\mathbf{r}_t - \mathbf{H}\mathbf{s}_t\|^2}{N_0} + \sum_{j \neq i} v_t[j] L_A^{(\phi)}(v_t[j]) \right\}}{\sum_{\mathbf{s}_t \in \chi_0^i} \exp \left\{ -\frac{\|\mathbf{r}_t - \mathbf{H}\mathbf{s}_t\|^2}{N_0} + \sum_{j \neq i} v_t[j] L_A^{(\phi)}(v_t[j]) \right\}}
 \end{aligned} \tag{2-4}$$

where χ_b^i is the subset of χ comprising all the multi-dimensional signal points for those the i -th bit of the binary representation of their labels is of value b . Note that $L_E^{(\phi)}(v_t[i])$'s also depend on the choices of χ and μ . The output LLRs of the demapper are then de-interleaved and serve as the *a priori* inputs $L_A^{(\psi)}(v_t[i])$'s of the decoder. Finally, the extrinsic outputs $L_E^{(\psi)}(v_t[i])$'s of the decoder generated by an appropriate soft-input soft-output decoding algorithm, e.g. BCJR algorithm [19], are fed to the demapper for next iteration of processing. The derivations of extrinsic information at demapper output and decoder output will be introduced in the next two subsections, respectively.

2-3-1 Demapper

As shown in Fig. 2-1, consider a BER-optimal MAP demapper ϕ that takes soft-input \mathbf{r}_t 's and the soft-input *a priori* LLR $L_A^{(\phi)}(v_t[i])$'s (i.e., the feedback LLR of $v_t[i]$'s from the decoder ψ) and then computes the *a posteriori* LLR [6], [7]

$$\begin{aligned}
& \ln \frac{\Pr(v_t[i] = 1 | \mathbf{r}_t)}{\Pr(v_t[i] = 0 | \mathbf{r}_t)} \\
&= \ln \frac{\Pr(v_t[i] = 1)}{\Pr(v_t[i] = 0)} + \ln \frac{\Pr(\mathbf{r}_t | v_t[i] = 1)}{\Pr(\mathbf{r}_t | v_t[i] = 0)} \\
&= \ln \frac{\Pr(v_t[i] = 1)}{\Pr(v_t[i] = 0)} + \ln \frac{\Pr(\mathbf{r}_t; v_t[i] = 1) / \Pr(v_t[i] = 1)}{\Pr(\mathbf{r}_t; v_t[i] = 0) / \Pr(v_t[i] = 0)} \\
&= \ln \frac{\Pr(v_t[i] = 1)}{\Pr(v_t[i] = 0)} + \ln \frac{\sum_{\mathbf{s}_t \in \mathcal{Z}_1^i} \Pr(\mathbf{r}_t; \mathbf{s}_t) / \Pr(v_t[i] = 1)}{\sum_{\mathbf{s}_t \in \mathcal{Z}_0^i} \Pr(\mathbf{r}_t; \mathbf{s}_t) / \Pr(v_t[i] = 0)} \\
&= \ln \frac{\Pr(v_t[i] = 1)}{\Pr(v_t[i] = 0)} + \ln \frac{\left[\sum_{\mathbf{s}_t \in \mathcal{Z}_1^i} \Pr(\mathbf{r}_t | \mathbf{s}_t) \cdot \Pr(\mathbf{s}_t) \right] / \Pr(v_t[i] = 1)}{\left[\sum_{\mathbf{s}_t \in \mathcal{Z}_0^i} \Pr(\mathbf{r}_t | \mathbf{s}_t) \cdot \Pr(\mathbf{s}_t) \right] / \Pr(v_t[i] = 0)} \\
&= \ln \frac{\Pr(v_t[i] = 1)}{\Pr(v_t[i] = 0)} + \ln \frac{\left[\sum_{\mathbf{s}_t \in \mathcal{Z}_1^i} \Pr(\mathbf{r}_t | \mathbf{s}_t) \cdot \prod_{j=0}^{mN_t-1} \Pr(v_t[j]) \right] / \Pr(v_t[i] = 1)}{\left[\sum_{\mathbf{s}_t \in \mathcal{Z}_0^i} \Pr(\mathbf{r}_t | \mathbf{s}_t) \cdot \prod_{j=0}^{mN_t-1} \Pr(v_t[j]) \right] / \Pr(v_t[i] = 0)} \\
&= \ln \frac{\Pr(v_t[i] = 1)}{\Pr(v_t[i] = 0)} + \ln \frac{\left[\sum_{\mathbf{s}_t \in \mathcal{Z}_1^i} \Pr(\mathbf{r}_t | \mathbf{s}_t) \cdot \prod_{j=0, j \neq i}^{mN_t-1} \Pr(v_t[j]) \right]}{\left[\sum_{\mathbf{s}_t \in \mathcal{Z}_0^i} \Pr(\mathbf{r}_t | \mathbf{s}_t) \cdot \prod_{j=0, j \neq i}^{mN_t-1} \Pr(v_t[j]) \right]} \\
&= L_A^{(\phi)}(v_t[i]) + \ln \frac{\sum_{\mathbf{s}_t \in \mathcal{Z}_1^i} \exp\left\{-\frac{\|\mathbf{r}_t - \mathbf{H}\mathbf{s}_t\|^2}{N_0} + \sum_{j \neq i} v_t[j] L_A^{(\phi)}(v_t[j])\right\}}{\sum_{\mathbf{s}_t \in \mathcal{Z}_0^i} \exp\left\{-\frac{\|\mathbf{r}_t - \mathbf{H}\mathbf{s}_t\|^2}{N_0} + \sum_{j \neq i} v_t[j] L_A^{(\phi)}(v_t[j])\right\}} \tag{2-5}
\end{aligned}$$

where in the last equation

$$L_A^{(\phi)}(v_t[i]) = \ln \frac{\Pr(v_t[i] = 1)}{\Pr(v_t[i] = 0)} \tag{2-6}$$

and from equation (2-1) the likelihood function is given by

$$\Pr(\mathbf{r}_t | \mathbf{s}_t) = \frac{\exp\left[-\frac{1}{N_0} \cdot \|\mathbf{r}_t - \mathbf{H}\mathbf{s}_t\|^2\right]}{(\pi N_0)^{N_R}}. \tag{2-7}$$

For the first round iteration, no *a priori* LLR is available and hence $L_A^{(\phi)}(v_t[i]) = 0, \forall i$.

The demapper outputs the *extrinsic a posteriori* LLR $L_E^{(\phi)}(v_t[i])$'s, where

$$\begin{aligned} L_E^{(\phi)}(v_t[i]) &\triangleq \ln \frac{\Pr(v_t[i] = 1 | \mathbf{r}_t)}{\Pr(v_t[i] = 0 | \mathbf{r}_t)} - L_A^{(\phi)}(v_t[i]) \\ &= \ln \frac{\sum_{s_t \in \mathcal{X}_1^i} \exp\left\{-\frac{\|\mathbf{r}_t - \mathbf{H}\mathbf{s}_t\|^2}{N_0} + \sum_{j \neq i} v_t[j] L_A^{(\phi)}(v_t[j])\right\}}{\sum_{s_t \in \mathcal{X}_0^i} \exp\left\{-\frac{\|\mathbf{r}_t - \mathbf{H}\mathbf{s}_t\|^2}{N_0} + \sum_{j \neq i} v_t[j] L_A^{(\phi)}(v_t[j])\right\}}, \end{aligned} \quad (2-8)$$

and then the soft-output $L_E^{(\phi)}(v_t[i])$'s are de-interleaved and serve as the *a priori* inputs $L_A^{(\psi)}(c[i])$'s of the decoder.

2-3-2 Decoder



The decoder takes $L_A^{(\psi)}(c[i])$'s and computes the *a posteriori* LLR of coded bits

$$\ln \frac{\Pr(c[i] = 1 | L_A^{(\psi)})}{\Pr(c[i] = 0 | L_A^{(\psi)})} \quad (2-9)$$

and the *a posteriori* LLR of information bits

$$\ln \frac{\Pr(b[i] = 1 | L_A^{(\psi)})}{\Pr(b[i] = 0 | L_A^{(\psi)})} \quad (2-10)$$

by an appropriate soft-input soft-output decoding algorithm, e.g. BCJR algorithm. The decoder produces the *extrinsic a posteriori* LLR $L_E^{(\psi)}(c[i])$'s, where

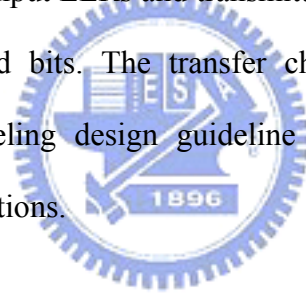
$$L_E^{(\psi)}(c[i]) = \ln \frac{\Pr(c[i] = 1 | L_A^{(\psi)})}{\Pr(c[i] = 0 | L_A^{(\psi)})} - L_A^{(\psi)}(c[i]), \quad (2-11)$$

and $L_E^{(\psi)}(c[i])$'s are interleaved and serve as the *a priori* inputs $L_A^{(\phi)}(v_t[i])$'s of the demapper.

Chapter 3

Exit-Chart Based Analysis

The EXIT chart is a powerful tool for analyzing the convergence behavior of iterative decoding schemes [8], [9], [20], which consists of two parallel or serial concatenated soft-input soft-output decoders. We use the EXIT chart for performance analysis to trace the effect of μ on BICM-ID, where two transfer characteristics for decoder and demapper are plotted in the same diagram. Each curve describes how the mutual information between input LLRs and transmitted bits transfers to that between output LLRs and transmitted bits. The transfer characteristics of demapper and decoder as well as the labeling design guideline based on EXIT-chart will be discussed in the following sections.



3-1 Transfer Characteristics of Demapper

The demapper ϕ takes channel observations \mathbf{r}_i 's and *a priori* input $L_A^{(\phi)}$'s from the decoder and calculates the *extrinsic a posteriori* $L_E^{(\phi)}$'s by equation (2-4). The information transfer can be controlled by the robustness of the *a priori* information. Several observations are obtained from [20]. 1) For large interleavers the *a priori* information $L_A^{(\phi)}$'s remain fairly uncorrelated from the respective channel observations \mathbf{r}_i 's over many iterations. 2) The probability density function of the *a priori* information approach Gaussian-like distribution with increasing number of iterations. Therefore, it is appropriate to model the *a priori* input $L_A^{(\phi)}$ in conjunction with the

known transmitted upmapped bit $v \in \{\pm 1\}$ as

$$L_A^{(\phi)} = \mu_A \cdot v + n_A, \quad (3-1)$$

where n_A is an independent Gaussian random variable with zero mean and variance σ_A^2 and according to [20]

$$\mu_A = \frac{\sigma_A^2}{2}. \quad (3-2)$$

The conditional probability density function of $L_A^{(\phi)}$ is

$$p_{L_A^{(\phi)}}(\xi | V = v) = \frac{e^{-((\xi - (\sigma_A^2/2) \cdot v)^2 / 2\sigma_A^2)}}{\sqrt{2\pi}\sigma_A}. \quad (3-3)$$

To measure the information contents of the *a priori* information, the mutual information $I_A^{(\phi)} = I(V; L_A^{(\phi)})$ between the transmitted bits V and the L-values $L_A^{(\phi)}$'s is used.

$$I_A^{(\phi)} = I(V; L_A^{(\phi)}) = \frac{1}{2} \sum_{v=-1,1} \int_{-\infty}^{+\infty} p_{L_A^{(\phi)}}(\xi | V = v) \cdot \log_2 \left(\frac{2 \cdot p_{L_A^{(\phi)}}(\xi | V = v)}{p_{L_A^{(\phi)}}(\xi | V = 1) + p_{L_A^{(\phi)}}(\xi | V = -1)} \right) d\xi \quad (3-4)$$

$$0 \leq I_A^{(\phi)} \leq 1. \quad (3-5)$$

With equation (3-2) and (3-3), equation (3-4) becomes

$$I_A^{(\phi)}(\sigma_A) = 1 - \int_{-\infty}^{+\infty} \frac{e^{-((\xi - (\sigma_A^2/2) \cdot v)^2 / 2\sigma_A^2)}}{\sqrt{2\pi}\sigma_A} \cdot \log_2(1 + e^{-\xi}) d\xi. \quad (3-6)$$

For abbreviation define

$$J(\sigma) = I_A^{(\phi)}(\sigma_A = \sigma) \quad (3-7)$$

with

$$\lim_{\sigma \rightarrow 0} J(\sigma) = 0, \quad \lim_{\sigma \rightarrow \infty} J(\sigma) = 1, \quad \sigma > 0. \quad (3-8)$$

Because equation (3-7) is monotonically increasing in σ ,

$$\sigma_A = J^{-1}(I_A^{(\phi)}). \quad (3-9)$$

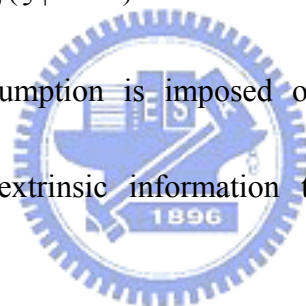
Thus, given an $I_A^{(\phi)}$ and a sequence of transmitted bits for a particular value of E_b / N_0 , we can use σ_A to generate the independent Gaussian random variables $L_A^{(\phi)}$'s. At the demapper output, the mutual information $I_E^{(\phi)} = I(V; L_E^{(\phi)})$ between the transmitted bits V and the L-values $L_E^{(\phi)}$'s is calculated.

$$I_E^{(\phi)} = I(V; L_E^{(\phi)})$$

$$= \frac{1}{2} \sum_{v=-1,1}^{+\infty} \int p_{L_E^{(\phi)}}(\xi | V = v) \cdot \log_2 \left(\frac{2 \cdot p_{L_E^{(\phi)}}(\xi | V = v)}{p_{L_E^{(\phi)}}(\xi | V = 1) + p_{L_E^{(\phi)}}(\xi | V = -1)} \right) d\xi, \quad (3-10)$$

$$0 \leq I_E^{(\phi)} \leq 1. \quad (3-11)$$

Note that the required pdf $p_{L_E^{(\phi)}}(\xi | V = v)$ can be estimated by generating the histogram of $L_E^{(\phi)}$ and no Gaussian assumption is imposed on this term. Therefore, given an $I_A^{(\phi)}$ and a E_b / N_0 , the extrinsic information transfer characteristics can be computed.



For example, Fig. 3-1 and Fig. 3-2 show the demapper transfer curves of Gray and Anti-Gray [21] labeling for 16QAM in AWGN channel respectively. It can be seen from these figures that the demapper curve is enhanced at all range of $I_A^{(\phi)}$ but not equally at higher E_b / N_0 . For Gray labeling, the transfer curve remains almost constant with the increasing of $I_A^{(\phi)}$, whereas the transfer curve of Anti-Gray labeling is very steep revealing the potential performance improvement over iterations.

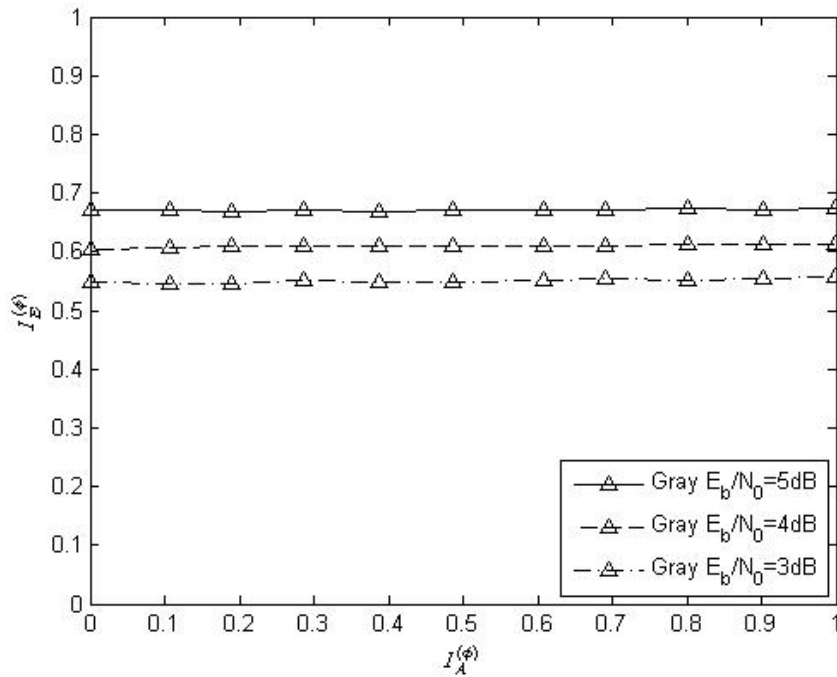


Fig. 3-1 Demapper transfer curve of Gray labeling for 16QAM in AWGN channel

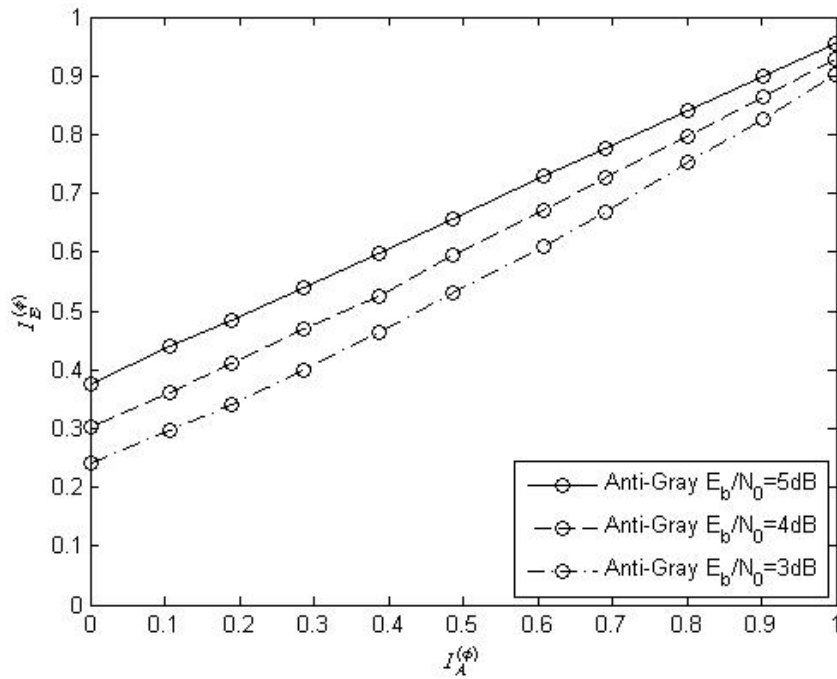


Fig. 3-2 Demapper transfer curve of Anti-Gray labeling for 16QAM in AWGN channel

3-2 Transfer Characteristics of Decoder

The decoder ψ takes the *a priori* input $L_A^{(\psi)}$'s from the demapper and calculates the *extrinsic a posteriori* $L_E^{(\psi)}$'s by equation (2-10). Because there is no channel observations in the decoder input, its transfer characteristics do not depend on E_b / N_0 . Define the mutual information between the coded bits and the decoder input and between the coded bits and the decoder output as $I_A^{(\psi)}$ and $I_E^{(\psi)}$, respectively. Assume $L_A^{(\psi)}$'s are independent Gaussian distributed, the extrinsic information transfer characteristics of the decoder can be computed by the same way as presented in the previous section.

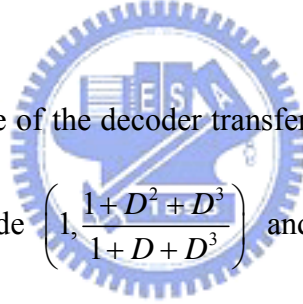


Fig. 3-3 shows an example of the decoder transfer curves of a rate-1/2 turbo code [22], [23] with constituent code $\left(1, \frac{1+D^2+D^3}{1+D+D^3}\right)$ and with 5 inner iterations as well as two convolutional codes with generator matrix $(1+D^2, 1+D+D^2)$ and $(1+D^2+D^3+D^5+D^6, 1+D+D^2+D^3+D^6)$. Note that the axes are swapped: the input is in the ordinate and the output is in the abscissa. It can be seen from the figure that the larger the code memory is, the flatter the decoder curve will be and the farther the curve may intersect with the demapper curve. Then, the resulting BER performance is better.

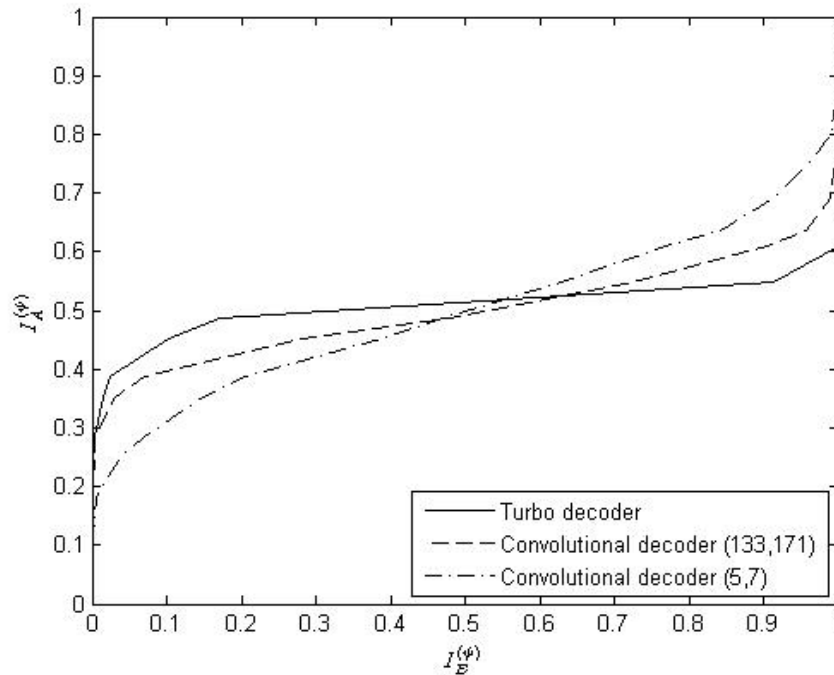


Fig. 3-3 Decoder transfer curves of turbo code and convolutional codes

3-3 Design Guideline Based on EXIT-chart

The transfer characteristics of the demapper and the decoder can be plotted in the same diagram with the axis of the decoder swapped. The exchange of extrinsic information between the demapper and the decoder can be visualized as the decoding trajectory in the EXIT-chart. Consider an example with the trajectory shown in Fig. 3-4, where $(I_A^{(\phi)}, I_E^{(\phi)})$ and $(I_A^{(\psi)}, I_E^{(\psi)})$ denote the mutual information of input and output LLRs of the demapper and decoder, respectively. The trajectory shows how the mutual information actually transfers between the decoder and the demapper. The farthest point that the trajectory can reach is the first intersection of the decoder transfer curve and the demapper transfer curve and it determines the performance limit of BICM-ID system.

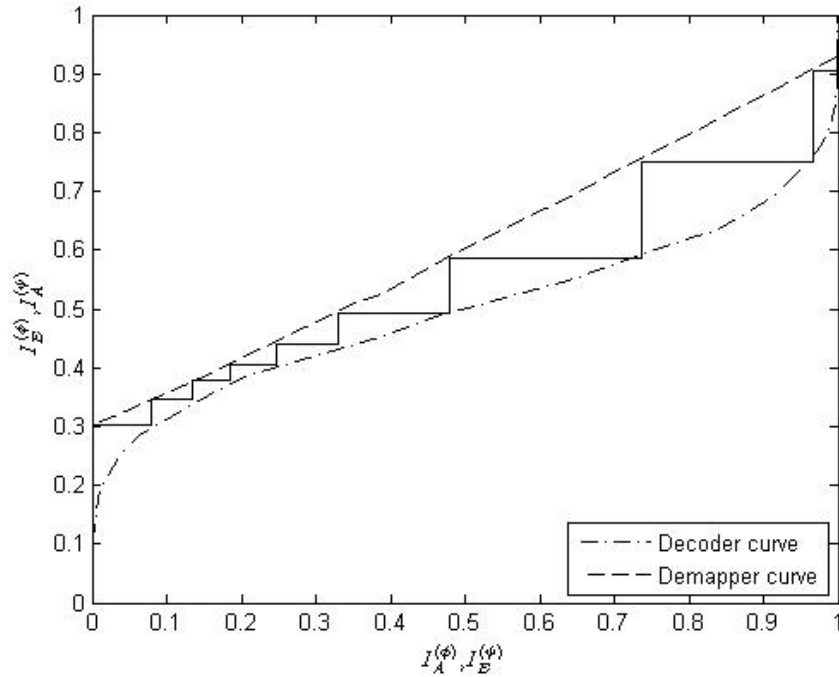


Fig. 3-4 An example of the EXIT-chart for BICM-ID at $E_b / N_0 = 4\text{dB}$ in AWGN channel

Given an outer code, a good labeling should be designed such that the demapper transfer curve and the decoder transfer curve can form a tunnel at SNR as low as possible to guarantee a low threshold for BICM-ID and have the first intersection at the farthest point to lower the undesired BER floor. Consider an example in Fig. 3-5, where two channel codes: a convolutional code with generator matrix $(1+D^2, 1+D+D^2)$ and a rate-1/2 turbo code with constituent code $(1, \frac{1+D^2+D^3}{1+D+D^3})$ are investigated with two kinds of labelings: Gray and Anti-Gray [21] at $E_b / N_0 = 4\text{dB}$ in AWGN channel. It can be observed from the figure that Gray is preferable to the turbo code while Anti-Gray is favorite to the convolutional code. This example suggests that the best labeling is different from code to code and therefore the labeling should be designed jointly with the outer code. Consider another example in Fig. 3-6, where a convolutional code with generator matrix $(1+D^2+D^3+D^5+D^6, 1+D+D^2+D^3+D^6)$ is investigated with two kinds of

labelings: MSEW [24] and M16a [11] at $E_b/N_0=4.5\text{dB}$ in AWGN channel. The MSEW is more preferred because the left-end point of its demapper curve is higher than that of M16a such that the tunnel can be opened at lower threshold and the right-end point is almost the same such that similar BER floor can be expected. This example advises that the transfer curve of the good labeling should be high at its two end points for an given outer code. Therefore, the design guideline can be summarized as: the best labeling should be designed such that its corresponding transfer curve not only matches a given outer code but is high at its two end points.

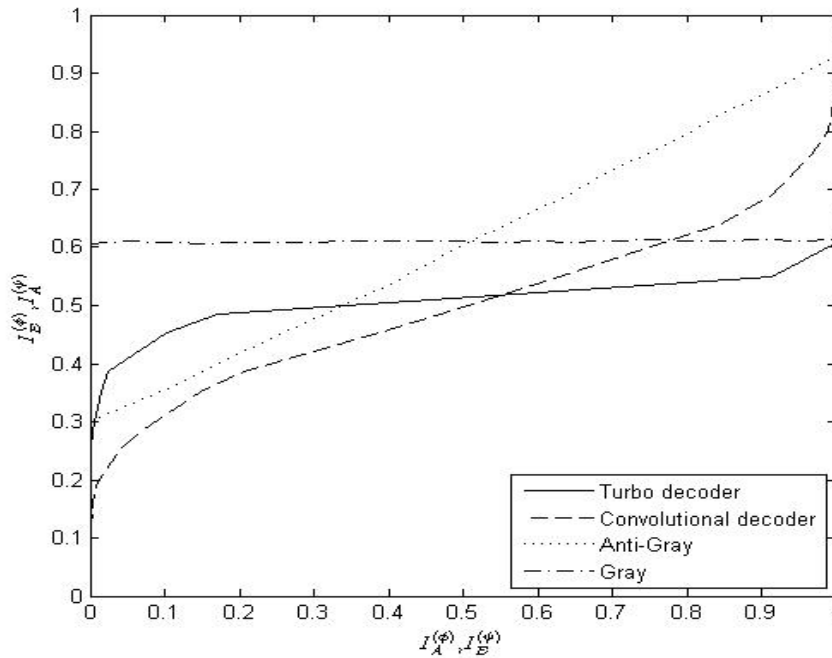


Fig. 3-5 Observation I for labeling design.

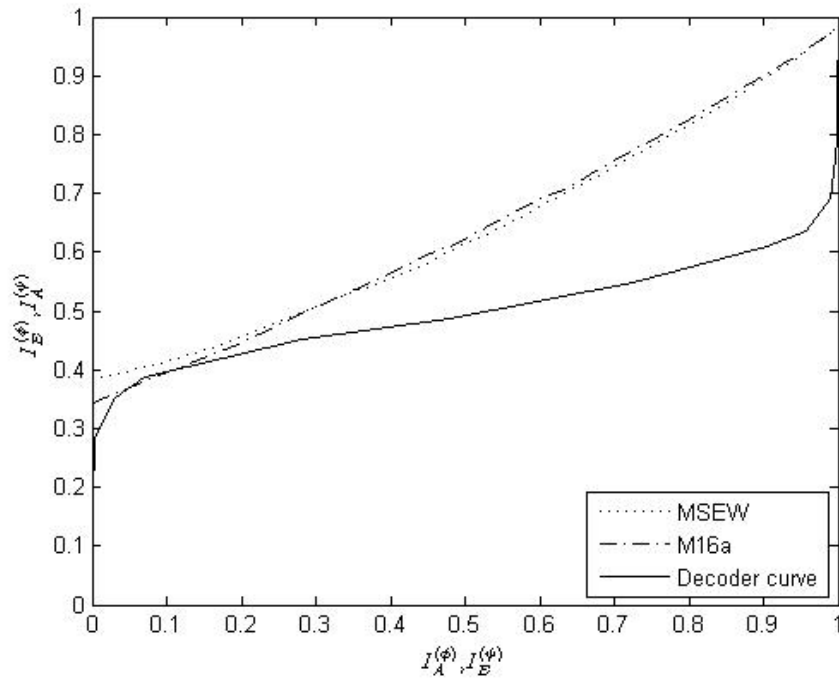
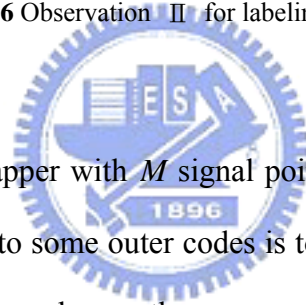


Fig. 3-6 Observation II for labeling design



For a one-dimensional mapper with M signal points, an intuitive way to find the optimal labeling with respect to some outer codes is to plot the demapper curve of all possible $M!$ labelings and then choose the one most matched to the outer code. However, for a large M , the high complexity required for exhaustive search is usually far beyond what a practical system can afford. To provide a practical search scheme for the optimal labeling, a systematic design methodology is proposed in next chapter.

Chapter 4

One-dimensional Labeling Design

The design guideline based on the EXIT-chart in chapter 3 pointed out that the best labeling should be designed such that its corresponding transfer curve not only matches a particular outer code but is high at its two end points. In this chapter, labeling design for regular one-dimensional constellation is concerned and the system model is reduced from the general system model Fig. 2-1 by employing a 1-D mapper as well as setting $N_T = 1$ and $N_R = 1$. Several criteria regarding the highness of two end points of demapper transfer curve will be presented first and then a systematic design method based on these criteria is proposed to design a set of lablings with good EXIT-chart characteristics. In this chapter, a one-dimensional M -ary complex constellation with $m = \log_2 M$ is assumed.

4-1 Design criteria

The mutual information between the demapper output and the coded bits when no *a priori* information is available (denoted as $I_E^{(\phi)}(I_A^{(\phi)} = 0)$) and when *a priori* information is ideally fed back (denoted as $I_E^{(\phi)}(I_A^{(\phi)} = 1)$) corresponds to the left-end and the right-end point of the demapper transfer curve, respectively. Several criteria deprived in previous works governing $I_E^{(\phi)}(I_A^{(\phi)} = 0)$ and $I_E^{(\phi)}(I_A^{(\phi)} = 1)$ will be investigated in this section.

4-1-1 Without A Priori Information

When *a priori* information from the decoder is not available (i.e., $I_A^{(\phi)} = 0$), it corresponds to the first iteration when the demapper takes only the channel observations r 's and computes the extrinsic *a posteriori* information $L_E^{(\phi)}$'s by assuming the probability of occurrence of bit 1 and bit 0 are equal likely. Higher $I_E^{(\phi)}$ corresponds with a lower BER P_b^0 of the hard-decisioned bits at the demapper output. The derivation of P_b^0 is as follows. By the union bound approximation, the pairwise symbol error probability $p(x_l \rightarrow x_k)$ when x_l is transmitted and erroneously decided as x_k can be written as

$$p(x_l \rightarrow x_k) \leq \sum_{k=0, k \neq l}^{M-1} p(x_l \rightarrow x_k). \quad (4-1)$$

Then the averaged symbol error rate p_e can be written as

$$p_e = \sum_{l=0}^{M-1} \sum_{k=0, k \neq l}^{M-1} p(x_l \rightarrow x_k) \cdot p(x_l). \quad (4-2)$$

The relationship between the symbol error probability p_e and the bit error probability p_{eb} of a MPSK or MQAM signal is as follows (assume the bit error probability in each bit position is equal likely)

$$\begin{aligned} p_e &= 1 - p_c \\ &= 1 - (p_{cb})^m \\ &= 1 - (1 - p_{eb})^m \\ &\approx m \cdot p_{eb} \quad (\text{By Taylor's expansion}) \end{aligned} \quad (4-3)$$

where p_c is the symbol correct probability and p_{cb} is the bit correct probability.

By equation (4-2) and (4-3), P_b^0 can be written as [14], [25]

$$P_b^0 = \sum_{l=0}^{M-1} \sum_{\substack{k=0 \\ k \neq l}}^{M-1} \frac{d_{Ham}(\mu(x_l), \mu(x_k))}{m} \Pr(x_l \rightarrow x_k) \cdot \Pr(x_l) \quad (4-4)$$

where $d_{Ham}(\cdot, \cdot)$ denotes the Hamming distance of two bit vectors and $\Pr(x_l) = 1/M$ owing to the lack of *a priori* information.

At a E_b / N_0 , the pairwise symbol error probability $p(x_l \rightarrow x_k)$ depends on the Euclidean distance between x_l and x_k : as the distance becomes smaller, the pairwise symbol error probability is larger. The nearest constellation points therefore contribute more in the symbol error probability and thus the BER P_b^0 . The average number of bits that differ between two closest constellation points is then the most important parameter that determines P_b^0 , which is denoted as [14]

$$N_{av} = \frac{1}{|\mathcal{X}|} \sum_{l=0}^{|\mathcal{X}|-1} \left[\frac{1}{N(l)} \sum_{x_k \in \mathcal{X}_l} d_{Ham}(\mu(x_l), \mu(x_k)) \right], \quad (4-5)$$

where \mathcal{X}_l contains the nearest neighbors of x_l and $|\mathcal{X}_l| = N(l)$. Hence, N_{av} can be used to determine $I_E^{(\phi)}(I_A^{(\phi)} = 0)$. Note that N_{av} depends on μ and not on E_b / N_0 and channel.

4-1-2 Ideal A Priori Information

When ideal *a priori* information from the decoder is available (i.e., $I_A^{(\phi)} = 1$), the demapper computes the *extrinsic a posteriori* information $L_E^{(\phi)}$'s based on the channel observations r 's and the *a priori* information $L_A^{(\phi)}$'s. Higher $I_E^{(\phi)}$ corresponds with a lower BER P_b^l . The BER upper bounds derived in [4], [6], [7] for AWGN channels and Rayleigh fading channels will be presented in this sections.

4-1-2-1 AWGN Channels

The union bound of probability of bit error for convolutional codes of rate k_c/n_c is given by [4]

$$P_b^l \leq \frac{1}{k_c} \sum_{d=d_f}^{\infty} W_t(d) f(d, \mu, \chi), \quad (4-6)$$

where $W_t(d)$ is the total information weight of error events at Hamming distance d , d_f is the minimum Hamming distance of the code and $f(d, \mu, \chi)$ is the average pairwise error probability (PEP) depending on Hamming distance d , a labeling μ and a signal constellation χ .

In AWGN channels, $f(d, \mu, \chi)$ is derived as [4] [11]

$$f(d, \mu, \chi) \sim \left[\frac{1}{m \cdot 2^m} \sum_{k=1}^m \sum_{b=0}^1 \sum_{x \in \chi_b^k} \sum_{\tilde{z} \in \chi_b^k} \exp\left(-\frac{\|x - \tilde{z}\|^2}{4N_0}\right) \right]^d, \quad (4-7)$$

where \tilde{z} is the only element in χ_b^k under the EFF assumption (i.e., other bits forming a channel symbol are known). For example, Fig. 4-1 shows the Gray labeling and the Set-partitioning labeling for 8-PSK; when *a priori* information is ideally fed back, the 8-PSK constellations can be partitioned into sets of BPSK constellations having larger

intersignal Euclidean distance. Therefore, equation (4-7) can be rewritten as

$$f(d, \mu, \chi) \sim \left[\frac{1}{m \cdot 2^m} \sum_{k=1}^m \sum_{b=0}^1 \sum_{x \in \chi_b^k} \exp\left(-\frac{\|x - \tilde{z}\|^2}{4N_0}\right) \right]^d. \quad (4-8)$$

It can be seen from equation (4-8) that $f(d, \mu, \chi)$ is dominated by the terms with the smallest square Euclidean distance, which is denoted as

$$d_{\min} = \min_{x \in \chi_b^k, \forall k, b} \|x - \tilde{z}\|^2. \quad (4-9)$$

The number of terms in equation (4-8) corresponding to d_{\min} can be equivalently expressed, up to a scaling factor, as the average number of nearest neighbors [15]

$$N_{\min} = \frac{1}{2^m} \sum_{i=0}^{2^m-1} N_{\min}(x_i, d_{\min}) \quad (4-10)$$

where $N_{\min}(x_i, d_{\min})$ is the number of nearest neighbors of x_i . Note that both d_{\min} and N_{\min} depend on the mapping and constellation. If a labeling has larger d_{\min} and smaller N_{\min} , this labeling can achieve lower BER P_b^1 and higher $I_E^{(\phi)}$ ($I_A^{(\phi)} = 1$) in AWGN channel.

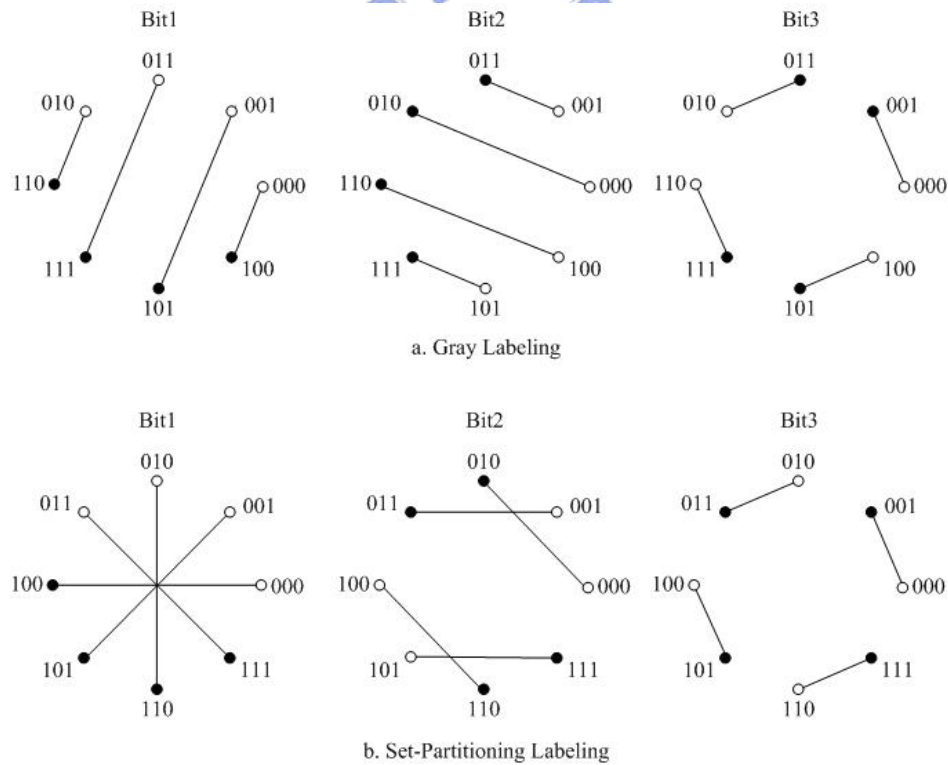


Fig. 4-1 Two mappings of 8-PSK constellation: (a) Gray and (b) Set-partitioning

4-1-2-2 Rayleigh Fading Channels

In [6] [7], the asymptotic performance of BICM-ID over Rayleigh fading channels can be approximated at high SNR by

$$\log_{10} P_b^1 \simeq -\frac{d_f}{10} \left[\left(R \Omega^2 \right)_{dB} + \left(\frac{E_b}{N_0} \right)_{dB} \right] + \text{const} \quad (4-11)$$

where d_f is the free Hamming distance of the code, R is the information rate (bits/dim) and Ω^2 is the harmonic mean of the squared Euclidean distances, defined as

$$\Omega^2 = \left[\frac{1}{m 2^m} \sum_{k=1}^m \sum_{b=0}^1 \sum_{x \in \chi_b^k} \left(\|x - \tilde{z}\|^2 \right)^{-1} \right]^{-1} \quad (4-12)$$

where $\tilde{z} \in \chi_b^k$ and $m = \log_2 M$. Note that under EFF assumption \tilde{z} is the only element in χ_b^k . The performance bound over Rayleigh fading channels primarily depends on d_f and Ω^2 and is not dominated by the minimum intersignal Euclidean distance as in AWGN channels. It can be seen from equation (4-11) that d_f controls the slope of the probability of bit error curve while Ω^2 provides the horizontal offset. Moreover, since d_f is a parameter of the channel code and Ω^2 is a function of the labeling μ and the signal set χ , the effect of the channel code and the labeling on BER P_b^1 can be separately optimized. If the minimum squared Euclidean distance between any pairs of modulated symbols which have only one distinct bit on their labels is increased, Ω^2 is increased and the resulting BER P_b^1 is lower. Then, $I_E^{(\phi)}$ is higher at the right-end point of the demapper transfer curve.

Hence we will investigate more on Ω^2 in the following. For each signal point x_i , define

$$\omega_i^2 \triangleq \left(\frac{1}{m} \sum_{k=1}^m \left(\|x_i - \tilde{z}\|^2 \right)^{-1} \right)^{-1} \quad (4-13)$$

where $x_i \in \mathcal{X}_b^k$, $\tilde{z} \in \mathcal{X}_b^k$. Each ω_i^2 is the harmonic mean of the squared Euclidean distances between x_i and other m constellation points whose labels differ in only one bit-position with x_i . With this definition, we can rewrite Ω^2 as the harmonic mean of ω_i^2 's

$$\Omega^2 = \left[\frac{1}{2^m} \sum_{i=0}^{2^m-1} \left(\omega_i^2 \right)^{-1} \right]^{-1}. \quad (4-14)$$

If taking partial derivative of Ω^2 with respect to ω_i^2 , the result is

$$\frac{\partial \Omega^2}{\partial (\omega_i^2)} = 2^m \cdot \left(\frac{\prod_{j=0, j \neq i}^{M-1} \omega_j^2}{\sum_{j=0}^{M-1} \sum_{k=j+1}^{M-1} \omega_j^2 \omega_k^2} \right)^2 \propto \left(\prod_{j=0, j \neq i}^{M-1} \omega_j^2 \right)^2. \quad (4-15)$$

If ω_i^2 is the minimum in ω_i^2 's, then $\partial \Omega^2 / \partial (\omega_i^2)$ is maximized. Therefore, we learn that the increment of the smallest term of ω_i^2 's maximizes the increase of Ω^2 . The large increment of Ω^2 lowers BER P_b^1 and enlarges $I_E^{(\phi)} (I_A^{(\phi)} = 1)$ maximally.

4-2 Design Method

Based on these design criteria regarding the highness of the two end points of the demapper transfer curve discussed in last section, we are ready to design a set of labelings (called the candidate set Γ) with desired good EXIT-chart characteristics (i.e., the demapper transfer curve matches the decoder transfer curve and is as high as possible at its two end points). Conventional Gray labeling, whose transfer curve is almost flat since the minimum intersignal Euclidean distance can not be increased through iterative decoding, is first chosen as the initial labeling. It can be observed that the demapper curve will be steeper if swapping any two labels of the Gray labeling. To design labelings with good EXIT-chart characteristics, the two labels to be swapped should be selected such that $I_E^{(\phi)}(I_A^{(\phi)} = 1)$ can be enhanced significantly and $I_E^{(\phi)}(I_A^{(\phi)} = 0)$ can be pulled down least. Through consecutive label swappings, we can get a set of labelings with good EXIT-chart characteristics.

More specifically, to make $I_E^{(\phi)}(I_A^{(\phi)} = 1)$ be enhanced significantly after swapping two labels in both AWGN and Rayleigh fading channels, the criteria presented in section 4-1-2 are used. In AWGN channels, larger d_{\min} and smaller N_{\min} can result in lower BER P_b^1 and higher $I_E^{(\phi)}$. Each swapping must ensure that N_{\min} can be reduced and d_{\min} can be gradually enlarged through consecutive swappings. Therefore, we require the signal point x_i to be swapped with another one should satisfy

$$\min \{ \|x_i - x_j\|^2 : \forall j \neq i, d_{\text{Ham}}(\mu(x_i), \mu(x_j)) = 1 \} = d_{\min}. \quad (4-16)$$

In Rayleigh fading channels, larger Ω^2 can result in lower BER P_b^1 and higher $I_E^{(\phi)}$ and the increasing of the smallest term of ω_i^2 's maximizes the increasing of Ω^2 .

Because many small terms in ω_i^2 's are usually about the same value, each swapping must guarantee that one of them can be enlarged such that Ω^2 can be increased significantly. Therefore, the signal point x_i to be swapped with another one is also required to satisfy

$$\omega_i^2 \leq \Omega^2. \quad (4-17)$$

On the other hand, to make $I_E^{(\phi)}(I_A^{(\phi)} = 0)$ be pulled down least, the criterion presented in section 4-1-1 suggests that N_{av} should be kept small after each swapping. Based on the above design principles, a systematic procedure is proposed as follows.

Procedure for searching Γ :

Step 1: Choose Gray mapping as the initial labeling.

Step 2: Calculate ω_i^2 of each constellation point x_i and Ω^2 .

Step 3: Generate a set of constellation points. Each one, say x_i , must satisfy equation (4-16) and the corresponding ω_i^2 must satisfy equation (4-17).

Step 4: Try to switch the label of each signal point in the set with the label of another signal point in the constellation and then calculate the resulting N_{av}' and Ω'^2 .

Step 5: Select a pair of signal points for label swapping and then store the resulting labeling in Γ . The selection rule is as follows:

1. Over the pairs satisfying $\Omega'^2 > \Omega^2$, select the pair with minimum N_{av}' .
2. If there are more than one pairs with the same minimum N_{av}' , select the pair with maximum Ω'^2 .

3. If there are still more than one pairs with the same maximum Ω'^2 , pick any one of them and store other pairs' resulting labelings after swapping in a temporary stack.

Step 6: If the swapping pair can be found in Step5, go back to Step 2 and continue the search procedure. If not (i.e., all the swapping pairs' corresponding $\Omega'^2 \leq \Omega^2$), go to Step 7.

Step 7: Replace the initial labeling with one labeling stored in the temporary stack. Remove this one from the temporary stack. Then, restart the search procedure. Stop until the temporary stack is empty.

Remarks:

When the search procedure is finished, we can get many labelings in Γ . There are two points to be noted :

1. If there are more than one lableings in Γ with the same value of Ω^2 and N_{av} , pick any one of them and discard others. These labelings may result in the same EXIT-chart characteristics and BER performance.
2. For those demapper transfer curves corresponding to the labelings in Γ , uniformly quantize $I_E^{(\phi)}(I_A^{(\phi)} = 0)$. With each discrete value at the left end, choose the labeling with the largest $I_E^{(\phi)}(I_A^{(\phi)} = 1)$.

4-3 Proposed Labelings

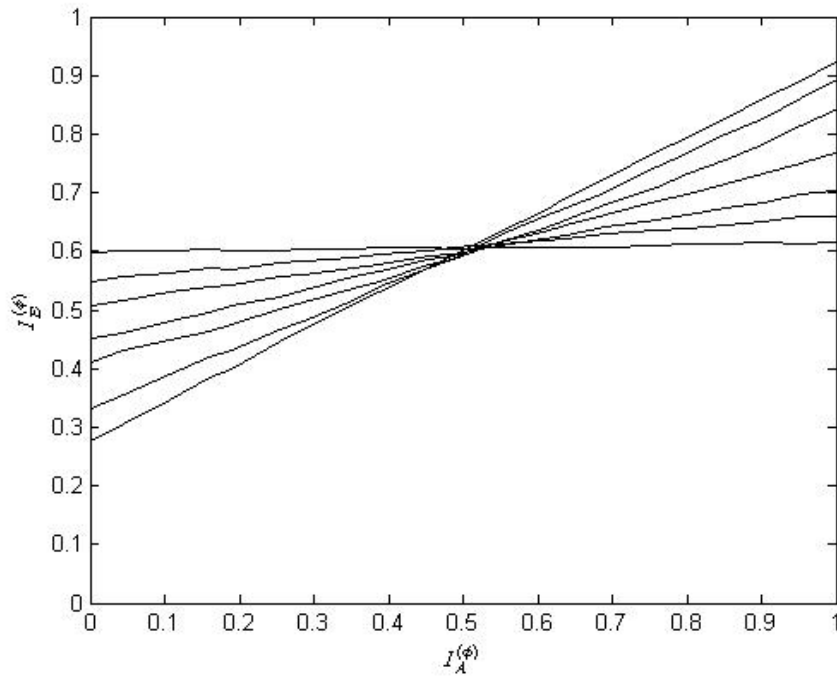
The searched Γ 's for 8-PSK, 16-QAM and 64-QAM are presented in Table 4-1, 4-2, 4-3, respectively, where the labelings are listed in a decreasing order in terms of $I_E^{(\phi)}(I_A^{(\phi)}=1)$. From Fig.4-2, Fig. 4-3 and Fig 4-4, the labeling are observed to generate the curves which are uniformly distributed in the left end and are high in the right end in both AWGN and Rayleigh fading channel. In addition, all the demapper curves can still keep the same order at various SNR and channel. Therefore, given an outer code, we can then choose a labeling form Γ which most matches the outer code to make tunnel open at low threshold and achieve acceptable BER at high SNR.



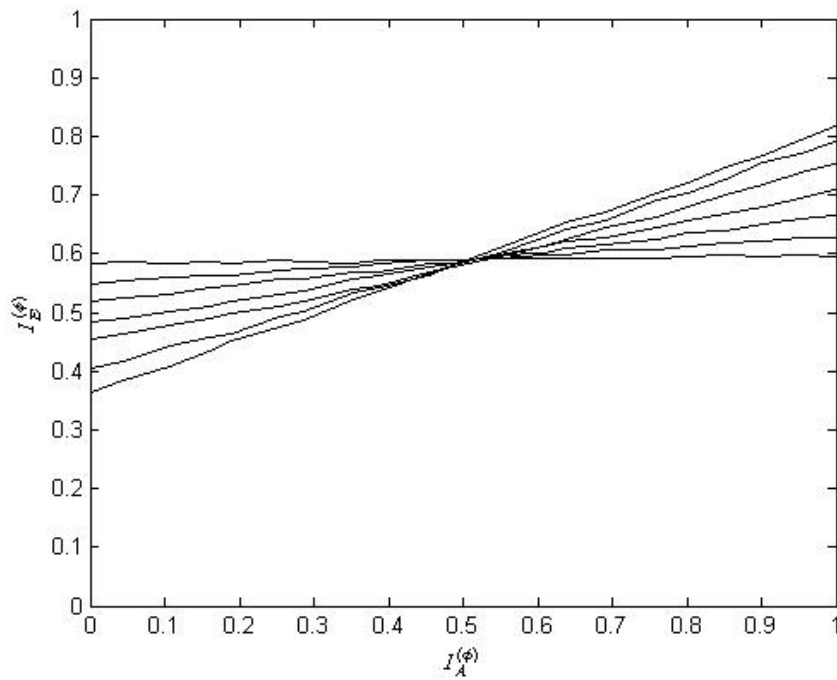
4-3-1 8-PSK

Table 4-1 Candidate set for 8-PSK

μ for 8PSK	$(\mu(x_0), \mu(x_1), \dots, \mu(x_7))$
A8	5,6,3,4,1,2,7,0
B8	5,0,3,6,1,2,4,7
C8	0,3,6,7,2,1,4,5
D8	0,6,7,1,3,2,4,5
E8	1,0,6,7,3,2,4,5
F8	1,0,3,2,6,7,5,4
Gray	0,1,3,2,6,7,5,4



(a)



(b)

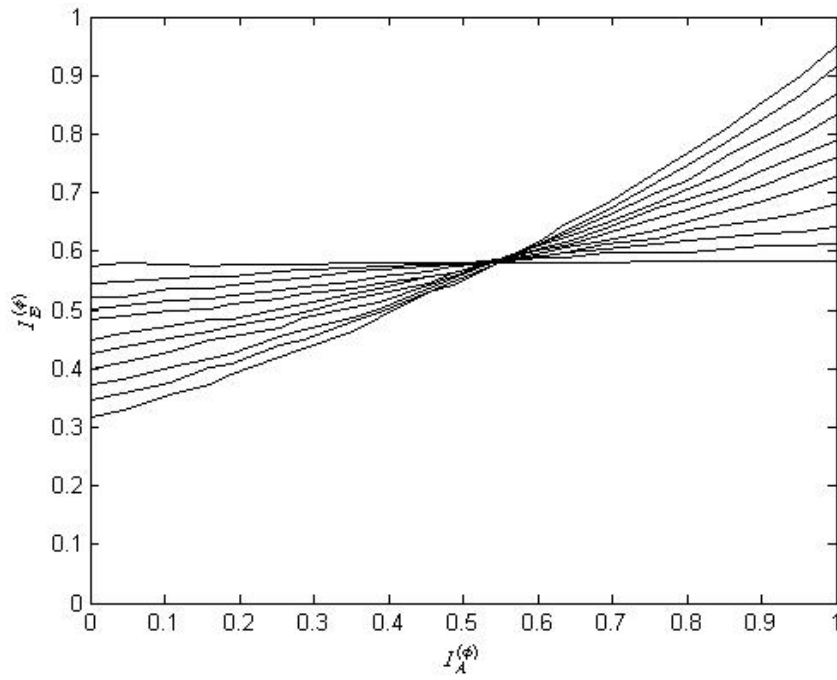
Fig. 4-2 Labelings for 8-PSK in Table 4-1 at (a) $E_b/N_0 = 3\text{dB}$ in AWGN channel and (b) $E_b/N_0 = 5\text{dB}$ in Rayleigh fading channel

4-3-2 16-QAM

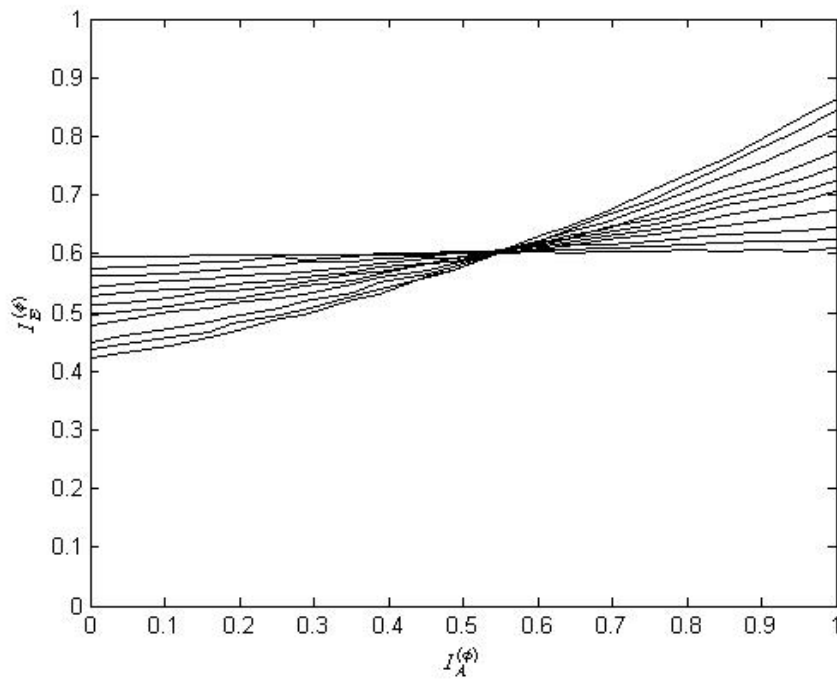
Table 4-2 Candidate set for 16-QAM

μ for 16QAM	$(\mu(x_0), \mu(x_1), \dots, \mu(x_{15}))$	
A16	(6,3,11,14,0,5,8,13,9,15,2,4,10,12,1,7)	
B16	(6,0,1,7,12,10,11,13,5,3,2,8,15,9,4,14)	
C16	(6,0,1,7,12,8,11,13,5,3,2,4,15,9,10,14)	
D16	(4,13,7,14,1,8,11,10,5,12,15,6,0,9,3,2)	
E16	(4,13,7,3,1,8,14,2,5,12,15,6,0,9,11,10)	
F16	(2,7,5,3,4,1,0,6,8,12,10,14,9,13,11,15)	
G16	(2,7,5,0,4,1,3,6,12,8,10,14,13,9,11,15)	
H16	(2,7,1,0,4,5,3,6,12,13,15,14,8,9,11,10)	
I16	(5,1,3,2,4,0,7,6,12,9,15,14,13,8,11,10)	
J16	(5,1,3,2,4,0,7,6,12,13,15,14,8,9,11,10)	
Gray	(0,1,3,2,4,5,7,6,12,13,15,14,8,9,11,10)	





(a)



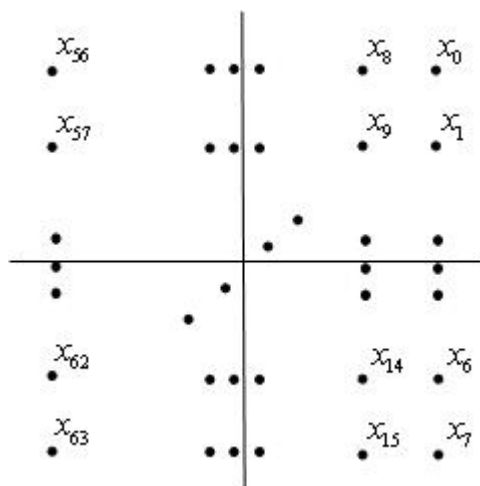
(b)

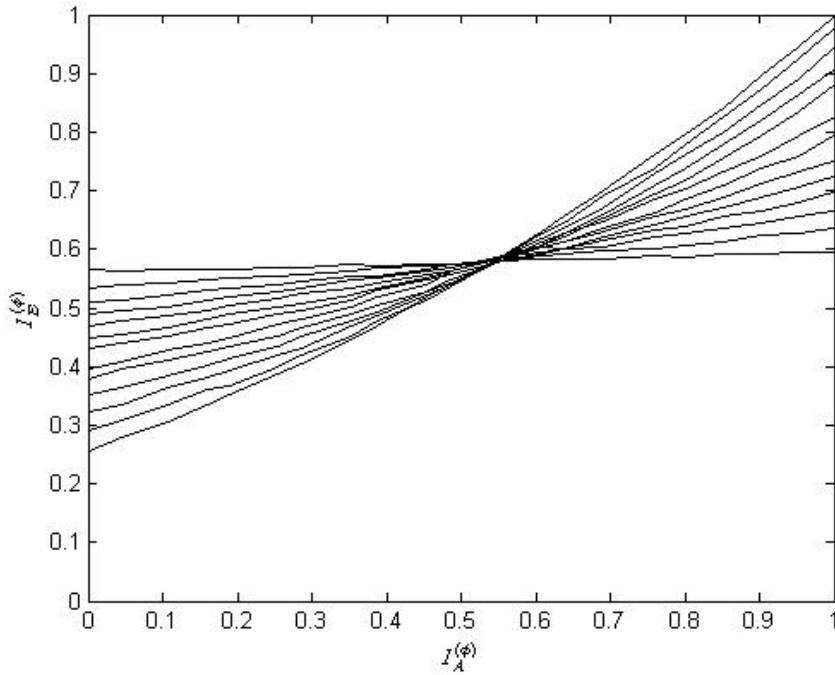
Fig. 4-3 Labelings for 16-QAM in Table 4-2 at (a) $E_b/N_0 = 3.5\text{dB}$ in AWGN channel and (b) $E_b/N_0 = 6\text{dB}$ in Rayleigh fading channel

4-3-3 64-QAM

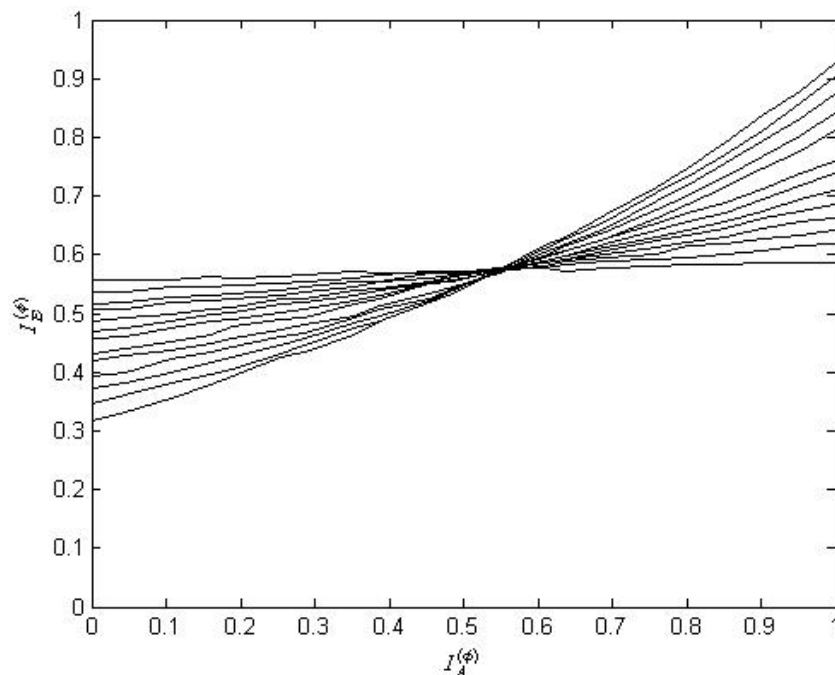
Table 4-3 Candidate set for 64-QAM

$\mu(x)$ for 64QAM	$(\mu(x_0), \mu(x_1), \dots, \mu(x_{63}))$
A64	(56,8,49,55,22,14,7,21,59,25,1,19,16,28,4,52,41,61,13,34,40,57,9,45,36,6,10,46,58,43,33,39,0,18,48,30,54,15,2,63,3,51,17,24,27,29,5,60,31,47,37,20,23,53,12,26,62,44,38,32,35,50,42,11)
B64	(30,11,1,8,4,9,29,15,23,35,2,26,14,3,5,12,53,50,22,62,42,32,17,20,57,27,21,31,25,49,59,18,48,24,13,6,19,55,61,28,54,60,46,36,16,7,37,52,39,63,58,40,33,38,47,44,45,43,51,34,0,10,41,56)
C64	(30,11,1,8,13,15,29,9,23,35,2,26,14,6,5,12,17,18,22,62,42,36,53,20,57,27,21,31,25,59,49,16,48,24,4,3,19,55,61,28,54,60,46,10,0,7,37,52,39,63,58,40,33,38,47,44,45,43,51,34,50,32,41,56)
D64	(26,59,49,16,22,14,28,61,56,25,1,19,55,7,4,21,8,40,13,11,31,15,12,45,0,48,24,58,62,39,5,53,3,3,34,10,18,54,23,20,52,17,51,3,27,63,30,29,60,57,9,37,35,46,42,41,44,43,47,38,50,6,2,32,36)
E64	(26,59,49,16,22,14,28,61,56,25,1,19,55,7,4,21,8,40,13,11,31,15,12,45,0,48,24,58,62,6,5,53,33,34,10,18,54,23,20,52,17,51,3,50,30,63,29,60,57,27,2,42,46,47,41,44,9,43,35,32,38,39,37,36)
F64	(9,1,2,8,12,5,15,14,0,3,11,26,30,6,13,28,16,18,17,25,60,54,53,20,24,27,29,31,62,22,21,4,48,57,49,19,59,55,61,52,32,41,34,10,35,7,37,23,50,56,58,40,46,38,47,63,42,43,51,33,39,36,44,45)
G64	(24,27,9,10,22,14,28,13,56,25,1,19,55,7,4,21,16,8,2,11,31,15,12,29,0,40,26,59,30,6,5,20,3,34,18,51,54,23,53,52,17,48,49,50,62,63,61,60,57,41,35,42,46,47,36,44,58,43,33,32,38,39,37,45)
H64	(1,8,2,10,12,5,15,14,0,9,3,11,13,6,30,28,16,24,17,25,31,7,21,4,18,27,23,59,62,22,52,20,48,57,51,19,54,55,53,29,49,56,50,26,58,63,61,45,35,32,42,40,46,47,36,60,43,41,33,34,38,39,37,44)
I64	(8,1,19,26,22,14,28,29,0,9,3,10,6,7,4,13,16,17,27,18,54,15,12,21,24,25,11,2,30,23,5,20,40,41,59,58,31,55,53,52,56,48,49,50,62,63,61,60,57,33,35,42,46,47,36,44,51,43,34,32,38,39,37,45)
J64	(1,0,2,10,14,12,15,13,8,9,3,11,7,6,5,4,26,24,27,25,31,30,29,28,19,17,18,16,22,23,21,20,48,57,51,58,54,55,53,52,49,56,50,59,62,63,61,60,33,32,42,40,46,47,36,44,43,41,35,34,38,39,37,45)
K64	(9,1,3,2,6,7,5,13,8,0,10,11,14,15,4,12,26,24,27,25,30,31,29,28,19,17,18,16,22,23,21,20,48,57,51,58,54,55,53,52,49,56,50,59,62,63,61,60,33,32,42,43,46,47,36,44,41,40,35,34,38,39,37,45)
L64	(9,1,3,2,6,7,5,13,8,0,10,11,14,15,4,12,25,24,27,26,30,31,29,28,16,17,18,19,22,23,21,20,48,49,50,51,54,55,53,52,57,56,58,59,62,63,61,60,40,32,42,43,46,47,36,44,41,33,35,34,38,39,37,45)
Gray	(0,1,3,2,6,7,5,4,8,9,11,10,14,15,13,12,24,25,27,26,30,31,29,28,16,17,19,18,22,23,21,20,48,49,51,50,54,55,53,52,56,57,59,58,62,63,61,60,40,41,43,42,46,47,45,44,32,33,35,34,38,39,37,36)





(a)



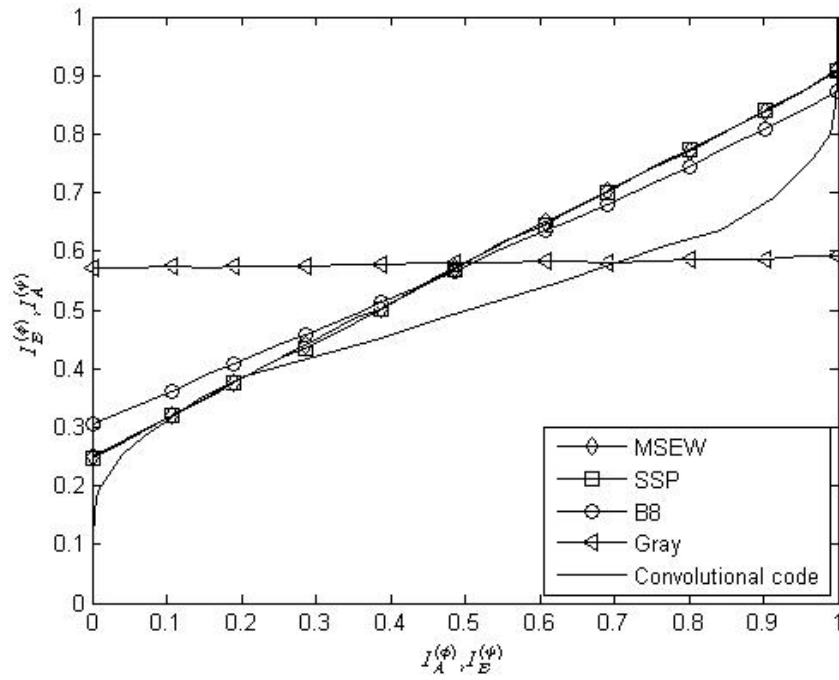
(b)

Fig. 4-4 Labelings for 64-QAM in Table 4-3 at (a) at $E_b / N_0 = 6\text{dB}$ in AWGN channel and (b) $E_b / N_0 = 8\text{dB}$ in Rayleigh fading channel

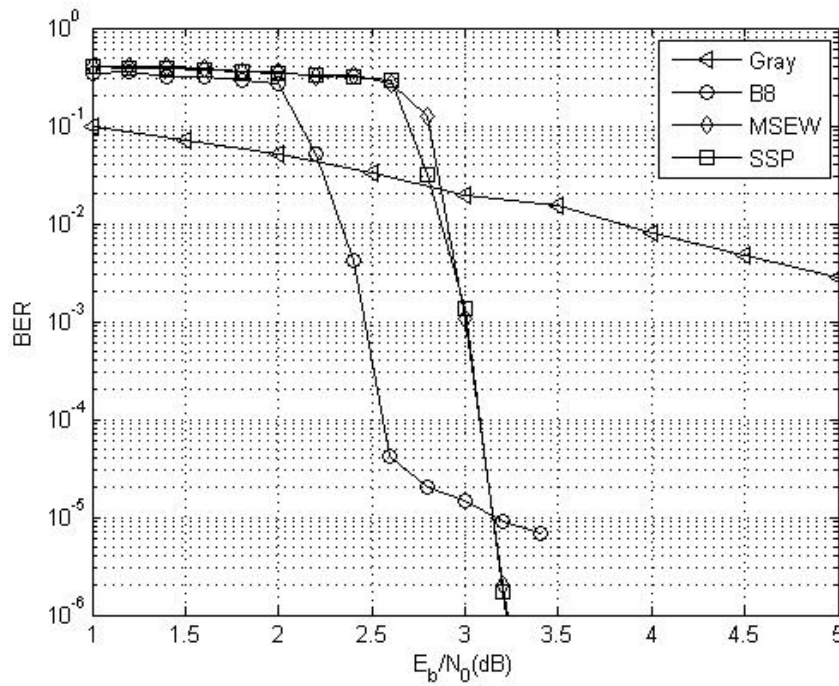
4-4 Simulation Results

To verify the superiority of our design over the conventional labelings, the BICM-ID system consisting of two kinds of rate-1/2 convolutional codes with generator matrix $(1+D^2, 1+D+D^2)$ and $(1+D^2+D^3+D^5+D^6, 1+D+D^2+D^3+D^6)$, a bit-interleaver of block length 24000 bits, and 8-PSK/16-QAM/64-QAM modulation is simulated for transmission over AWGN and Rayleigh channels. The demapper in (2-4) and BCJR decoder of the outer code are employed for iterative decoding with 40 iterations. For 8-PSK modulation, conventional designs suggest MSEW and SSP with the steepest demapper curves as the optimal labelings for BICM-ID. However, it can be seen from Fig. 4-5, Fig. 4-6 and Fig. 4-7 that the labeling that most match the outer code is B8, C8 and B8, respectively, as revealed from the EXIT-chart in Fig. 4-5(a) at 2.6dB, in 4-6(a) at 3dB and in 4-7(a) at 4.8dB. These labelings can provide SNR gain at BER around 10^{-5} . For example in Fig. 4-6(a), the first intersection of the demapper and decoder curves for C8 is observed to have $I_E^{(\phi)}$ larger than which of Gray, MSEW and SSP; the tunnel between both curves opens for C8 but not for MSEW and SSP. Therefore, based on the design guideline in section 3-3, C8 is expected to provide the best decoding performance, followed by Gray and then MSEW/SSP. The corresponding BER curves in Fig. 4-6(b) agree with the above analysis, which also show that our design can achieve 1.7 dB SNR gain over MSEW and SSP at BER 10^{-5} .

Similarly, simulation results in Fig. 4-8 to Fig. 4-10 confirm the most matched labelings for 16-QAM and 64-QAM modulation in the candidate sets can provide remarkable SNR gain over the conventional ones.

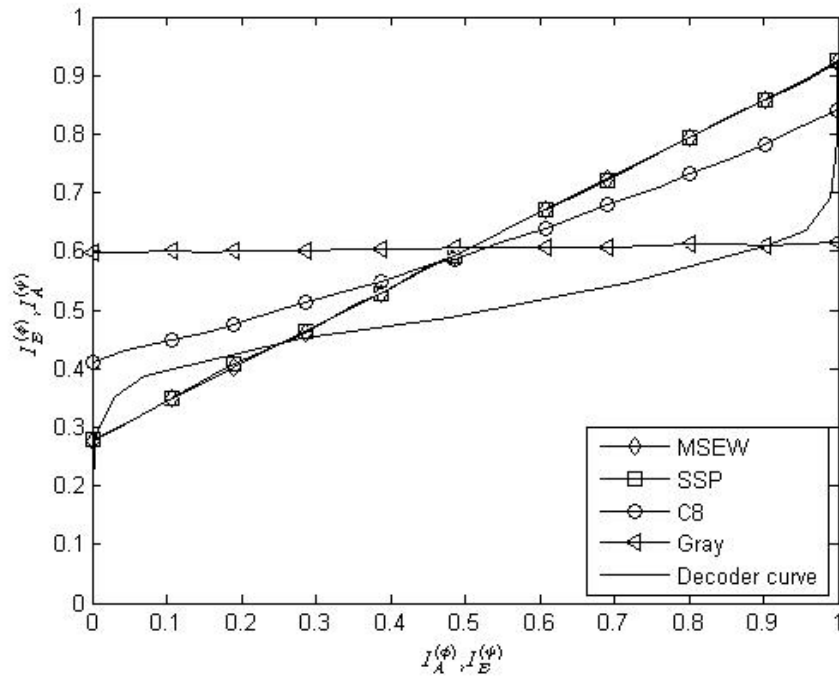


(a)

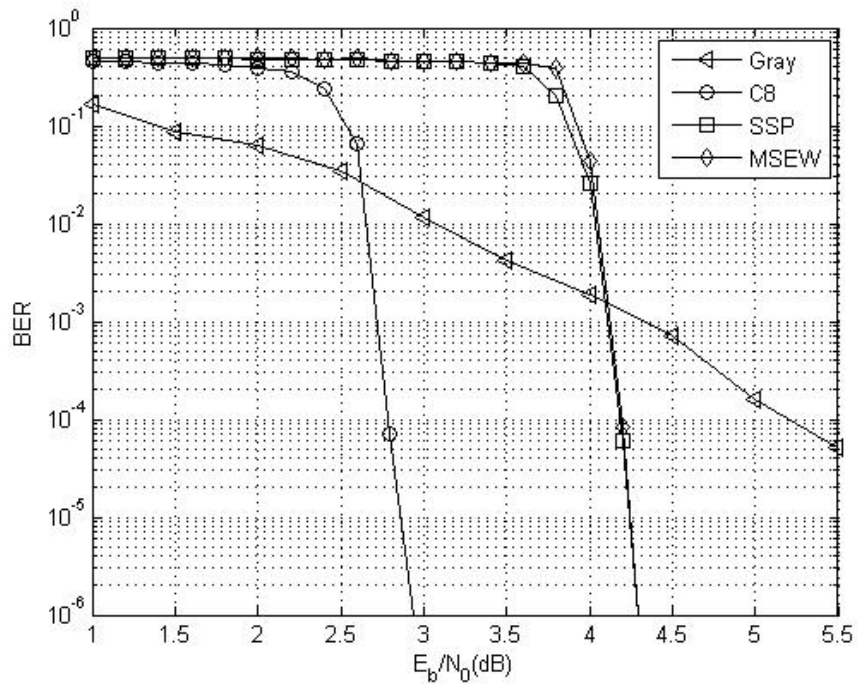


(b)

Fig. 4-5 (a) EXIT-chart at $E_b / N_0 = 2.6$ dB and (b) performance plots of the BICM-ID system with 8-PSK and (5, 7) convolutional code in AWGN channel

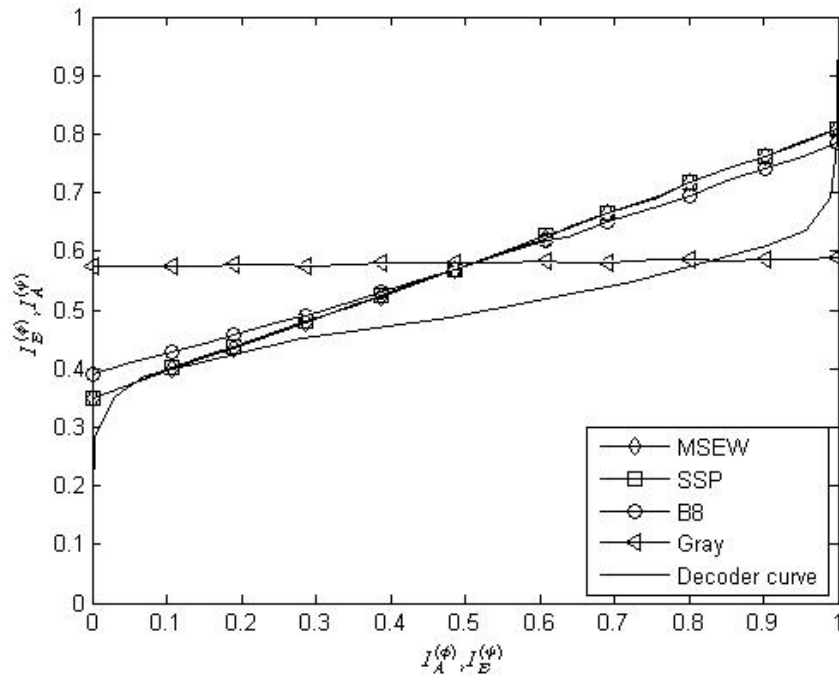


(a)

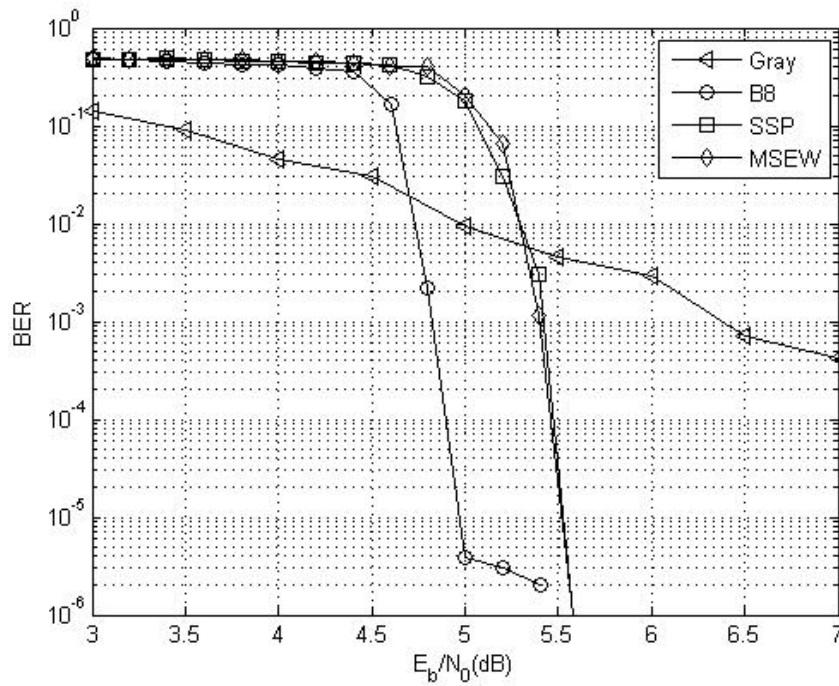


(b)

Fig. 4-6 (a) EXIT-chart at $E_b / N_0 = 3\text{dB}$ and (b) performance plots of the BICM-ID system with 8-PSK and (133, 171) convolutional code in AWGN channel

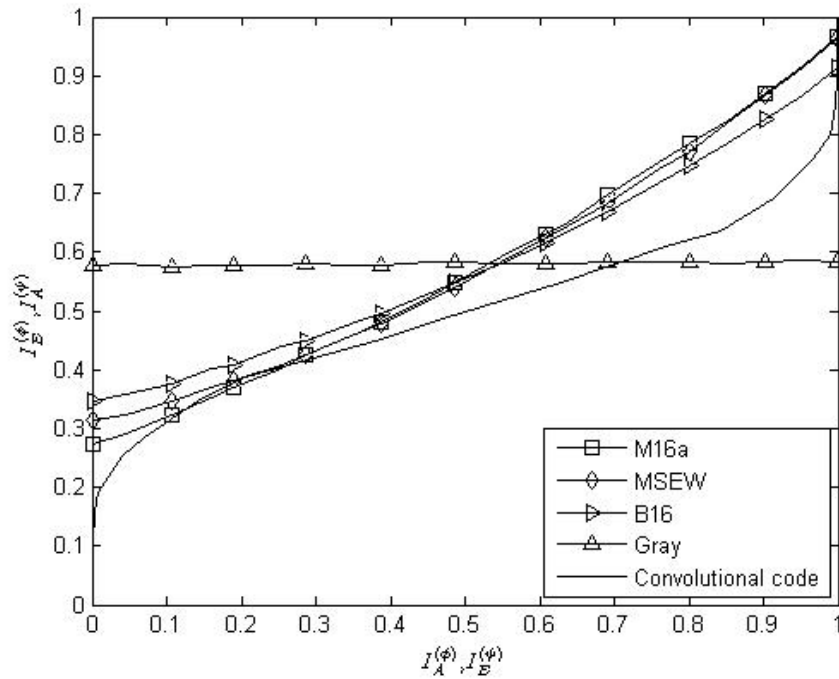


(a)

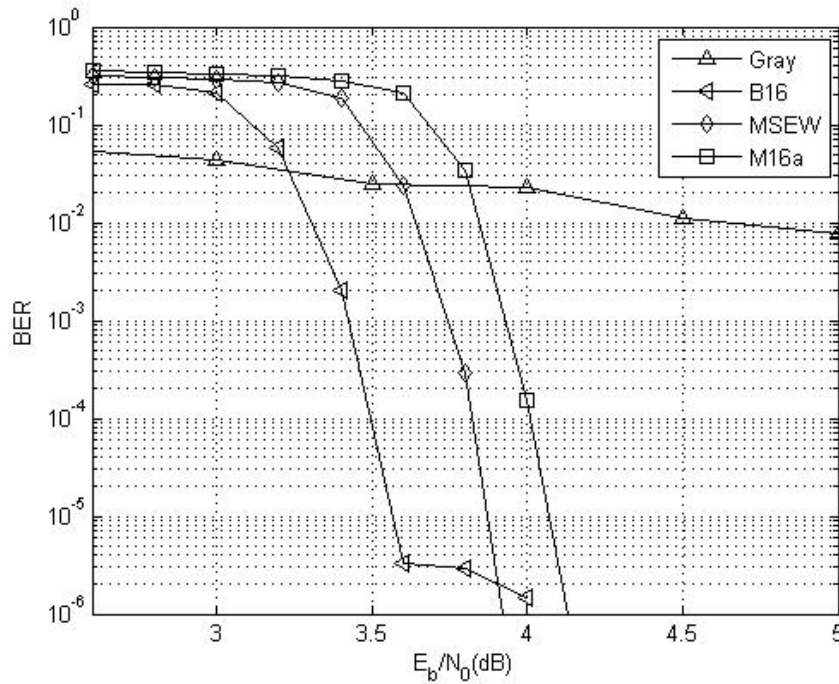


(b)

Fig. 4-7 (a) EXIT-chart at $E_b / N_0 = 4.8$ dB and (b) performance plots of the BICM-ID system with 8-PSK and (133, 171) convolutional code in Rayleigh channel



(a)



(b)

Fig. 4-8 (a) EXIT-chart at $E_b / N_0 = 3.5\text{dB}$ and (b) performance plots of the BICM-ID system with 16-QAM and (5, 7) convolutional code in AWGN channel

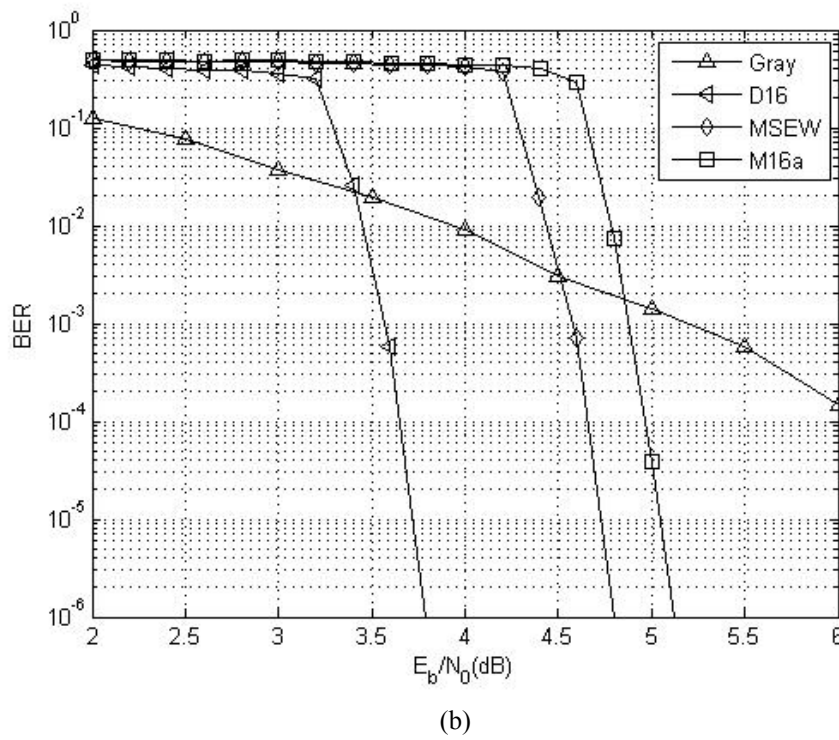
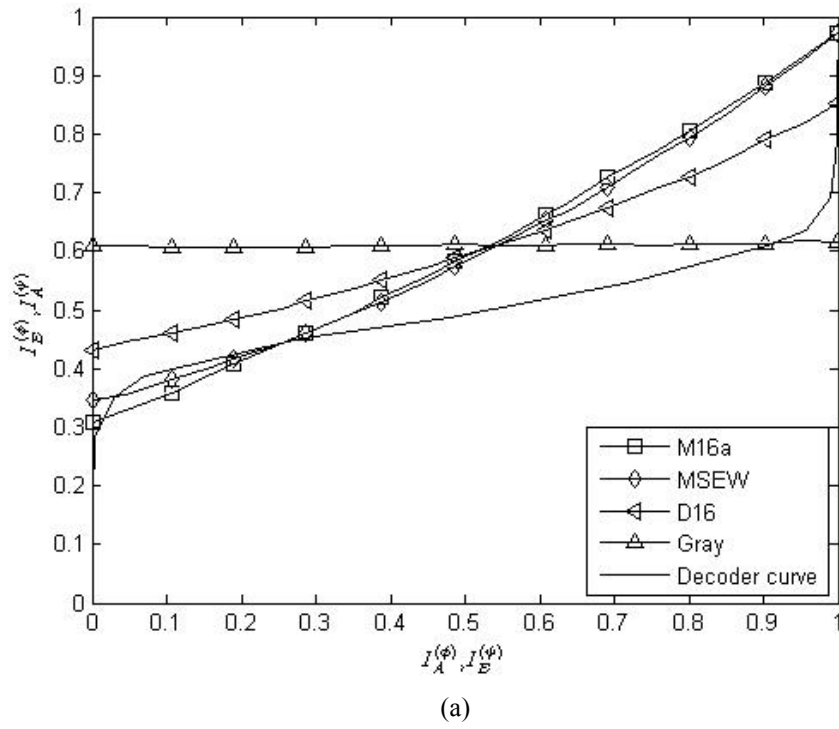


Fig. 4-9 (a) EXIT-chart at $E_b / N_0 = 4$ dB and (b) performance plots of the BICM-ID system with 16-QAM and (133, 171) convolutional code in AWGN channel

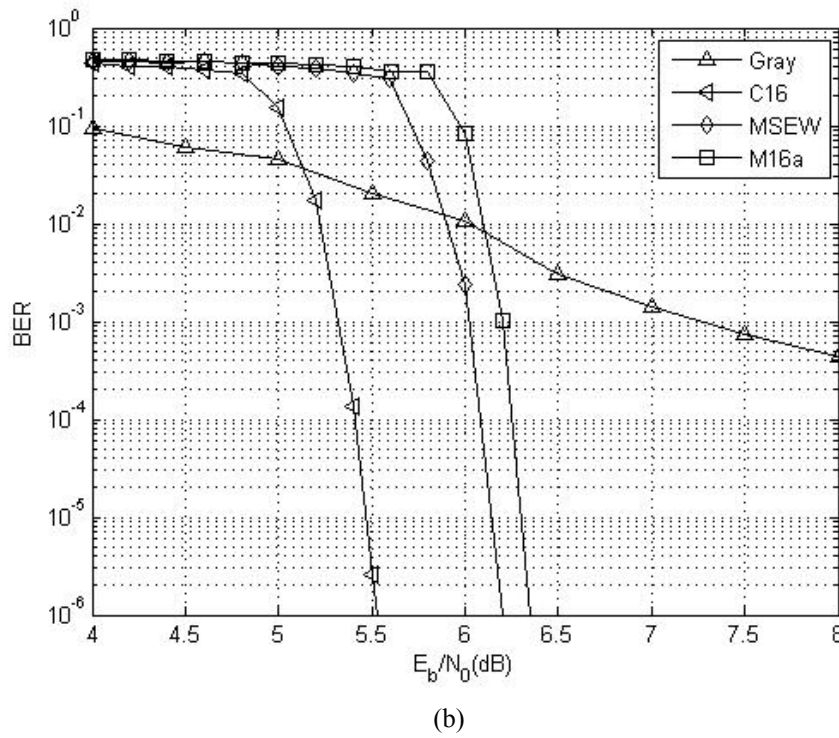
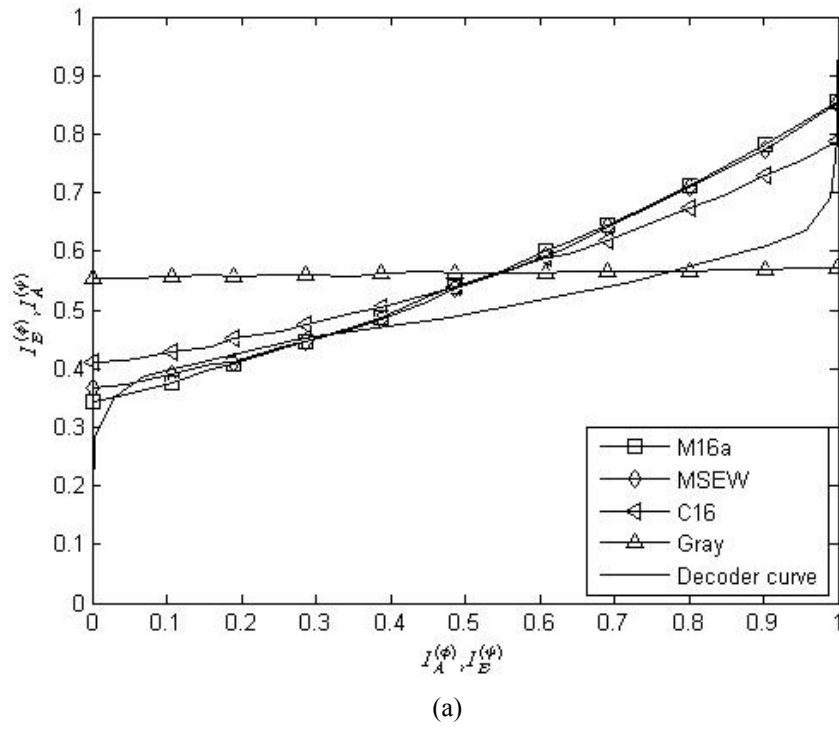
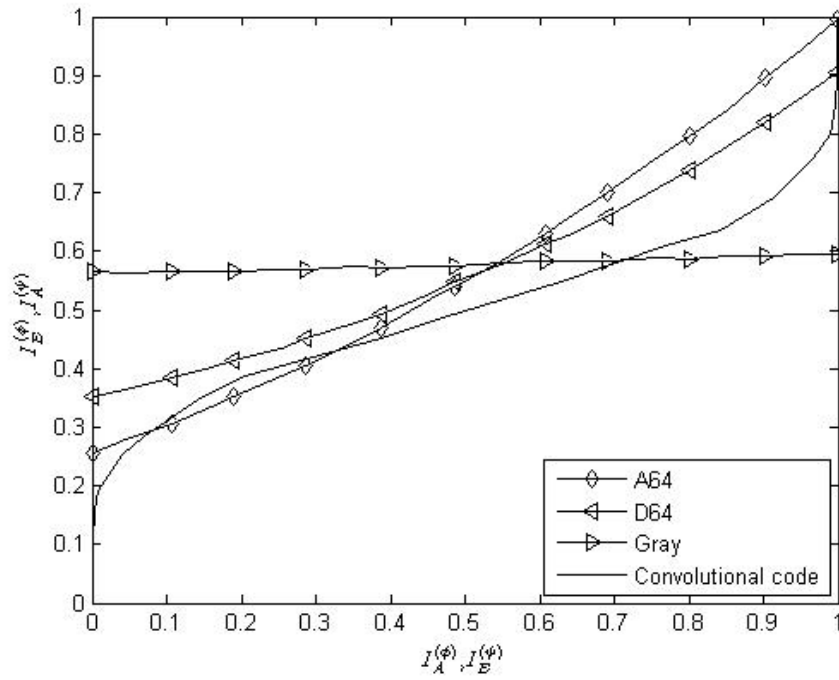
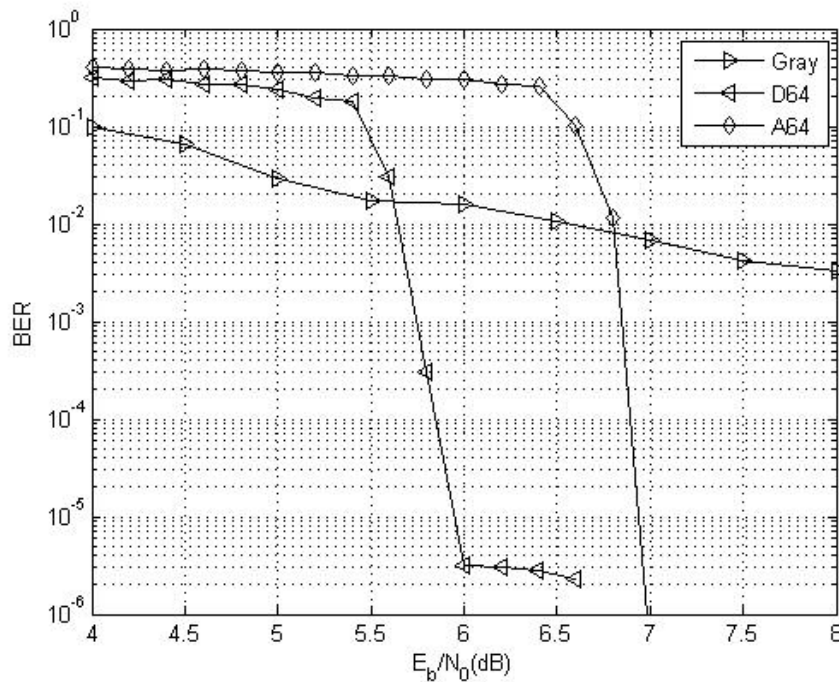


Fig. 4-10 (a) EXIT-chart at $E_b / N_0 = 5.2\text{dB}$ and (b) performance plots of the BICM-ID system with 16-QAM and (133, 171) convolutional code in Rayleigh channel

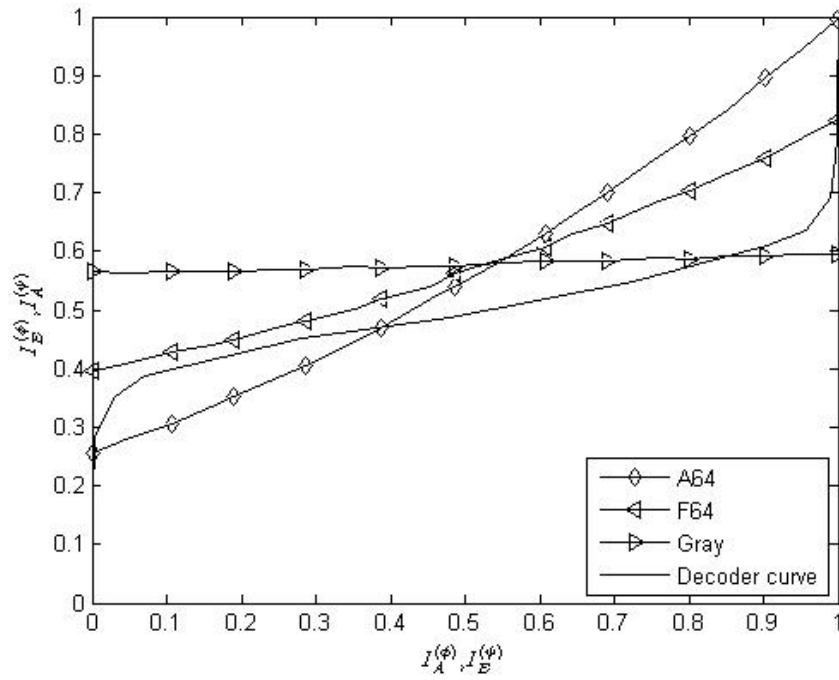


(a)

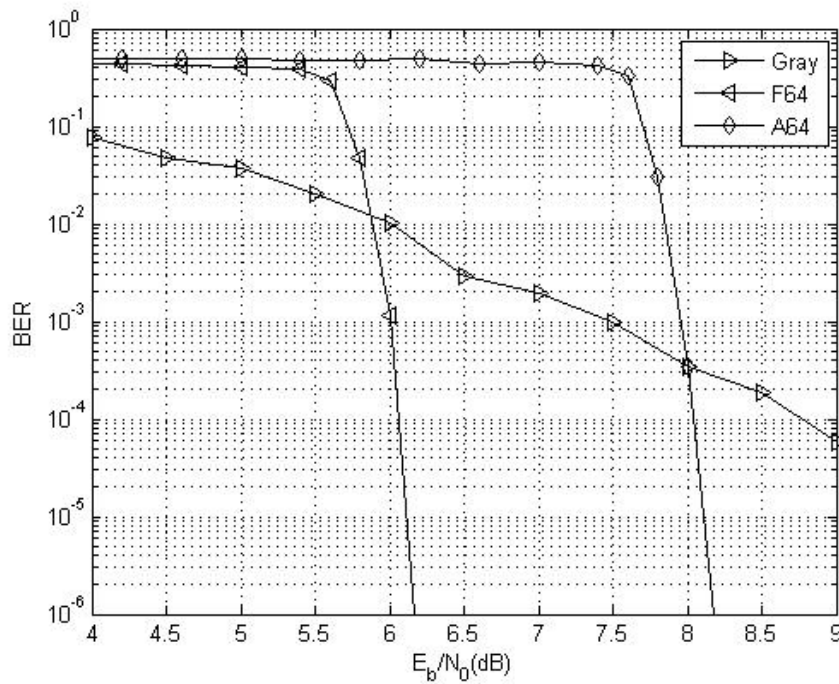


(b)

Fig. 4-11 (a) EXIT-chart at $E_b / N_0 = 6$ dB and (b) performance plots of the BICM-ID system with 64-QAM and (5, 7) convolutional code in AWGN channel

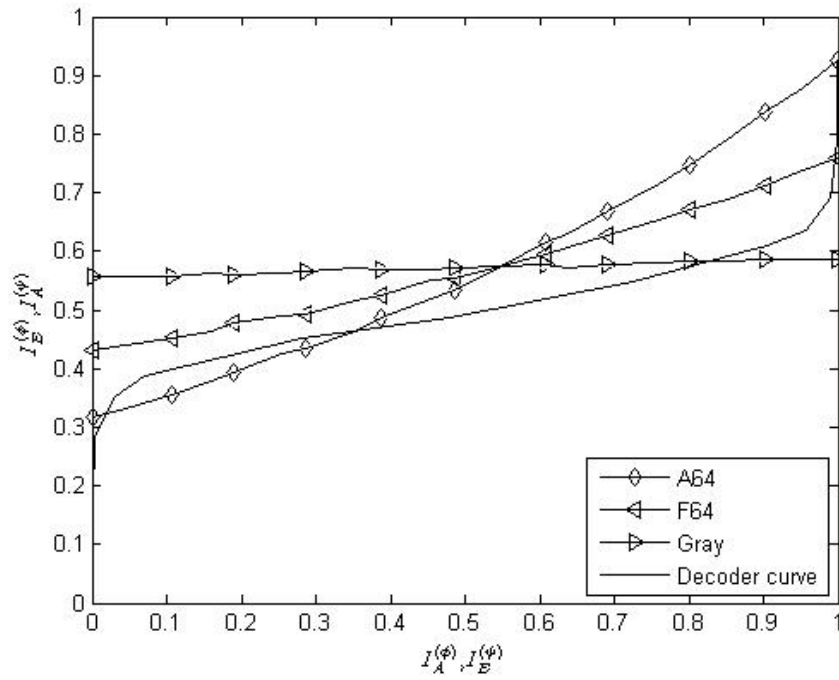


(a)

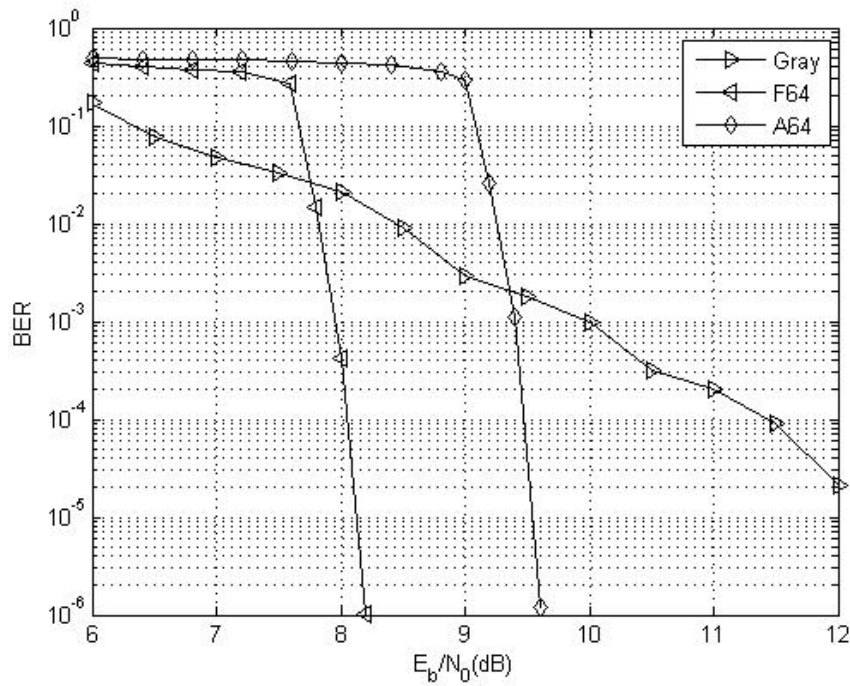


(b)

Fig. 4-12 (a) EXIT-chart at $E_b / N_0 = 6$ dB and (b) performance plots of the BICM-ID system with 64-QAM and (133, 171) convolutional code in AWGN channel



(a)



(b)

Fig. 4-13 (a) EXIT-chart at $E_b / N_0 = 8$ dB and (b) performance plots of the BICM-ID system with 64-QAM and (133, 171) convolutional code in Rayleigh channel

Chapter 5

Multi-dimensional Labeling Design

Multi-dimensional modulation scheme was proposed in [26] for TCM systems for several advantages compared with conventional one-dimensional mappings such as flexibility and higher code rate. When combined with BICM-ID systems, such a large constellation in higher dimensional space makes labeling design more flexible and allows potential performance improvements. For a N -dimensional signal \mathbf{x} , it is generated by taking the N -fold Cartesian product of the one-dimensional constellation (i.e., a block of coded bits were mapped to a vector of N symbols), denoted as


$$\mathbf{x} = [s_t^1, s_t^2, \dots, s_t^N], \quad (5-1)$$

where the sub index t indicates that the signal are generated at time t . The multi-dimensional signal can be transmitted in a SISO system over time domain or a MIMO system over spatial domain. We are going to design multi-dimensional labelings with good EXIT-chart characteristics for BICM-ID systems in both system configurations. Design criteria regarding the highness of both ends of the demapper transfer curve will be presented. Then, labeling design method for one-dimensional constellation can be directly extended to multi-dimensional constellation with the criteria changed.

5-1 Design Criteria

5-1-1 Multi-dimensional Mapping over Spatial Domain

The design of bit-interleaved space-time coded modulation with iterative decoding (BI-STCM-ID) over block Rayleigh fading channels with N_T transmit antennas and N_R receive antennas was proposed in [27] to capture both space and time diversity. In this section, we consider employing a MD mapper and spatial multiplexing in the BI-STCM-ID system. Several criteria governing two end points of the demapper curve when *a priori* information is not available and when *a priori* information is ideally fed back, respectively, will be presented.

5-1-1-1 Without A Priori Information

The derivation of BER P_b^0 is the same as in section 4-1-1 except that super-symbols are considered here. By the union bound approximation, the pairwise super-symbol error probability $p(\mathbf{x}_l \rightarrow \mathbf{x}_k)$ when \mathbf{x}_l is transmitted and erroneously decided as \mathbf{x}_k can be written as

$$p(\mathbf{x}_l \rightarrow \mathbf{x}_k) \leq \sum_{k=0, k \neq l}^{2^{mN}-1} p(\mathbf{x}_l \rightarrow \mathbf{x}_k). \quad (5-2)$$

The averaged super-symbol error rate p_e can be written as

$$p_e = \sum_{l=0}^{2^{mN}-1} \sum_{k=0, k \neq l}^{2^{mN}-1} p(\mathbf{x}_l \rightarrow \mathbf{x}_k) \cdot p(\mathbf{x}_l). \quad (5-3)$$

The relationship between super-symbol error probability p_e and bit error probability p_{eb} of a multi-dimensional signal is as follows (assume bit error probability in each bit position of the super-symbol is equal likely)

$$\begin{aligned}
p_e &= 1 - p_c \\
&\approx 1 - (p_{cb})^{mN} \\
&= 1 - (1 - p_{eb})^{mN} \\
&\approx mN \cdot p_{eb} \quad (\text{By Taylor's expansion}) \tag{5-4}
\end{aligned}$$

where p_c is the super-symbol correct probability and p_{cb} is the bit correct probability.

From equation (5-3) and (5-4), BER P_b^0 can therefore be written as

$$P_b^0 = \sum_{l=0}^{2^{mN}-1} \sum_{\substack{k=0 \\ k \neq l}}^{2^{mN}-1} \frac{d_{Ham}(\mu(\mathbf{x}_l), \mu(\mathbf{x}_k))}{mN} \Pr(\mathbf{x}_l \rightarrow \mathbf{x}_k) \cdot \Pr(\mathbf{x}_l) \tag{5-5}$$

where $d_{Ham}(\cdot, \cdot)$ denotes the Hamming distance of two bit vectors and $\Pr(x_l) = 1/2^{mN}$ due to the lack of *a priori* information.

At a E_b/N_0 , the pairwise super-symbol error probability $p(\mathbf{x}_l \rightarrow \mathbf{x}_k)$ depends on the Euclidean distance between \mathbf{x}_l and \mathbf{x}_k . Since the nearest constellation points contribute more in the super-symbol error probability and the BER P_b^0 , the average number of bits that differ between two closest signal points is then the most important parameter that determines the BER P_b^0 , which is denoted as [14]

$$N_{av} = \frac{1}{|\mathcal{X}|} \sum_{l=0}^{|\mathcal{X}|-1} \left[\frac{1}{N(l)} \sum_{\mathbf{x}_k \in \mathcal{X}_l} d_{Ham}(\mu(\mathbf{x}_l), \mu(\mathbf{x}_k)) \right], \tag{5-6}$$

where \mathcal{X}_l contains the nearest neighbors of \mathbf{x}_l and $|\mathcal{X}_l| = N(l)$. Hence, N_{av} can be used to determine $I_E^{(\phi)}(I_A^{(\phi)} = 0)$. Note that N_{av} depends on μ and not on E_b/N_0 and the channel.

5-1-1-2 Ideal A Priori Information

In [12], \mathbf{X} is defined as a $L \times N_T$ space-time codeword matrix, where L is the number of time slots for transmitting one space-time codeword. The asymptotic performance of BI-STCM-ID over block Rayleigh fading channels under EFF assumption can be approximated by

$$\log_{10} P_b^1 \simeq -\frac{\tilde{r}N_R d_f}{10} \left[(R\Omega^2)_{dB} + \left(\frac{E_b}{N_0} \right)_{dB} \right] + \text{const}. \quad (5-7)$$

Here, d_f is the minimum Hamming distance of the code, R is the information rate (bits/dim), \tilde{r} is the rank of the matrix $\mathbf{A} = (\mathbf{X} - \tilde{\mathbf{Z}})^H (\mathbf{X} - \tilde{\mathbf{Z}})$ where \mathbf{X} and $\tilde{\mathbf{Z}}$ differ in the k -th bit-position of their corresponding labels and Ω^2 is defined as

$$\Omega^2 = \left[\frac{1}{mN_T \cdot 2^{mN_T} \sum_{k=1}^{mN_T} \sum_{b=0}^1 \sum_{\mathbf{x} \in \mathcal{X}_b^k} \left(\prod_{i=1}^{\tilde{r}} \tilde{\lambda}_i \right)^{-N_R}} \right]^{\frac{1}{\tilde{r}N_R}} \quad (5-8)$$

where $\tilde{\lambda}_i$'s are the nonzero eigenvalues of the \mathbf{A} .

We can take advantage of the above performance analysis in our system configuration by assuming $L=1$, $N_T=N$ and a N -dimensional mapper. Then \mathbf{X} becomes a $1 \times N$ space-time codeword matrix representing a N -dimensional signal \mathbf{x}

$$\mathbf{x} = [s_t^1, s_t^2, \dots, s_t^N], \quad (5-9)$$

and $\tilde{\mathbf{Z}}$ can also be seen as a N -dimensional signal $\tilde{\mathbf{z}}$. It can then be verified that \mathbf{A} is a rank-1 matrix with the eigenvalue $\|\mathbf{x} - \tilde{\mathbf{z}}\|^2$. Therefore, Ω^2 can be rewritten as

$$\Omega^2 = \left[\frac{1}{mN \cdot 2^{mN} \sum_{k=1}^{mN} \sum_{b=0}^1 \sum_{\mathbf{x} \in \mathcal{X}_b^k} \left(\|\mathbf{x} - \tilde{\mathbf{z}}\|^2 \right)^{-N_R}} \right]^{\frac{1}{N_R}}. \quad (5-10)$$

Note that equation (5-10) is just the N_R -th power mean of the squared Euclidean

distances associated with all pairs of N -dimensional signals whose labels differ only in one bit-position. Hence if the minimum squared Euclidean distance between any pairs of multi-dimensional signals which have only one distinct bit on their labels is increased, then Ω^2 is increased, the resulting BER P_b^1 is lower and $I_E^{(\phi)}(I_A^{(\phi)} = 1)$ is higher.

For each N -dimensional signal \mathbf{x}_i , define

$$\omega_i^2 \triangleq \left(\frac{1}{mN} \sum_{k=1}^{mN} (\|\mathbf{x}_i - \tilde{\mathbf{z}}\|^2)^{-N_R} \right)^{-N_R} \quad (5-11)$$

where $\mathbf{x}_i \in \mathcal{X}_b^k$, $\tilde{\mathbf{z}} \in \mathcal{X}_b^k$. Each ω_i^2 is the N_R -th power mean of the squared Euclidean distances between \mathbf{x}_i and other mN signal points whose labels differ in only one bit-position with \mathbf{x}_i . With this definition, we can rewrite Ω^2 as the N_R -th power mean of ω_i^2 's:

$$\Omega^2 = \left[\frac{1}{2^{mN}} \sum_{i=0}^{2^{mN}-1} (\omega_i^2)^{-N_R} \right]^{-N_R}. \quad (5-12)$$

For the same reason as in section 4-1-2-2, the increase of the smallest term maximizes the increase of Ω^2 . The large increase of Ω^2 lowers BER P_b^1 and increases $I_E^{(\phi)}(I_A^{(\phi)} = 1)$ maximally.

5-1-2 Multi-dimensional Mapping over Time Domain

In this section, we employ a multi-dimensional mapper in the conventional BICM-ID whereby the multi-dimensional signals are transmitted in consecutive time slots over a SISO channel. Several criteria governing $I_E^{(\phi)}(I_A^{(\phi)} = 0)$ and $I_E^{(\phi)}(I_A^{(\phi)} = 1)$ when *a priori* information is not available and when *a priori* information is ideally fed back, respectively, will be presented.

5-1-2-1 Without A Priori Information

The derivation of BER P_b^0 is the same as in section 5-1-1-1 and can be expressed as equation (5-5). The most important parameter that determines P_b^0 is the average number of bits that differ between two closest MD signal points, denoted as N_{av} in equation (5-6). N_{av} is used to determine $I_E^{(\phi)}(I_A^{(\phi)} = 0)$.

5-1-2-2 Ideal A Priori Information

The BICM union bound of probability of bit error is expressed in equation (4-6) except MD signal is considered here. Under EFF assumption, the average PEP is presented in the following.

5-1-2-2-1 AWGN Channels

The average PEP $f(d, \mu, \chi)$ derived in [15], [16] can be approximated as

$$f(d, \mu, \chi) \sim \frac{1}{2} [\Delta_c(\mu, \chi)]^d, \quad (5-13)$$

where

$$\Delta_c(\mu, \chi) = \frac{1}{mN \cdot 2^{mN}} \sum_{k=1}^{mN} \sum_{b=0}^1 \sum_{\mathbf{x} \in \mathcal{X}_b^k} \exp\left(-\frac{\|\mathbf{x} - \tilde{\mathbf{z}}\|^2}{4N_0}\right). \quad (5-14)$$

Here, $\tilde{\mathbf{z}}$ differs from \mathbf{x} only in the k -th bit-position of their corresponding labels. It can be seen from equation (5-14) that the average PEP $f(d, \mu, \chi)$ is dominated by the smallest square Euclidean distance, which is denoted as

$$d_{\min} = \min_{\mathbf{x} \in \mathcal{X}_b^k, \forall k, b} \|\mathbf{x} - \tilde{\mathbf{z}}\|^2 \quad (5-15)$$

The number of terms in (5-14) corresponding to d_{\min} can be equivalently expressed, up to a scaling factor, as the average number of nearest neighbors [15]

$$N_{\min} = \frac{1}{2^m} \sum_{i=0}^{2^m-1} N_{\min}(\mathbf{x}_i, d_{\min}) \quad (5-16)$$

where $N_{\min}(\mathbf{x}_i, d_{\min})$ is the number of nearest neighbors of \mathbf{x}_i . Note that both d_{\min} and N_{\min} depend on the mapping and constellation. If a labeling has larger d_{\min} and still can keep N_{\min} small, this labeling can achieve lower BER P_b^1 and higher $I_E^{(\phi)}(I_A^{(\phi)} = 1)$. Note that if setting $N = 1$, equation (5-15) is exactly the same as equation (4-8).

5-1-2-2-2 Rayleigh Fading Channels [16]

When each element of the N -dimensional signal fades independently, the average PEP $f(d, \mu, \chi)$ can be approximated as

$$f(d, \mu, \chi) \sim \frac{1}{2} [\Delta_A(\mu, \chi)]^d, \quad (5-17)$$

where

$$\Delta_A(\mu, \chi) = \frac{1}{mN \cdot 2^{mN}} \sum_{k=1}^{mN} \sum_{b=0}^1 \sum_{\mathbf{x} \in \chi_b^k} \prod_{n=1}^N \left(1 + \frac{\|s_t^n - \tilde{s}_t^n\|^2}{4N_0} \right)^{-1}. \quad (5-18)$$

Here, define $\tilde{\mathbf{z}}$ as

$$\tilde{\mathbf{z}} = [\tilde{s}_t^1, \tilde{s}_t^2, \dots, \tilde{s}_t^N], \quad (5-19)$$

where the labels corresponding to \mathbf{x} and $\tilde{\mathbf{z}}$ differ only in the k -th bit-position. When each element fades simultaneously, the average PEP $f(d, \mu, \chi)$ can be approximated as

$$f(d, \mu, \chi) \sim \frac{1}{2} [4N_0 \cdot \Delta_B(\mu, \chi)]^d \quad (5-20)$$

where

$$\Delta_B(\mu, \chi) = \frac{1}{mN \cdot 2^{mN}} \sum_{k=1}^{mN} \sum_{b=0}^1 \sum_{\mathbf{x} \in \chi_b^k} \|\mathbf{x} - \tilde{\mathbf{z}}\|^{-2}. \quad (5-21)$$

$\Delta_A(\mu, \chi)$ and $\Delta_B(\mu, \chi)$ characterize the influence of μ on the BER performance. Note that $\Delta_B(\mu, \chi)^{-1}$ is the harmonic mean of the squared Euclidean distances associated with all pairs of N -dimensional signals whose labels differ in only one bit-position and it is exactly the same as equation (4-12) if setting $N = 1$.

From equation (5-18) and (5-21), we consider each MD signal in $\Delta_A(\mu, \chi)^{-1}$ and $\Delta_B(\mu, \chi)^{-1}$ in the same way as the one-dimensional case. Then, we can rewrite

$\Delta_A(\mu, \chi)^{-1}$ as

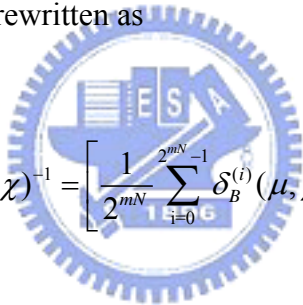
$$\Delta_A(\mu, \chi)^{-1} = \left(\frac{1}{2^{mN}} \sum_{i=0}^{2^{mN}-1} \delta_A^{(i)}(\mu, \chi)^{-1} \right)^{-1}. \quad (5-22)$$

where

$$\delta_A^{(i)}(\mu, \chi) \triangleq \left(\frac{1}{mN} \sum_{k=1}^{mN} \prod_{n=1}^N \left(1 + \frac{\|s_{t,i}^n - \tilde{s}_{t,i}^n\|^2}{4N_0} \right)^{-1} \right)^{-1}. \quad (5-23)$$

Here, $\mathbf{x}_i = [s_{t,i}^1, s_{t,i}^2, \dots, s_{t,i}^N]$ and $\tilde{\mathbf{z}} = [\tilde{s}_{t,i}^1, \tilde{s}_{t,i}^2, \dots, \tilde{s}_{t,i}^N]$ differ in the k -th bit-position in their

label. And $\Delta_B(\mu, \chi)^{-1}$ can be rewritten as



$$\Delta_B(\mu, \chi)^{-1} = \left[\frac{1}{2^{mN}} \sum_{i=0}^{2^{mN}-1} \delta_B^{(i)}(\mu, \chi)^{-1} \right]^{-1}. \quad (5-24)$$

where

$$\delta_B^{(i)}(\mu, \chi) \triangleq \left(\frac{1}{mN} \sum_{k=1}^{mN} \left(\|\mathbf{x}_i - \tilde{\mathbf{z}}\|^2 \right)^{-1} \right)^{-1}. \quad (5-25)$$

Each $\delta_B^{(i)}(\mu, \chi)$ is the harmonic mean of the squared Euclidean distances between \mathbf{x}_i and other mN signal points whose labels differ only in one bit-position with \mathbf{x}_i . The increase of the smallest term of $\delta_A^{(i)}(\mu, \chi)$'s ($\delta_B^{(i)}(\mu, \chi)$'s) maximizes the increase of $\Delta_A(\mu, \chi)^{-1}$ ($\Delta_B(\mu, \chi)^{-1}$), which is evident from section 4-1-2-2, and then the resulting BER P_b^1 is lowered and $I_E^{(\phi)}(I_A^{(\phi)} = 1)$ is enhanced maximally.

5-2 Design Method

The procedure for one-dimensional labeling design is directly extended for MD constellation with design parameters replaced by those introduced in this chapter. We summarize the labeling design parameters in Table 5-1.

Table 5-1 Summary of design criteria.

		$I_A^{(\phi)} = 0$	$I_A^{(\phi)} = 1$	
One-dimensional design Fast Rayleigh fading, AWGN channels		N_{av} (4-5)	Ω^2 (4-12) ω_i^2 (4-13) d_{\min} (4-9)	
Multi-dimensional design	Spatial domain Fast Rayleigh fading channels	N_{av} (5-6)	Ω^2 (5-10) ω_i^2 (5-11) d_{\min} (5-15)	
	Time domain	Fast Rayleigh fading, AWGN channels	N_{av} (5-6)	$\Delta_A(\mu, \chi)^{-1}$ (5-22) $\delta_A^{(i)}(\mu, \chi)$ (5-23) d_{\min} (5-15)
		Block Rayleigh fading, AWGN channels	N_{av} (5-6)	$\Delta_B(\mu, \chi)^{-1}$ (5-24) $\delta_B^{(i)}(\mu, \chi)$ (5-25) d_{\min} (5-15)

5-3 Proposed Labelings

Since multi-dimensional labeling design is more flexible in the larger space, we can find the labelings with better EXIT-chart characteristics than one-dimensional ones. Multi-dimensional mapping over spatial and time domain will be proposed in this section.

5-3-1 Multi-dimensional Mapping over Spatial Domain

N -dimensional signals are generated by taking the N -fold Cartesian product of M -ary one-dimensional constellation and is assumed to be transmitted by N transmit antennas. An equivalent and convenient way to describe the multi-dimensional mapper is shown in Fig. 5-1, where Gray labeling is employed as the constituent one-dimensional mapper as shown in Fig. 5-2 and the block \mathcal{M} is a one-to-one mapping function of the coded bits forming a super-symbol. Therefore, the labeling of multi-dimensional constellation can be conveniently described by \mathcal{M} . The searched Γ 's for multi-dimensional constellation are presented in the same way as in section 4-3.

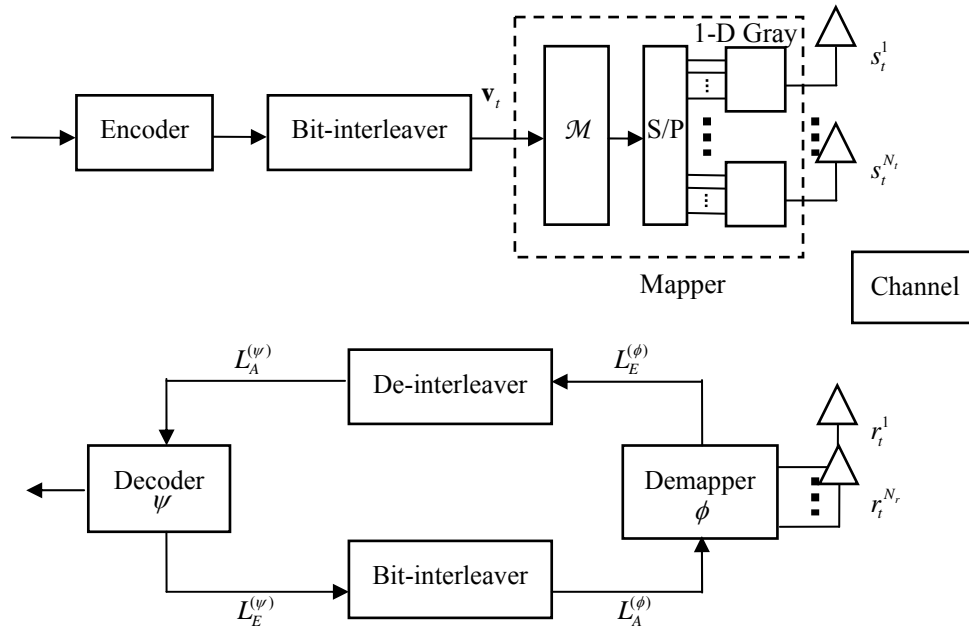


Fig. 5-1 Equivalent and convenient model of the multi-dimensional mapper over spatial domain

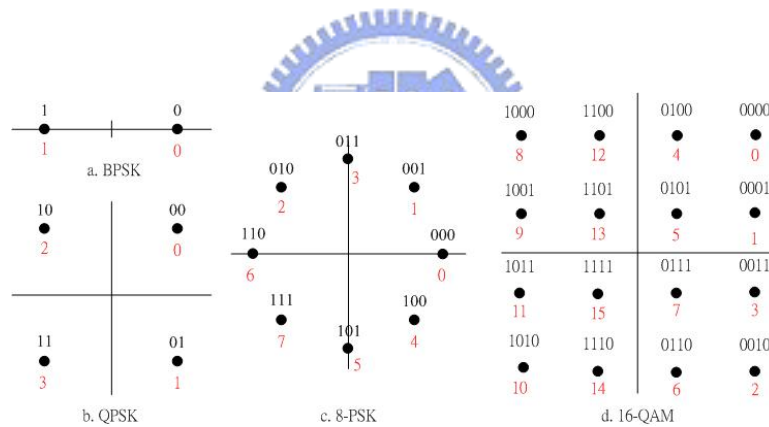


Fig. 5-2 Constituent one-dimensional mappers: (a) BPSK (b) QPSK (c) 8-PSK (d) 16-QAM

5-3-1-1 $N \times \text{BPSK}$

5-3-1-1-1 $2 \times \text{BPSK}$

Table 5-2 Candidate set for $2 \times \text{BPSK}$

\mathcal{M} for $2 \times \text{BPSK}$	$(\mathcal{M}(0), \dots, \mathcal{M}(3))$
Anti-Gray	(1,0,2,3)
Gray	(0,1,2,3)

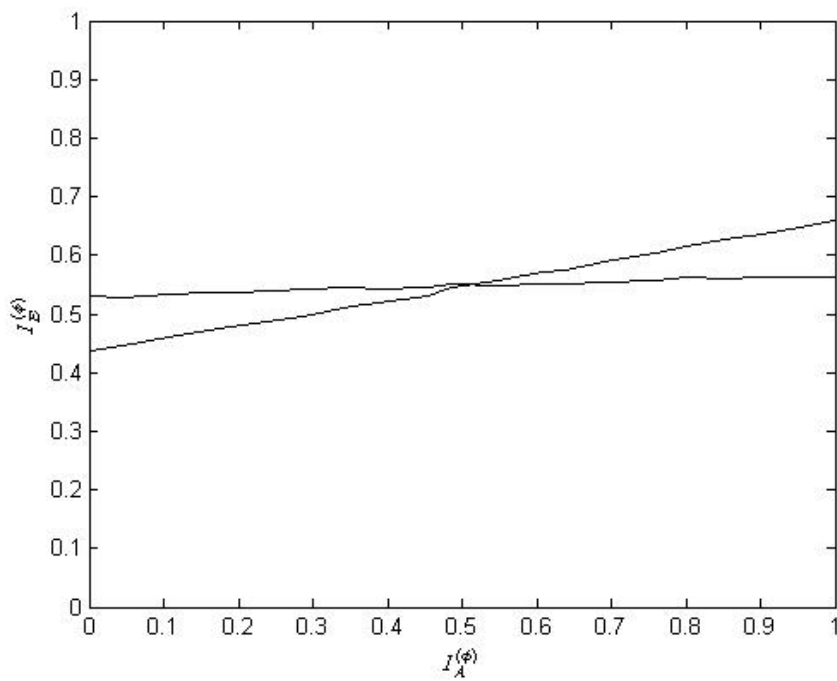


Fig. 5-3 Labelings for $2 \times \text{BPSK}$ in Table 5-2 at $E_b / N_0 = 2\text{dB}$ in 2×2 fast Rayleigh fading channel

5-3-1-1-2 3×BPSK

Table 5-3 Candidate set for 3×BPSK

\mathcal{M} for 3×BPSK	$(\mathcal{M}(0), \mathcal{M}(1), \dots, \mathcal{M}(7))$
3DA2	(3,4,6,1,5,2,0,7)
3DB2	(3,6,4,1,5,2,0,7)
3DC2	(1,6,4,3,5,2,0,7)
3DD2	(1,6,2,3,4,5,0,7)
3DE2	(1,0,2,3,4,5,6,7)
Gray	(0,1,2,3,4,5,6,7)

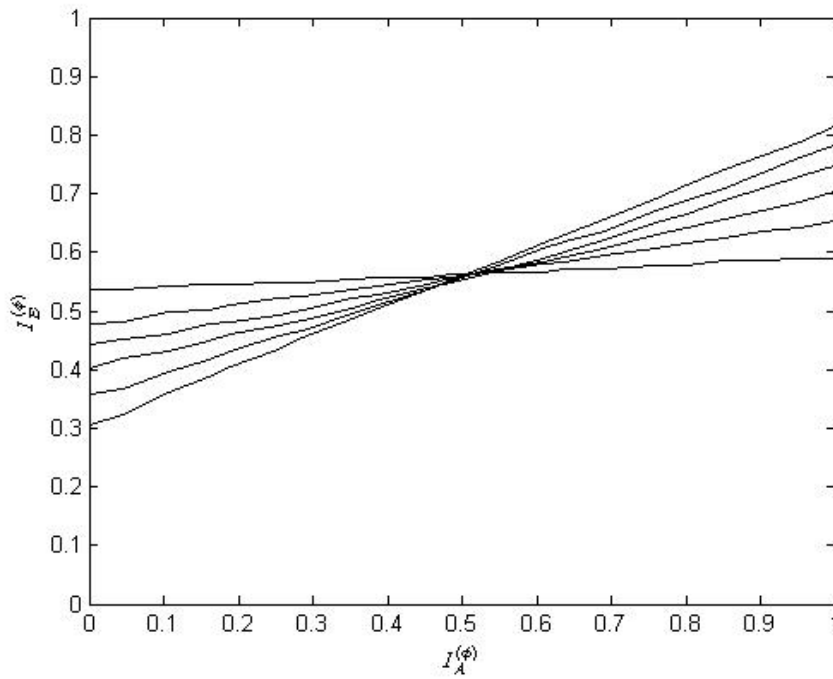


Fig. 5-4 Labelings for 3×BPSK in Table 5-3 at $E_b / N_0 = 2\text{dB}$ in 3×3 fast Rayleigh fading channel

5-3-1-1-3 4×BPSK

Table 5-4 Candidate set for 4xBPSK

\mathcal{M} for 4×BPSK	$(\mathcal{M}(0), \mathcal{M}(1), \dots, \mathcal{M}(15))$
4DA2	(15,4,0,11,2,9,13,6,8,3,7,12,5,14,10,1)
4DB2	(1,15,14,9,12,0,3,13,6,8,11,7,2,5,4,10)
4DC2	(0,15,14,9,12,1,3,13,4,8,10,7,2,5,6,11)
4DD2	(2,13,6,9,12,1,8,15,4,3,10,7,0,5,14,11)
4DE2	(8,13,6,15,12,1,2,3,4,9,10,7,0,5,14,11)
4DF2	(1,4,2,3,0,5,7,6,8,9,11,10,12,13,14,15)
4DG2	(1,0,2,3,4,5,7,6,9,8,11,10,12,13,14,15)
4DH2	(1,0,2,3,4,5,7,6,8,9,10,11,12,13,14,15)
4DI2	(1,0,2,3,4,5,6,7,8,9,10,11,12,13,14,15)
Gray	(0,1,2,3,4,5,6,7,8,9,10,11,12,13,14,15)

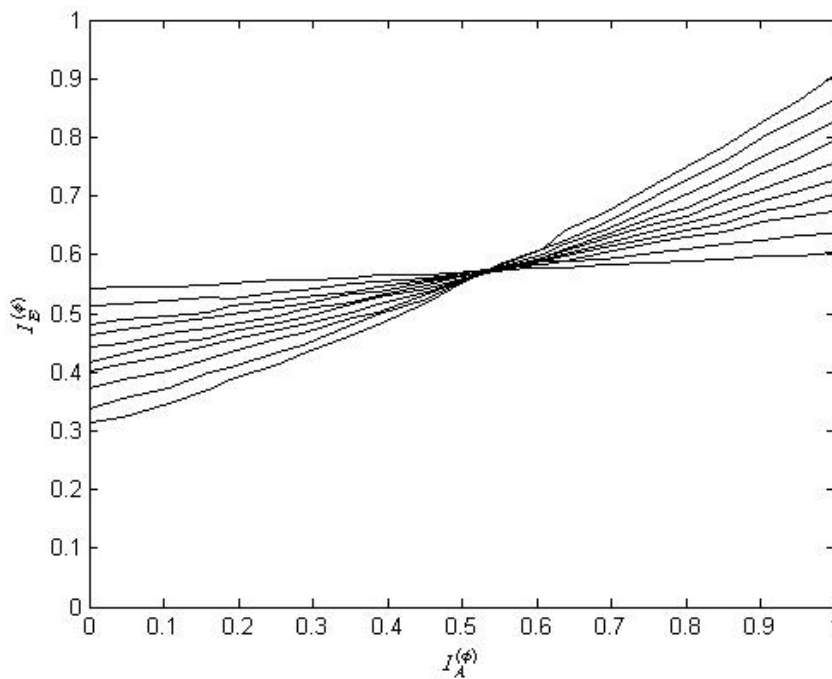


Fig. 5-5 Labelings for 4xBPSK in Table 5-4 at $E_b / N_0 = 2\text{dB}$ in 4x4 fast Rayleigh fading channel

5-3-1-2 $N \times \text{QPSK}$

5-3-1-2-1 $2 \times \text{QPSK}$

Table 5-5 Candidate set for $2 \times \text{QPSK}$

\mathcal{M} for $2 \times \text{QPSK}$	$(\mathcal{M}(0), \mathcal{M}(1), \dots, \mathcal{M}(15))$
2DA4	(15,4,0,9,2,11,13,6,8,3,7,12,5,14,10,1)
2DB4	(13,4,0,9,2,1,15,6,8,3,7,12,5,14,10,11)
2DC4	(6,5,1,12,11,4,14,3,9,8,2,13,10,7,15,0)
2DD4	(2,3,1,0,11,4,14,5,9,8,10,13,6,7,15,12)
2DE4	(8,13,6,9,12,1,2,3,4,15,10,7,0,5,14,11)
2DF4	(1,4,2,3,0,5,7,6,8,9,11,10,12,13,14,15)
2DG4	(1,0,2,3,4,5,7,6,9,8,11,10,12,13,14,15)
2DH4	(1,0,2,3,4,5,7,6,8,9,10,11,12,13,14,15)
2DI4	(1,0,2,3,4,5,6,7,8,9,10,11,12,13,14,15)
Gray	(0,1,2,3,4,5,6,7,8,9,10,11,12,13,14,15)

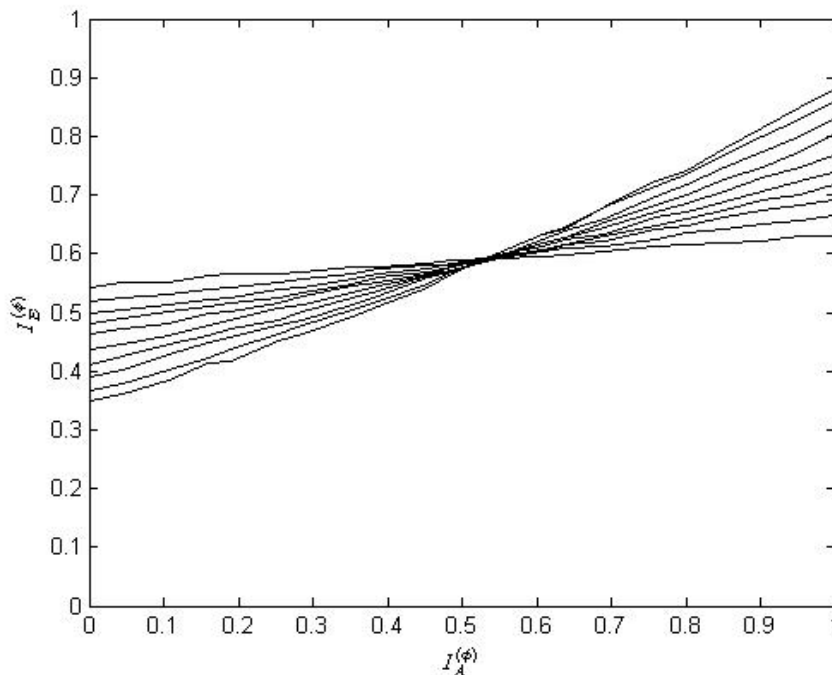


Fig. 5-6 Labelings for $2 \times \text{QPSK}$ in Table 5-5 at $E_b / N_0 = 3\text{dB}$ in 2×2 fast Rayleigh fading channel

5-3-1-2-2 3×QPSK

Table 5-6 Candidate set for 3xQPSK

\mathcal{M} for 3×QPSK	$(\mathcal{M}(0), \mathcal{M}(1), \dots, \mathcal{M}(63))$
3DA4	(45,10,0,35,6,37,47,28,2,33,43,8,41,30,4,39,16,51,59,24,63,14,20,55,57,26,18,49,22,53,61,12,42,1,15,40,13,46,36,7,9,58,32,3,38,5,11,44,27,56,48,19,52,23,31,60,34,17,25,50,29,62,54,21)
3DB4	(51,44,14,17,12,19,49,46,36,59,25,6,27,4,38,57,28,3,33,62,35,60,30,1,11,20,54,41,52,43,9,22,10,21,55,40,53,42,8,23,29,2,32,63,34,61,31,0,37,58,24,7,26,5,39,56,50,45,15,16,13,18,48,47)
3DC4	(4,17,19,6,21,8,10,23,9,12,14,11,0,29,31,2,1,20,22,3,24,7,5,26,28,25,27,30,13,16,18,15,49,36,38,51,40,53,55,42,44,41,43,46,61,32,34,63,52,33,35,58,37,56,54,39,57,48,62,59,60,45,47,50)
3DD4	(3,48,50,1,36,5,7,38,40,9,11,42,15,60,46,13,32,17,19,34,21,52,54,23,25,56,58,27,44,29,31,62,0,35,33,2,37,4,6,39,41,8,10,43,28,47,45,30,49,16,18,51,20,53,55,22,24,57,59,26,63,12,14,61)
3DE4	(1,4,2,3,0,5,15,6,8,17,11,10,13,12,14,7,16,25,27,18,29,20,22,31,9,24,26,19,28,21,23,30,36,33,35,38,37,32,34,39,49,40,46,43,44,45,47,42,57,48,50,59,52,61,63,54,56,41,51,58,53,60,62,55)
3DF4	(1,0,2,3,4,5,15,14,8,9,11,10,13,12,6,7,16,17,19,26,21,20,30,23,29,24,18,27,28,25,31,22,32,33,43,42,45,44,46,47,41,40,34,35,36,37,38,39,49,56,58,51,60,53,54,55,48,57,50,59,61,52,62,63)
3DG4	(3,2,0,1,4,5,7,6,8,9,11,10,13,12,14,15,16,19,17,18,21,20,22,23,25,24,26,27,28,29,31,30,32,35,33,34,37,36,38,39,41,40,42,43,45,44,47,46,48,51,50,49,52,53,54,55,56,57,58,59,61,60,62,63)
3DH4	(1,0,2,3,4,5,7,6,8,9,11,10,13,12,14,15,16,17,19,18,21,20,22,23,25,24,26,27,28,29,30,31,32,33,35,34,37,36,38,39,41,40,42,43,44,45,46,47,48,49,51,50,53,52,54,55,56,57,58,59,60,61,62,63)
3DI4	(1,0,2,3,4,5,7,6,8,9,11,10,13,12,14,15,16,17,19,18,21,20,22,23,25,24,26,27,28,29,30,31,32,33,34,35,36,37,38,39,40,41,42,43,44,45,46,47,48,49,50,51,52,53,54,55,56,57,58,59,60,61,62,63)
3DJ4	(1,0,2,3,4,5,7,6,8,9,11,10,13,12,14,15,16,17,18,19,20,21,22,23,24,25,26,27,28,29,30,31,32,33,34,35,36,37,38,39,40,41,42,43,44,45,46,47,48,49,50,51,52,53,54,55,56,57,58,59,60,61,62,63)
Gray	(0,1,2,3,4,5,6,7,8,9,10,11,12,13,14,15,16,17,18,19,20,21,22,23,24,25,26,27,28,29,30,31,32,33,34,35,36,37,38,39,40,41,42,43,44,45,46,47,48,49,50,51,52,53,54,55,56,57,58,59,60,61,62,63)

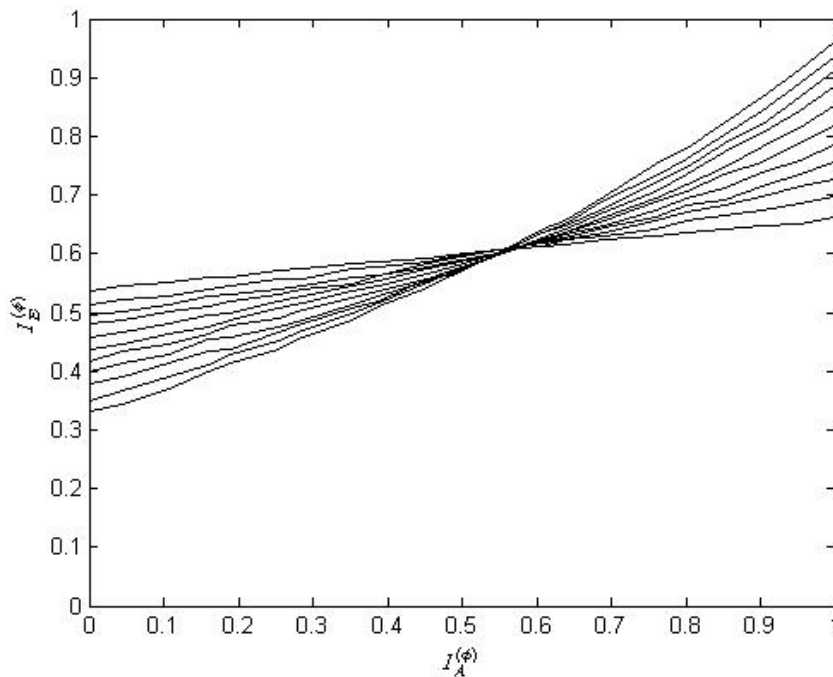


Fig. 5-7 Labelings for 3xQPSK in Table 5-6 at $E_b / N_0 = 3\text{dB}$ in 3x3 fast Rayleigh fading channel

5-3-1-3 $N \times 8$ -PSK

5-3-1-3-1 2×8 -PSK

Table 5-7 Candidate set for 2×8 -PSK

\mathcal{M} for 2×8 -PSK	$(\mathcal{M}(0), \mathcal{M}(1), \dots, \mathcal{M}(63))$
2DA8	(34,20,22,33,16,39,36,18,44,26,24,47,30,41,42,28,21,35,32,23,38,17,19,37,27,45,46,25,40,31,13,58,53,3,0,54,6,48,51,5,10,61,62,8,56,14,29,43,2,52,55,1,49,7,4,50,60,11,9,63,15,57,59,12)
2DB8	(48,33,2,19,4,61,22,7,8,56,58,10,60,13,15,63,1,16,18,3,20,5,6,23,40,9,14,47,12,45,42,11,0,51,50,35,52,37,34,55,41,25,26,59,28,53,62,27,49,32,38,17,36,21,54,39,24,57,43,31,44,29,30,46)
2DC8	(6,7,4,1,0,3,2,5,12,11,14,15,10,13,8,9,16,19,30,17,22,21,20,23,18,29,28,25,24,27,26,31,32,51,38,39,34,53,36,55,58,47,56,57,60,59,46,45,50,33,48,49,52,35,54,37,40,41,62,63,42,61,44,43)
2DD8	(0,37,34,35,6,1,2,7,44,9,10,43,8,45,46,15,52,53,22,19,48,49,54,55,28,61,26,27,56,29,62,63,36,33,4,5,32,39,38,3,12,41,42,11,40,13,14,47,20,17,18,23,16,21,50,51,60,25,30,59,24,57,58,31)
2DE8	(32,37,6,33,2,3,34,7,40,41,14,11,12,45,10,15,16,17,22,23,20,21,18,19,24,25,62,31,28,29,30,27,36,1,0,39,4,5,38,35,8,9,46,43,44,13,42,47,48,49,54,51,52,53,50,55,56,57,58,63,60,61,26,59)
2DF8	(0,1,38,35,36,5,34,39,40,9,14,11,12,13,10,15,16,17,22,19,20,21,18,23,24,25,26,31,28,29,30,27,32,33,6,3,4,37,2,7,8,41,46,43,44,45,42,47,48,49,50,55,52,53,54,51,56,57,62,59,60,61,58,63)
2DG8	(0,3,2,1,4,5,6,7,24,27,26,11,28,13,14,15,16,19,18,17,20,53,54,55,8,25,10,9,12,29,30,31,32,35,34,33,36,37,38,39,40,43,42,41,44,45,46,47,48,49,50,51,52,21,22,23,56,59,58,57,60,61,62,63)
2DH8	(0,3,2,1,32,37,6,7,12,9,10,11,8,13,14,15,16,17,18,19,20,21,22,23,24,25,26,27,28,29,30,31,4,33,34,35,36,5,38,39,40,41,42,43,44,45,46,47,48,49,50,51,52,53,54,55,56,57,58,59,60,61,62,63)
Gray	(0,1,2,3,4,5,6,7,8,9,10,11,12,13,14,15,16,17,18,19,20,21,22,23,24,25,26,27,28,29,30,31,32,33,34,35,36,37,38,39,40,41,42,43,44,45,46,47,48,49,50,51,52,53,54,55,56,57,58,59,60,61,62,63)

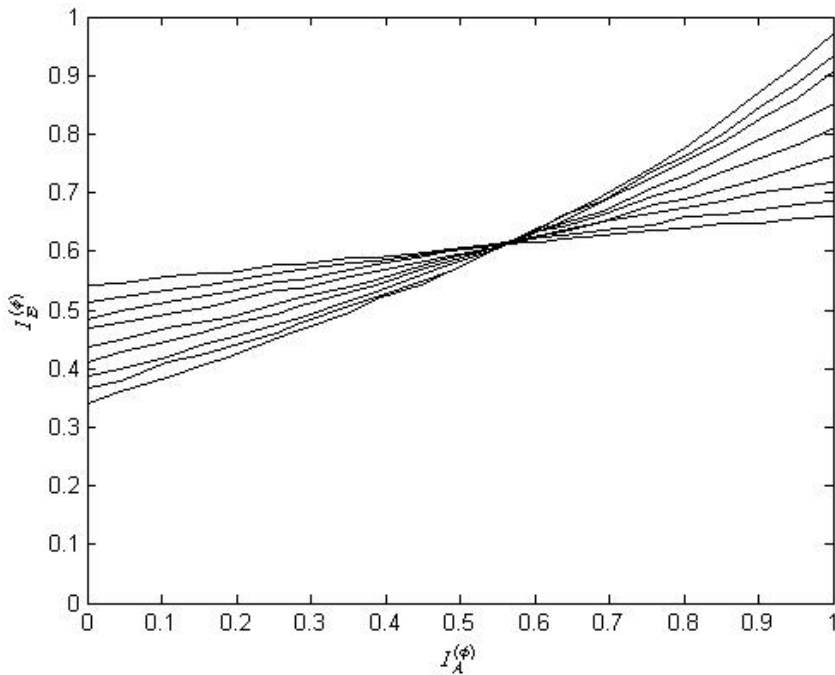


Fig. 5-8 Labelings for 2×8 -PSK in Table 5-7 at $E_b / N_0 = 5$ dB in 2×2 fast Rayleigh fading channel

5-3-1-4 $N \times 16$ -QAM

5-3-1-4-1 2×16 -QAM

Table 5-8 Candidate set for 2×16 -QAM

\mathcal{M} for 2×16 -QAM	$(\mathcal{M}(0), \mathcal{M}(1), \dots, \mathcal{M}(255))$
2DA16	(148,19,18,147,228,197,74,101,86,217,251,25,156,23,28,159,48,193,134,113,196,53,119,151,124,26,27,130,30,221,158,31,32,209,182,98,87,37,102,215,187,57,88,155,60,214,223,29,212,49,17,146,52,213,150,21,59,170,186,24,220,61,63,190,96,47,250,114,22,100,247,7,72,104,46,203,108,77,10,111,1,97,112,3,116,5,2,117,58,9,82,234,204,171,62,207,208,33,115,183,36,85,6,35,42,73,219,106,76,45,110,14,40,211,66,99,192,175,103,56,8,41,120,210,44,13,191,127,224,131,16,50,132,55,23,1,177,136,237,232,138,236,157,78,239,0,245,178,135,244,133,198,166,91,137,142,249,141,169,168,143,144,229,118,145,160,149,20,230,92,153,154,89,152,93,23,8,38,165,129,90,167,128,161,162,34,185,123,226,139,94,174,216,95,68,181,243,195,164,69,202,54,172,201,75,235,140,109,254,79,240,65,194,241,4,253,179,199,200,233,248,15,252,205,206,255,173,80,218,51,84,39,246,71,176,105,43,242,222,189,188,107,64,225,227,67,180,81,70,163,122,83,11,121,12,125,126,184)
2DB16	(64,129,147,2,44,65,6,98,45,8,26,171,12,108,47,14,145,80,66,23,84,21,151,82,156,61,63,10,59,30,94,29,33,5,106,35,69,100,39,7,9,41,169,42,37,13,107,34,208,49,179,126,36,144,148,183,57,24,58,31,28,53,11,43,97,4,70,99,68,101,103,131,72,109,111,74,237,76,78,123,48,88,243,181,112,22,247,25,81,90,127,52,125,92,86,73,32,163,110,96,120,71,231,121,248,38,91,60,117,75,40,113,242,122,87,124,85,119,50,62,89,95,46,93,56,54,223,133,119,210,202,197,173,130,200,137,235,206,141,172,138,176,16,152,19,146,149,210,154,3,153,17,27,187,188,205,191,222,192,165,161,234,135,128,132,167,105,168,174,139,77,143,189,15,177,162,250,51,2,12,181,55,186,136,217,155,170,157,236,176,159,0,193,102,198,229,134,199,164,233,216,202,251,204,207,239,142,21,201,150,83,116,213,180,214,220,201,185,158,209,184,218,255,225,166,195,227,196,228,160,67,140,203,249,238,224,104,118,253,182,244,115,178,241,246,254,245,240,232,190,219,252,221,79,114)
2DC16	(0,17,18,147,20,129,70,39,26,15,158,25,46,173,28,10,48,1,134,55,4,21,54,5,40,89,27,11,30,13,143,31,32,145,182,51,22,33,102,151,104,57,59,155,60,159,190,29,5,64,98,83,52,100,150,103,88,170,186,24,220,61,63,174,130,65,80,115,68,245,222,7,72,108,250,74,124,77,78,111,64,113,90,3,112,197,2,119,58,92,91,12,117,62,75,208,37,114,183,36,85,47,35,42,73,219,106,76,45,110,223,116,81,66,99,97,53,226,87,8,41,122,217,44,221,86,127,164,131,16,19,132,165,38,17,136,233,232,138,92,157,14,239,128,177,146,135,176,133,198,23,248,137,142,187,141,237,94,207,144,229,231,211,160,149,148,246,172,153,154,234,152,93,238,191,228,209,50,16,7,96,161,162,34,171,121,166,139,168,175,216,230,84,241,243,195,180,69,6,247,236,201,202,235,140,109,254,79,240,193,194,179,196,253,118,199,200,249,251,2,03,252,205,206,255,224,181,218,227,156,101,242,215,184,105,43,185,212,189,188,107,192,225,178,67,244,213,214,163,199,210,123,204,125,126,95)
2DD16	(64,33,2,67,36,69,78,23,40,65,74,90,76,45,10,207,17,89,130,19,84,37,22,71,88,57,26,83,60,93,158,30,32,105,106,35,68,39,38,111,104,41,42,99,12,109,102,47,232,48,18,123,52,127,126,55,24,121,122,59,116,63,46,119,1,73,194,3,196,5,6,79,72,9,11,75,44,77,206,14,80,49,50,91,20,85,70,21,56,81,86,27,156,61,62,87,248,0,34,1,07,4,101,110,7,8,97,98,43,108,13,15,103,16,249,234,51,236,53,54,255,112,25,58,115,28,117,118,29,129,201,66,147,197,145,191,199,200,144,79,138,188,205,142,222,153,148,146,131,180,221,134,95,168,137,155,203,92,176,94,159,184,161,178,171,181,173,174,151,128,169,186,163,124,177,183,231,164,185,187,162,132,14,9,150,167,136,160,82,154,172,125,166,223,192,213,242,195,100,189,198,254,193,229,202,211,204,209,190,143,212,217,219,10,157,228,246,135,216,208,11,4,21,8,244,141,220,31,225,233,170,227,252,133,182,175,96,241,243,235,245,237,230,215,152,165,226,251,224,253,238,214,120,113,250,139,140,210,247,239)
2DE16	(13,1,67,27,112,69,78,3,28,5,10,75,4,8,66,71,17,29,26,19,20,0,18,31,12,25,86,59,24,21,30,91,48,165,110,35,36,97,32,167,44,105,34,43,104,173,46,33,52,49,118,18,116,183,62,51,120,60,58,187,190,121,50,189,65,77,74,6,80,8,0,2,15,76,9,70,7,72,79,14,73,116,64,22,247,81,93,94,83,56,216,90,192,89,82,23,228,99,98,111,96,237,238,59,40,229,42,11,109,41,38,239,246,245,122,115,84,113,114,255,124,57,54,251,88,191,254,231,193,151,134,130,132,208,194,135,136,137,138,139,140,14,1,142,143,150,144,146,149,209,133,148,211,152,159,154,155,156,157,156,63,164,176,162,107,240,37,166,163,169,172,170,171,45,185,174,47,160,53,180,179,182,241,178,55,61,153,188,123,184,168,186,175,100,128,195,215,129,197,198,131,200,201,202,203,204,205,206,95,192,213,214,147,212,145,210,221,252,217,218,87,220,85,222,207,161,236,106,235,196,225,102,199,108,233,226,103,232,101,234,227,244,177,242,119,224,253,126,243,248,117,250,223,125,249,230,127)
2DF16	(32,49,18,2,20,5,7,21,8,9,74,59,12,29,62,15,16,13,17,0,19,22,6,24,25,58,43,28,159,14,31,48,33,98,55,4,53,54,35,44,57,122,11,61,13,10,63,36,51,178,39,52,37,38,2,3,56,41,46,27,45,60,30,47,80,65,66,81,68,117,84,70,88,91,90,75,94,77,78,127,64,113,242,103,86,101,67,85,72,73,42,89,76,95,92,11,96,12,50,99,116,69,226,119,104,105,106,123,108,125,126,79,82,97,102,115,100,87,118,71,120,121,26,107,124,109,110,93,144,137,166,147,132,149,148,135,136,145,189,168,141,143,255,128,153,146,131,150,165,134,151,172,129,138,155,158,157,156,142,224,185,34,167,180,133,162,191,40,152,174,187,169,190,171,176,161,130,179,228,181,1,82,163,248,177,154,239,188,173,170,189,192,209,208,203,214,197,198,213,232,193,202,219,140,223,254,207,210,201,194,211,164,215,246,199,200,217,218,195,222,205,206,221,240,225,230,243,196,245,212,227,216,249,250,175,244,233,234,247,160,241,114,231,252,229,83,188,236,237,238,251,204,253,220,235)
2DG16	(4,1,130,67,0,81,70,135,72,89,74,15,88,11,107,79,116,13,86,19,12,133,22,83,40,9,26,95,20,93,126,27,48,113,98,35,100,37,34,119,120,41,42,75,44,125,110,47,96,49,50,114,52,101,118,39,8,121,90,59,108,45,58,127,80,5,66,3,92,64,6,71,68,73,14,107,28,69,78,31,84,17,18,91,21,77,214,23,24,85,94,25,76,29,30,87,116,33,38,99,36,117,102,55,56,105,106,43,124,61,46,111,32,97,115,51,244,53,54,103,104,57,62,123,60,109,122,63,193,141,194,131,134,65,150,195,137,140,138,139,152,153,142,143,148,129,146,215,192,157,246,151,136,213,154,155,156,132,158,159,228,161,178,227,167,229,165,166,184,249,170,171,172,173,174,175,176,177,178,179,180,181,182,149,183,247,232,169,186,187,168,237,190,191,201,209,2,199,144,197,198,7,200,217,202,203,216,196,206,207,208,205,82,147,210,145,128,211,220,204,218,219,212,221,222,223,180,241,243,162,240,176,182,231,248,185,234,235,172,253,238,239,160,177,179,226,164,245,230,181,188,233,250,251,252,189,254,255)
2DH16	(0,65,66,3,70,56,199,72,9,138,107,12,205,78,143,112,17,18,83,20,85,86,23,8,89,218,155,92,29,158,87,104,33,34,67,36,109,102,39,40,105,106,43,110,37,46,111,1,6,121,118,51,124,53,54,127,120,57,58,123,52,117,126,63,64,12,99,4,69,68,71,24,73,74,11,76,141,14,79,48,81,82,19,84,21,22,29,88,25,154,91,28,93,22,159,32,97,98,35,108,45,38,103,96,41,42,75,44,101,100,47,80,49,50,115,60,125,114,55,56,113,122,59,116,61,62,119,192,129,194,195,132,172,197,198,7,174,175,240,181,178,179,172,142,207,148,177,210,147,212,145,150,215,216,153,26,219,152,221,94,31,160,161,162,163,164,165,166,167,168,169,170,171,172,173,174,175,176,177,178,179,180,181,6,213,182,183,184,185,186,187,252,189,190,191,128,193,130,131,196,133,134,135,200,137,10,203,136,77,206,15,208,149,146,211,244,209,214,151,156,217,90,27,220,157,30,223,224,225,226,227,228,229,230,231,232,233,234,235,236,237,238,239,180,241,242,243,144,245,246,247,248,249,250,251,188,253,254,255)
2DI16	(16,1,66,27,4,21,22,7,8,25,26,11,30,13,14,31,32,17,18,3,20,37,70,23,24,9,74,19,12,29,28,95,0,49,50,35,52,5,38,55,56,41,42,59,44,61,62,47,48,33,98,51,36,53,54,39,104,57,58,43,60,45,46,63,64,65,82,67,68,69,67,72,73,10,75,76,77,79,15,80,81,2,83,84,85,86,87,88,89,90,91,92,93,78,79,112,97,34,115,100,125,118,103,40,121,1,22,107,124,109,110,119,96,113,114,99,116,101,102,127,120,105,106,123,108,117,126,111,128,129,130,131,132,133,134,135,136,137,138,139,140,141,142,143,14,4,145,146,147,148,149,150,151,152,153,154,155,156,157,158,159,176,161,162,167,168,161,180,167,168,177,186,171,190,173,174,191,160,185,178,163,182,165,166,183,184,189,170,179,172,189,188,175,192,193,194,195,196,197,198,199,200,201,202,203,204,205,206,207,208,209,210,211,212,213,214,215,216,217,218,219,220,221,222,223,224,249,242,227,244,229,230,255,248,233,234,243,236,245,254,239,240,225,226,251,228,253,246,231,232,241,250,235,252,237,238,247)
2DJ16	(2,1,3,0,5,4,6,7,9,72,10,11,12,13,15,14,17,16,18,19,22,21,23,20,24,25,27,26,29,28,30,31,33,96,34,35,36,37,39,38,40,41,42,43,44,45,46,47,48,49,50,51,52,53,54,55,56,57,58,59,60,61,62,63,64,65,66,67,68,69,70,71,8,73,74,75,76,77,78,79,80,81,82,83,84,85,86,87,88,89,90,91,92,93,94,95,96,101,98,99,100,97,102,103,104,105,10,6,107,108,109,110,111,116,113,114,119,112,117,118,115,120,121,122,123,124,125,126,127,128,129,130,131,132,133,134,135,136,137,138,139,140,141,142,143,14,44,145,146,147,148,149,150,151,152,153,154,155,156,157,158,159,160,161,162,163,164,165,166,167,168,169,170,171,172,173,174,175,176,177,178,179,180,181,182,183,184,185,186,187,188,189,190,191,192,193,194,195,196,197,198,199,200,201,202,203,204,205,206,207,212,209,214,215,208,213,210,211,216,217,218,219,220,221,222,223,224,225,226,227,228,229,230,231,232,233,234,235,236,237,238,239,240,241,242,243,244,245,246,247,248,249,250,251,252,253,254,255)
2DK16	(0,5,2,3,4,1,6,7,8,9,10,11,12,13,14,15,20,17,22,23,16,21,18,19,24,25,26,27,28,29,30,31,32,33,34,39,36,37,38,35,40,41,42,43,44,45,46,47,48,53,54,51,52,49,50,55,5,6,57,58,59,60,61,62,63,64,65,66,67,68,69,70,71,8,73,74,75,76,77,78,79,80,81,82,83,84,85,86,87,88,89,90,91,92,93,94,95,96,101,98,99,100,97,102,103,104,105,10,6,107,108,109,110,111,116,113,114,119,112,117,118,115,120,121,122,123,124,125,126,127,128,129,130,131,132,133,134,135,136,137,138,139,140,141,142,143,14,44,145,146,147,148,149,150,151,152,153,154,155,156,157,158,159,160,161,162,163,164,165,166,167,168,169,170,171,172,173,174,175,176,177,178,179,180,181,182,183,184,185,186,187,188,189,190,191,192,193,194,195,196,197,198,199,200,201,202,203,204,205,206,207,212,209,214,215,208,213,210,211,216,217,218,219,220,221,222,223,224,225,226,227,228,229,230,231,232,233,234,235,236,237,238,239,240,241,242,243,244,245,246,247,248,249,250,251,252,253,254,255)
Gray	(0,1,2,3,4,5,6,7,8,9,10,11,12,13,14,15,16,17,18,19,20,21,22,23,24,25,26,27,28,29,30,31,32,33,34,35,36,37,38,39,40,41,42,43,44,45,46,47,48,49,50,51,52,53,54,55,5,57,58,59,60,61,62,63,64,65,66,67,68,69,70,71,72,73,74,75,76,77,78,79,80,81,82,83,84,85,86,87,88,89,90,91,92,93,94,95,96,97,98,99,100,101,102,103,104,105,10,6,107,108,109,110,111,112,113,114,115,116,117,118,119,120,121,122,123,124,125,126,127,128,129,130,131,132,133,134,135,136,137,138,139,140,141,142,143,14,44,145,146,147,148,149,150,151,152,153,154,155,156,157,158,159,160,161,162,163,164,165,166,167,168,169,170,171,172,173,174,175,176,177,178,179,180,181,182,183,184,185,186,187,188,189,190,191,192,193,194,195,196,197,198,199,200,201,202,203,204,205,206,207,208,209,210,211,212,213,214,215,216,217,218,219,220,221,222,223,224,225,226,227,228,229,230,231,232,233,234,235,236,237,238,239,240,241,242,243,244,245,246,247,248,249,250,251,252,253,254,255)

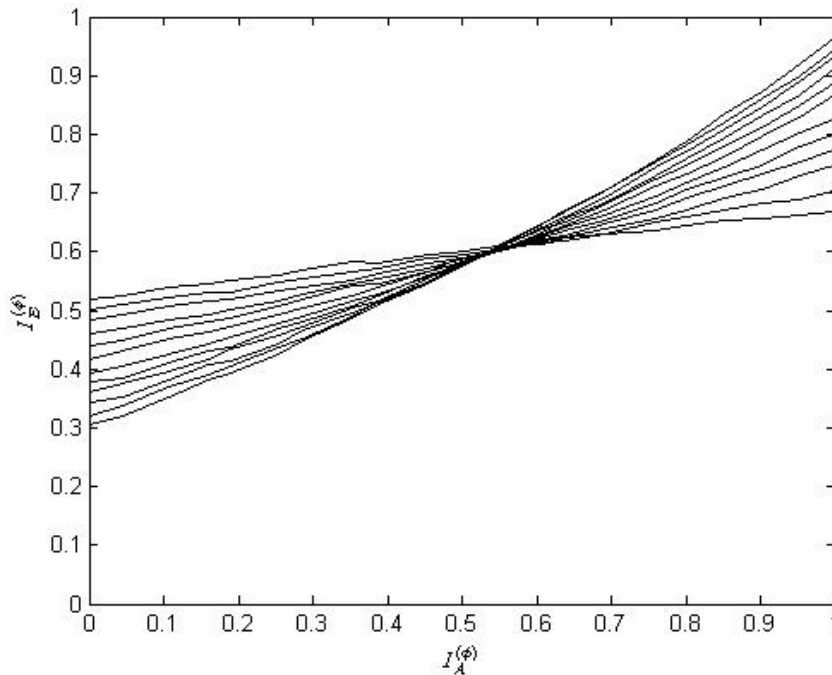


Fig. 5-9 Labelings for 2x16-QAM in Table 5-8 at $E_b / N_0 = 6\text{dB}$ in 2x2 fast Rayleigh fading channel



5-3-2 Multi-dimensional Mapping over Time Domain

N -dimensional signals are generated by taking the N -fold Cartesian product of one-dimensional constellation and transmitted over N consecutive time slots. An equivalent and convenient way to describe the multi-dimensional mapper is shown in Fig. 5-10, where Gray labeling is employed as the constituent two-dimensional mapper as shown in Fig. 5-2 and the block \mathcal{M} is a one-to-one mapping function of the coded bits forming a super-symbol. Therefore, the labeling of multi-dimensional constellation can be conveniently described by \mathcal{M} . In this section, we will present the case when N one-dimensional symbols of a N -dimensional signal fade simultaneously.

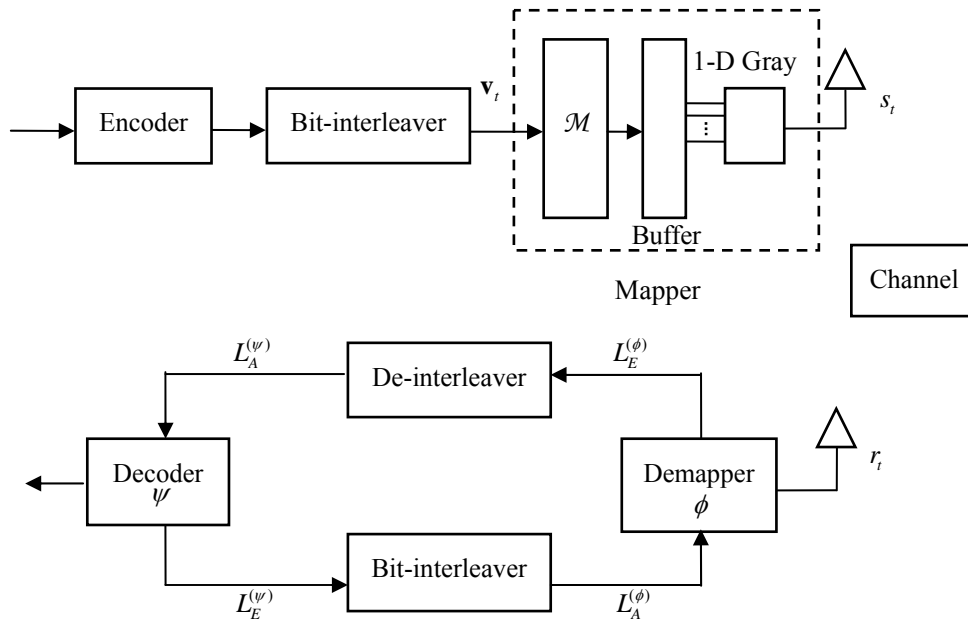


Fig. 5-10 Equivalent and convenient model of the multi-dimensional mapper over time domain

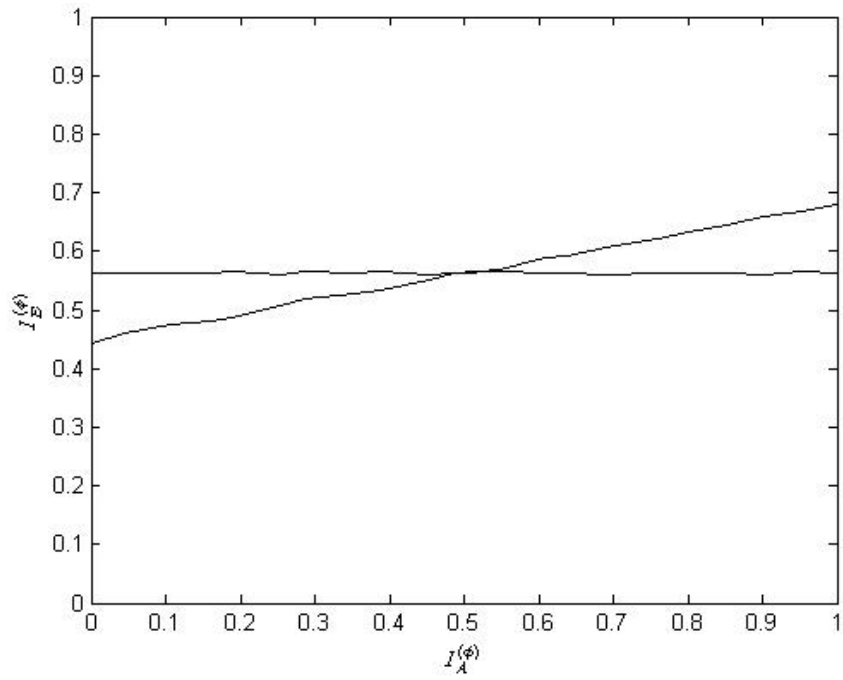
5-3-2-1 $N \times \text{BPSK}$



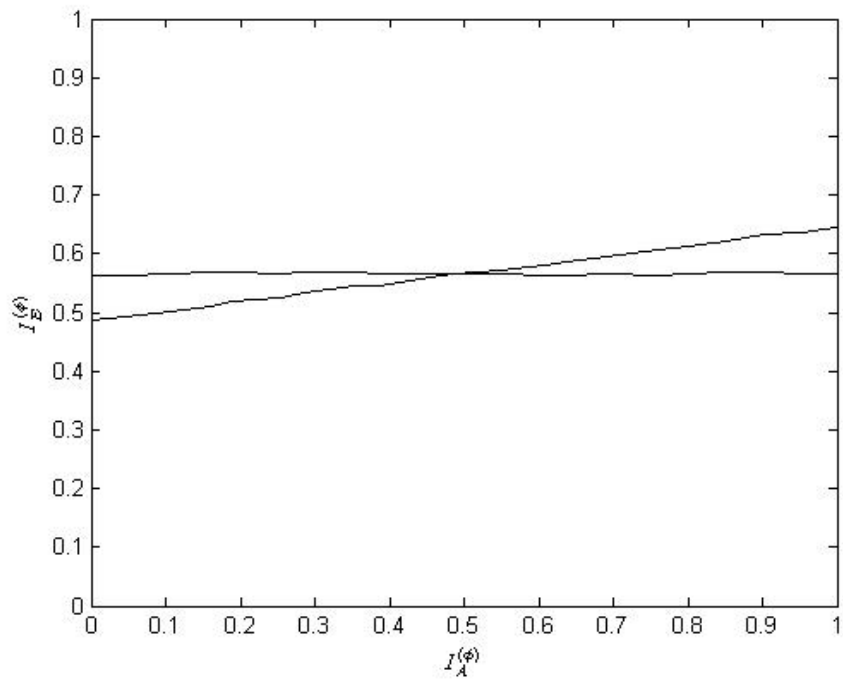
5-3-2-1-1 $2 \times \text{BPSK}$

Table 5-9 Candidate set for $2 \times \text{BPSK}$

\mathcal{M} for $2 \times \text{BPSK}$	$(\mathcal{M}(0), \dots, \mathcal{M}(3))$
Anti-Gray	(1,0,2,3)
Gray	(0,1,2,3)



(a)



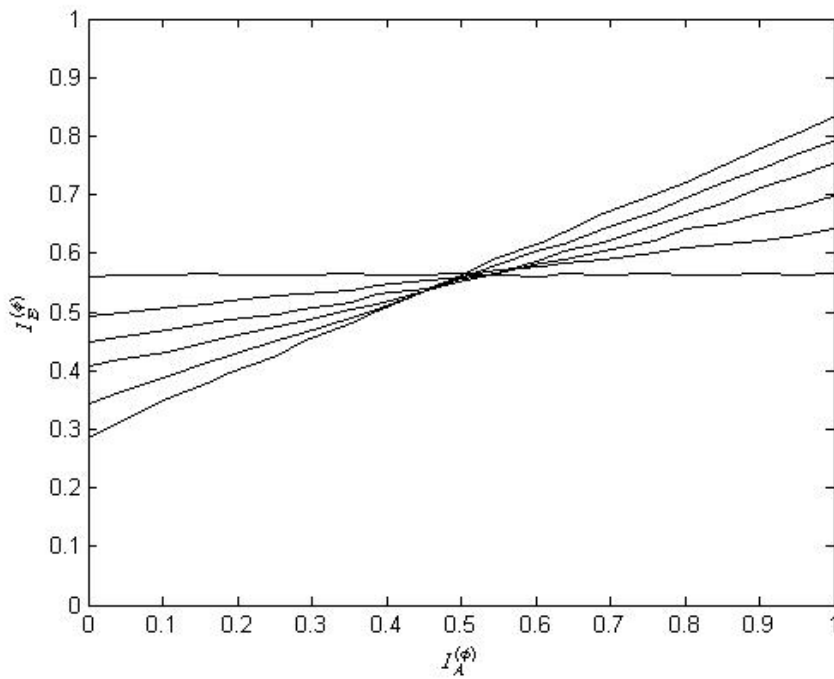
(b)

Fig. 5-11 Labelings for 2x2BPSK in Table 5-9 at (a) at $E_b / N_0 = 1\text{dB}$ in AWGN channel and (b) $E_b / N_0 = 3\text{dB}$ in block Rayleigh fading channel

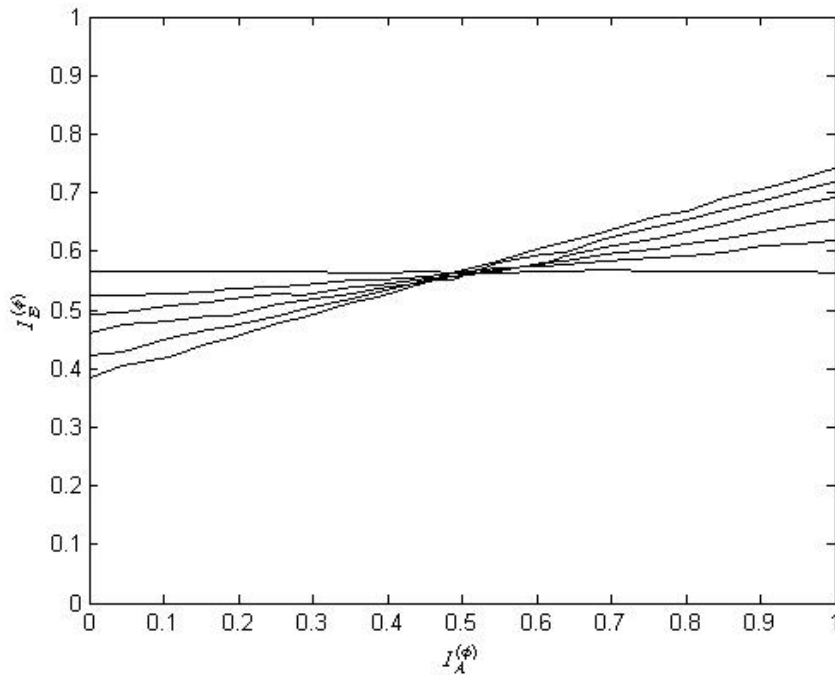
5-3-2-1-2 3×BPSK

Table 5-10 Candidate set for 3×BPSK

\mathcal{M} for 3×BPSK	$(\mathcal{M}(0), \mathcal{M}(1), \dots, \mathcal{M}(7))$
3DA2	(3,4,6,1,5,2,0,7)
3DB2	(3,6,4,1,5,2,0,7)
3DC2	(1,6,4,3,5,2,0,7)
3DD2	(1,6,2,3,4,5,0,7)
3DE2	(1,0,2,3,4,5,6,7)
Gray	(0,1,2,3,4,5,6,7)

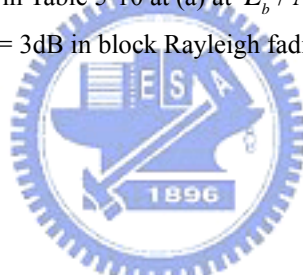


(a)



(b)

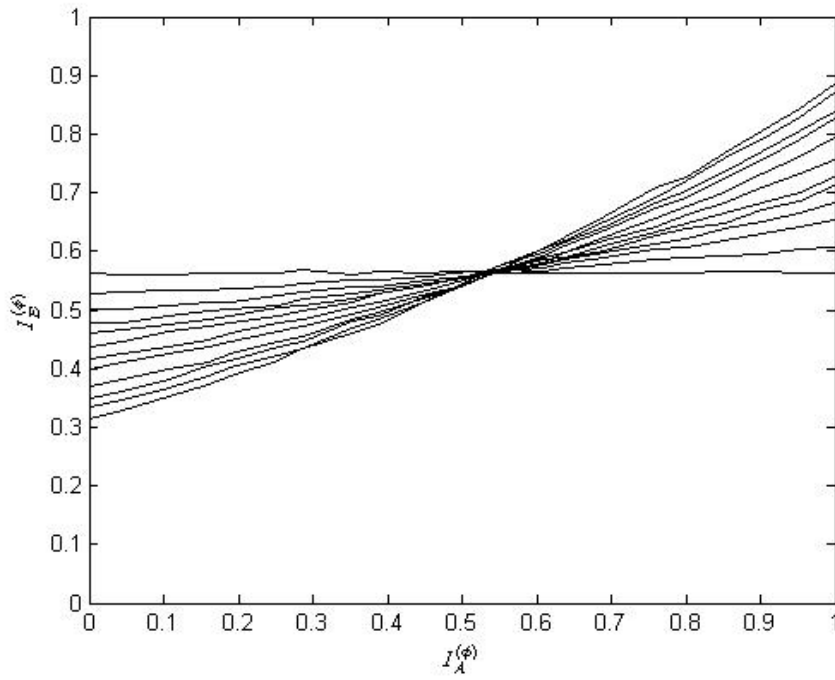
Fig. 5-12 Labelings for 3xBPSK in Table 5-10 at (a) at $E_b / N_0 = 1\text{dB}$ in AWGN channel and (b) $E_b / N_0 = 3\text{dB}$ in block Rayleigh fading channel



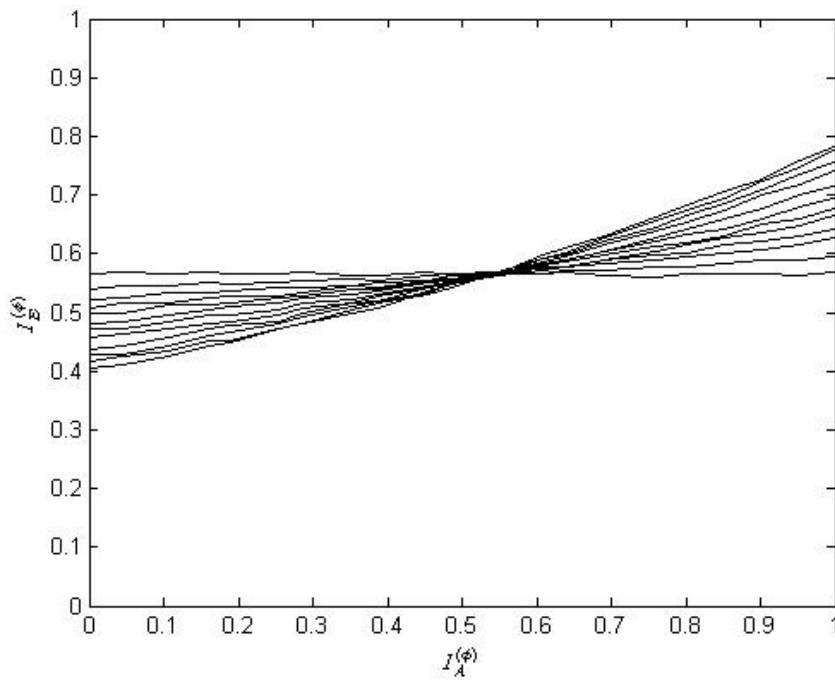
5-3-2-1-3 4x BPSK

Table 5-11 Candidate set for 4x BPSK

\mathcal{M} for 4x BPSK	$(\mathcal{M}(0), \mathcal{M}(1), \dots, \mathcal{M}(15))$
4DA2	(4,10,11,5,9,6,7,8,3,14,13,2,12,1,0,15)
4DB2	(1,15,14,9,12,0,3,13,6,8,11,7,2,5,4,10)
4DC2	(1,12,10,3,14,5,7,8,4,13,11,2,9,0,6,15)
4DD2	(8,1,3,12,5,14,4,15,9,10,0,11,2,13,7,6)
4DE2	(0,13,6,9,12,1,8,15,4,3,10,7,2,5,14,11)
4DF2	(3,0,2,1,4,7,5,6,11,9,13,10,12,8,14,15)
4DG2	(3,0,2,1,4,7,5,6,8,9,11,10,12,13,14,15)
4DH2	(3,0,2,1,4,5,7,6,8,9,11,10,12,13,14,15)
4DI2	(1,0,2,3,4,5,7,6,9,8,11,10,12,13,14,15)
4DJ2	(1,0,2,3,4,5,7,6,8,9,10,11,12,13,14,15)
4DK2	(1,0,2,3,4,5,6,7,8,9,10,11,12,13,14,15)
Gray	(0,1,2,3,4,5,6,7,8,9,10,11,12,13,14,15)



(a)



(b)

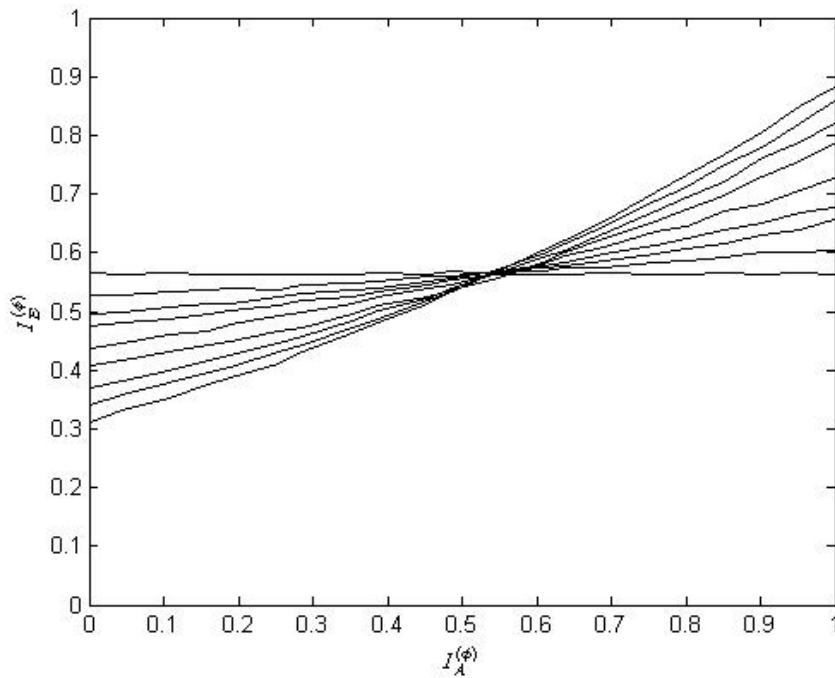
Fig. 5-13 Labelings for 4xBPSK in Table 5-11 at (a) $E_b/N_0 = 1\text{dB}$ in AWGN channel and (b) $E_b/N_0 = 3\text{dB}$ in block Rayleigh fading channel

5-3-2-2 $N \times \text{QPSK}$

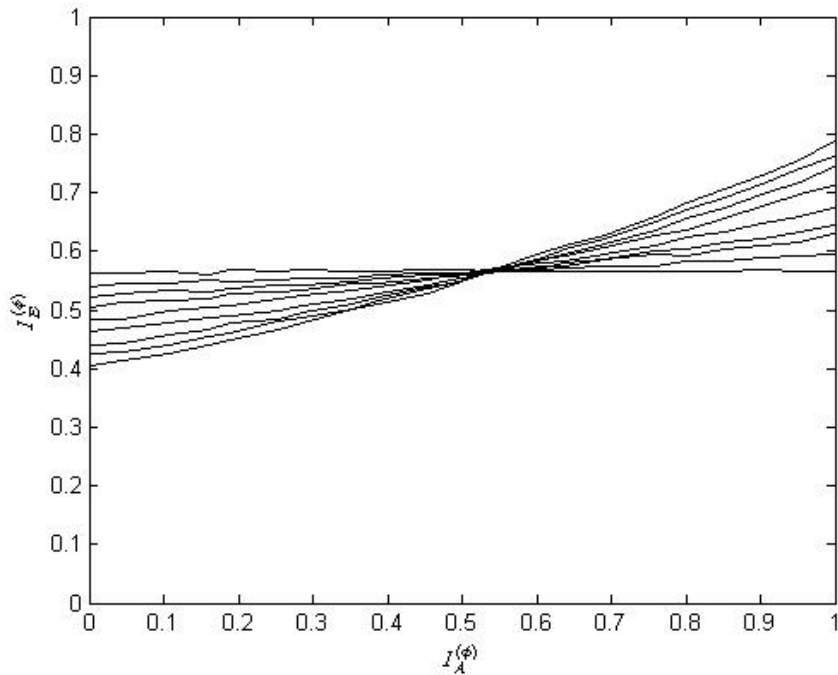
5-3-2-2-1 $2 \times \text{QPSK}$

Table 5-12 Candidate set for $2 \times \text{QPSK}$

\mathcal{M} for $2 \times \text{QPSK}$	$(\mathcal{M}(0), \mathcal{M}(1), \dots, \mathcal{M}(15))$
2DA4	(4,10,11,5,9,6,7,8,3,14,13,2,12,1,0,15)
2DB4	(1,15,14,9,12,0,3,13,6,8,10,7,2,5,4,11)
2DC4	(8,1,3,12,5,14,4,15,9,10,0,11,2,13,7,6)
2DD4	(2,13,6,9,12,1,8,15,4,3,10,7,0,5,14,11)
2DE4	(3,0,2,1,4,7,5,6,8,9,11,10,12,13,14,15)
2DF4	(1,0,2,3,4,5,7,6,9,8,11,10,12,13,14,15)
2DG4	(1,0,2,3,4,5,7,6,8,9,10,11,12,13,14,15)
2DH4	(1,0,2,3,4,5,6,7,8,9,10,11,12,13,14,15)
Gray	(0,1,2,3,4,5,6,7,8,9,10,11,12,13,14,15)



(a)



(b)

Fig. 5-14 Labelings for 2xQPSK in Table 5-12 at (a) $E_b / N_0 = 1\text{dB}$ in AWGN channel and (b) $E_b / N_0 = 3\text{dB}$ in block Rayleigh fading channel

5-3-2-2-2 $3 \times \text{QPSK}$

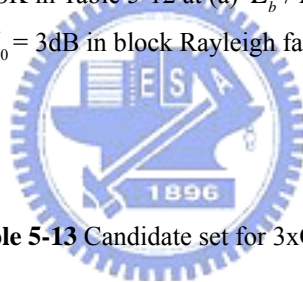
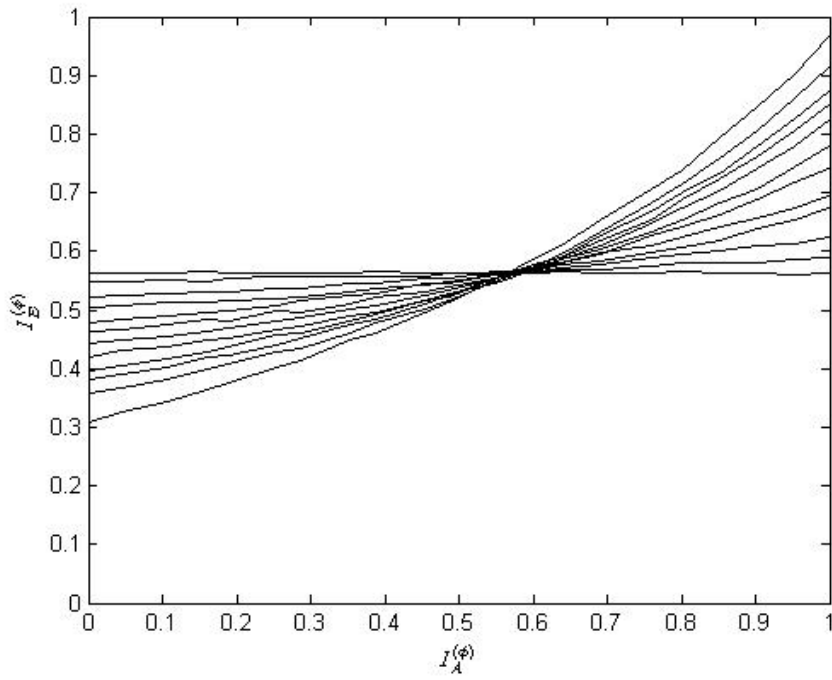
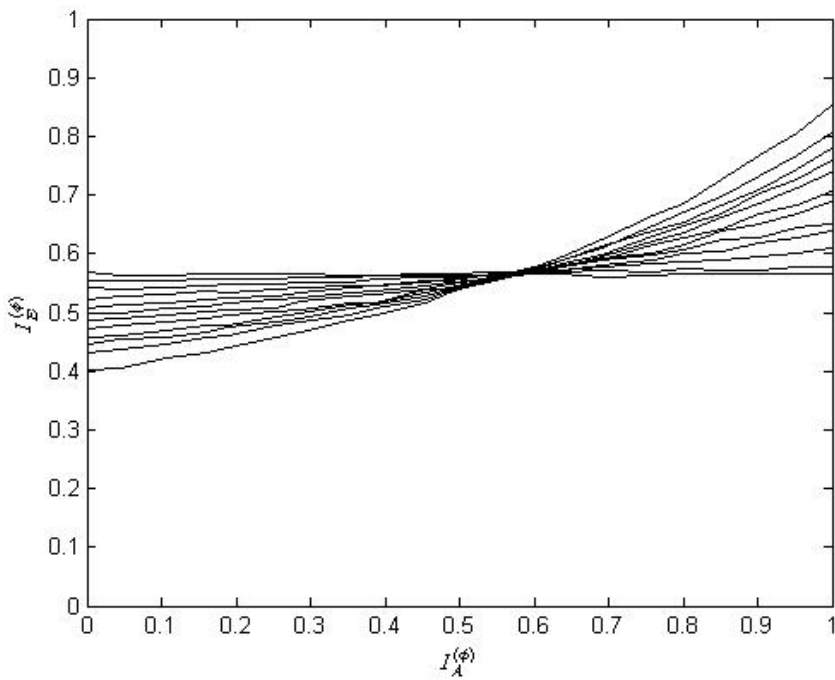


Table 5-13 Candidate set for $3 \times \text{QPSK}$

\mathcal{M} for $3 \times \text{QPSK}$	$(\mathcal{M}(0), \mathcal{M}(1), \dots, \mathcal{M}(63))$
3DA4	(1,0,2,3,4,37,38,23,8,9,46,27,44,13,10,47,17,16,18,19,20,21,22,55,24,25,26,43,28,61,62,31,32,33,34,7,36,5,6,39,40,41,42,11,12,45,14,15,48,49,50,35,52,53,54,51,56,57,58,59,60,29,30,63)
3DB4	(16,1,2,7,20,5,6,3,24,9,10,11,12,29,30,15,0,17,18,23,4,21,22,19,8,25,26,27,28,13,14,31,40,41,50,35,52,37,54,39,48,33,42,43,44,45,46,63,56,57,34,51,36,53,38,55,32,49,58,59,60,61,62,47)
3DC4	(0,3,2,19,4,5,22,7,12,9,10,11,8,13,14,31,16,1,18,17,20,21,6,23,28,25,26,27,24,29,30,15,34,33,32,35,36,39,38,63,40,41,42,43,44,61,62,47,50,51,48,49,52,37,54,55,56,57,58,59,60,45,46,53)
3DD4	(0,3,34,1,6,5,4,7,40,9,42,11,12,15,14,13,18,17,16,19,20,23,22,21,24,27,26,25,28,29,30,31,2,3,32,35,36,39,38,37,8,41,10,43,44,45,46,47,48,49,50,51,52,55,54,53,56,57,58,59,60,63,62,61)
3DE4	(10,1,2,3,4,7,6,5,8,11,42,9,14,13,12,15,48,17,26,19,20,21,22,23,56,25,18,27,28,29,30,31,32,3,5,34,33,38,37,36,39,0,41,40,43,44,47,46,45,16,49,50,51,52,53,54,55,24,57,58,59,60,61,62,63)
3DF4	(1,0,2,3,4,5,6,15,8,9,26,11,13,12,14,7,16,17,18,19,21,20,22,23,25,24,10,27,28,29,30,31,32,33,34,35,36,37,54,39,41,40,42,43,45,44,46,47,49,48,50,51,52,53,38,55,56,57,58,59,61,60,62,63)
3DG4	(0,5,34,3,36,1,38,35,12,9,10,15,8,13,14,11,20,17,18,23,16,21,22,19,24,29,26,27,28,25,30,31,4,37,2,7,32,33,6,39,40,41,42,43,44,45,46,47,48,49,50,51,52,53,54,55,56,57,58,59,60,61,62,63)
3DH4	(1,0,2,3,4,5,7,6,8,9,11,10,13,12,14,15,16,17,19,18,21,20,22,23,25,24,26,27,28,29,30,31,33,32,35,34,36,37,39,38,40,41,42,43,44,45,46,47,48,49,50,51,52,53,54,55,56,57,58,59,60,61,62,63)
3DI4	(1,0,2,3,4,5,7,6,9,8,10,11,12,13,15,14,16,17,19,18,28,29,22,23,24,25,27,26,20,21,30,31,33,32,34,35,36,37,38,39,41,40,42,43,44,45,47,46,48,49,50,51,52,53,54,55,56,57,58,59,60,61,62,63)
3DJ4	(1,0,2,3,4,5,7,6,8,9,11,10,13,12,14,15,17,16,19,18,20,21,22,23,24,25,26,27,28,29,30,31,32,33,34,35,36,37,38,39,40,41,42,43,44,45,46,47,48,49,50,51,52,53,54,55,56,57,58,59,60,61,62,63)
3DK4	(1,0,2,3,4,5,7,6,8,9,10,11,12,13,14,15,16,17,18,19,20,21,22,23,24,25,26,27,28,29,30,31,32,33,34,35,36,37,38,39,40,41,42,43,44,45,46,47,48,49,50,51,52,53,54,55,56,57,58,59,60,61,62,63)
Gray	(0,1,2,3,4,5,6,7,8,9,10,11,12,13,14,15,16,17,18,19,20,21,22,23,24,25,26,27,28,29,30,31,32,33,34,35,36,37,38,39,40,41,42,43,44,45,46,47,48,49,50,51,52,53,54,55,56,57,58,59,60,61,62,63)



(a)



(b)

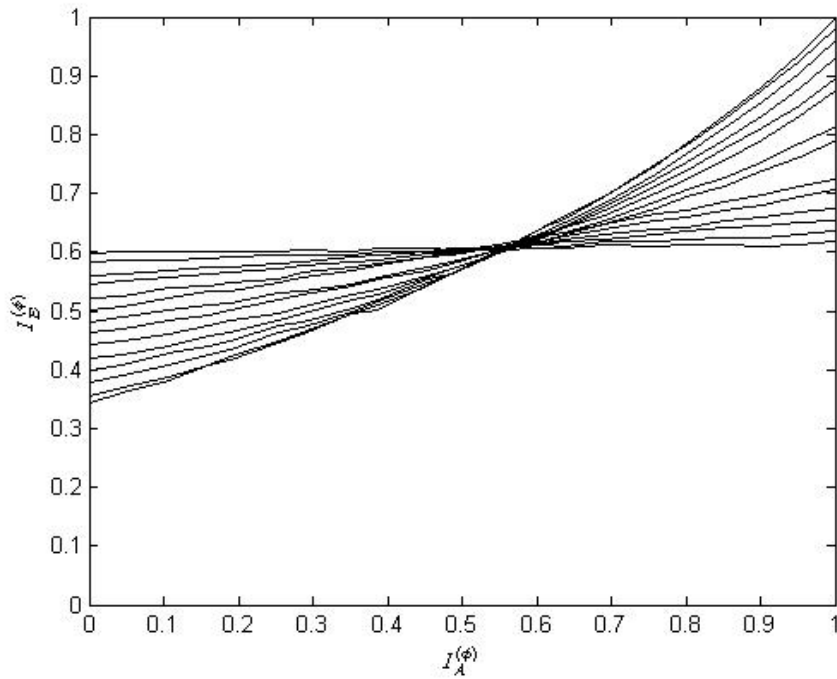
Fig. 5-15 Labelings for 3xQPSK in Table 5-13 at (a) $E_b/N_0 = 1\text{dB}$ in AWGN channel and (b) $E_b/N_0 = 3\text{dB}$ in block Rayleigh fading channel

5-3-2-3 $N \times 8$ -PSK

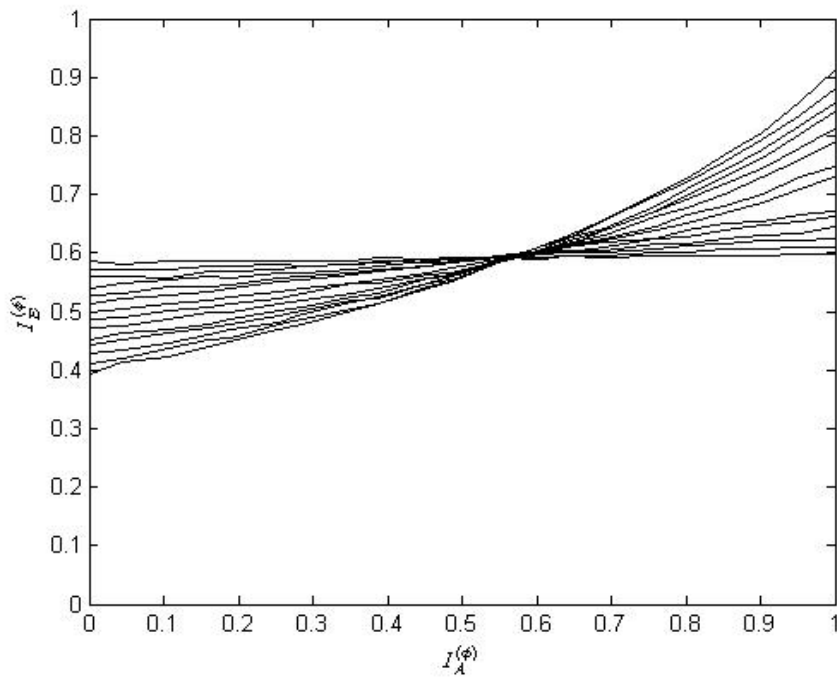
5-3-2-3-1 2×8 -PSK

Table 5-14 Candidate set for 2×8 -PSK

\mathcal{M} for 2×8 -PSK	$(\mathcal{M}(0), \mathcal{M}(1), \dots, \mathcal{M}(63))$
2DA8	(50,4,6,48,0,55,53,3,12,58,56,15,63,9,11,61,37,18,16,38,22,33,35,21,43,28,30,40,24,47,45,27,5,51,49,7,54,1,2,52,59,13,14,41,8,62,60,10,19,36,39,17,32,23,20,34,29,42,57,31,46,25,26,44)
2DB8	(1,21,23,35,20,0,6,19,40,9,26,47,8,41,42,31,52,3,2,18,4,17,50,37,24,45,46,11,60,13,30,43,48,33,34,55,32,49,54,7,28,63,62,27,56,29,14,57,38,53,22,39,16,5,36,51,44,25,10,59,12,61,58,15)
2DC8	(4,33,10,5,2,23,32,3,14,13,12,11,8,25,6,31,18,21,20,19,16,17,22,7,28,41,26,15,30,29,40,27,34,37,36,35,0,1,38,39,60,43,42,61,62,63,56,9,52,59,50,53,54,55,48,49,58,45,44,51,24,57,46,47)
2DD8	(2,3,0,5,4,39,38,1,12,13,14,9,42,11,8,15,20,21,22,23,18,19,16,55,58,59,24,31,28,29,62,25,32,37,6,35,34,33,36,7,10,43,40,45,60,47,46,41,50,51,48,49,52,53,54,17,56,61,30,57,26,27,44,63)
2DE8	(38,33,4,35,0,39,34,21,24,59,42,11,46,9,28,47,16,51,18,3,54,1,20,55,58,25,12,27,8,63,62,29,32,49,2,5,6,7,36,37,40,41,10,43,44,45,14,15,50,17,48,19,52,53,22,23,56,57,26,13,30,31,60,61)
2DF8	(4,3,10,5,2,1,32,7,12,13,26,11,8,9,6,31,20,21,18,19,22,17,16,23,28,25,14,15,24,29,30,27,34,37,36,35,0,39,38,33,44,43,42,45,46,41,40,47,52,51,50,53,48,55,54,49,58,61,60,59,62,63,56,57)
2DG8	(4,5,34,35,32,33,2,7,44,9,14,15,12,13,10,11,18,17,16,19,20,21,22,23,24,25,30,31,26,29,28,27,36,1,6,39,0,37,38,3,8,45,42,43,40,41,46,47,52,53,50,51,54,49,48,55,60,61,58,59,56,57,62,63)
2DH8	(32,33,6,7,36,1,2,3,12,13,14,11,8,9,10,15,16,23,22,17,20,21,18,19,28,25,30,31,24,29,26,27,4,5,38,35,0,37,34,39,40,41,46,47,44,45,42,43,54,53,48,49,52,55,50,51,56,61,62,57,58,59,60,63)
2DI8	(32,1,6,35,36,37,38,3,8,9,14,11,12,13,10,15,48,49,54,51,52,53,50,55,24,25,30,27,28,29,26,31,0,33,34,7,4,5,2,39,40,41,42,43,44,45,46,47,16,17,22,19,20,21,18,23,56,57,62,59,60,61,58,63)
2DJ8	(4,1,2,35,0,5,6,7,12,25,10,11,28,13,14,15,16,17,18,3,20,21,22,23,24,9,26,27,8,29,30,31,36,33,34,51,32,37,38,39,56,41,58,43,40,61,62,63,48,49,50,19,52,53,54,55,44,57,42,59,60,45,46,47)
2DK8	(4,1,2,35,0,5,6,7,12,25,10,11,28,13,14,15,16,17,22,19,20,21,18,23,24,9,26,27,8,29,30,31,36,33,34,3,32,37,38,39,40,41,42,43,44,45,46,47,48,49,54,51,52,53,50,55,56,57,62,59,60,61,58,63)
2DL8	(0,3,2,1,4,5,6,7,24,27,26,11,12,13,14,15,16,19,18,17,20,21,22,23,8,25,10,9,28,29,30,31,32,33,34,35,36,37,38,39,40,41,42,43,44,45,46,47,48,49,50,51,52,53,54,55,56,57,58,59,60,61,62,63)
2DM8	(4,1,2,35,0,5,6,7,8,9,10,11,12,13,14,15,16,17,18,19,20,21,22,23,24,25,26,27,28,29,30,31,32,33,34,3,36,37,38,39,40,41,42,43,44,45,46,47,48,49,50,51,52,53,54,55,56,57,58,59,60,61,62,63)
Gray	(0,1,2,3,4,5,6,7,8,9,10,11,12,13,14,15,16,17,18,19,20,21,22,23,24,25,26,27,28,29,30,31,32,33,34,35,36,37,38,39,40,41,42,43,44,45,46,47,48,49,50,51,52,53,54,55,56,57,58,59,60,61,62,63)

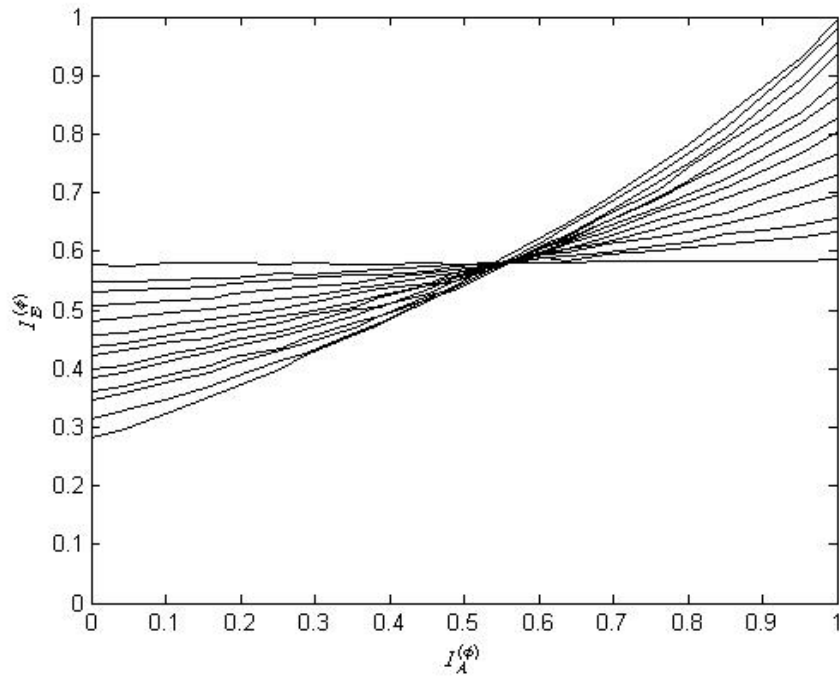


(a)

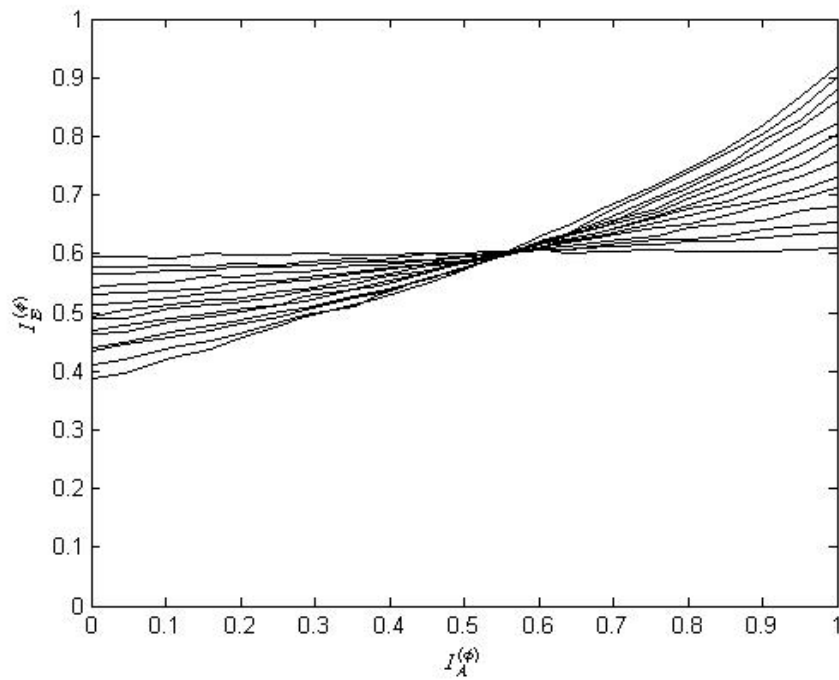


(b)

Fig. 5-16 Labelings for 2x8-PSK in Table 5-14 at (a) $E_b/N_0 = 3\text{dB}$ in AWGN channel and (b) $E_b/N_0 = 5\text{dB}$ in block Rayleigh fading channel



(a)



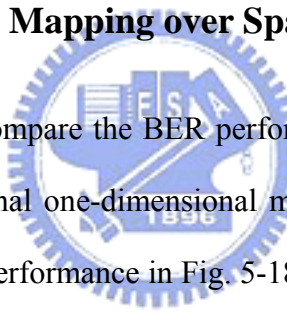
(b)

Fig. 5-17 Labelings for 2x8-PSK in Table 5-15 at (a) $E_b / N_0 = 3.5\text{dB}$ in AWGN channel and (b) $E_b / N_0 = 6\text{dB}$ in block Rayleigh fading channel

5-4 Simulation Results

To verify the advantage of multi-dimensional mapping, the convolutional code with generator matrix $(1+D^2, 1+D+D^2)$ is particularly chosen as the outer code in this section. From section 4-4 with our proposed labelings, the simulation results employing this code usually have about the same waterfall threshold with the code with generator matrix $(1+D^2+D^3+D^5+D^6, 1+D+D^2+D^3+D^6)$ but exhibit early BER floor around 10^{-5} . We will show that with a proper multi-dimensional labeling, this BER floor can be improved. Then, the good performance with the memory-6 convolutional code can also be expected.

5-4-1 Multi-dimensional Mapping over Spatial Domain



In a MIMO system, we compare the BER performance with a multi-dimensional mapper and with a conventional one-dimensional mapper. For $N \times N$ BPSK and BPSK modulation, we simulate the performance in Fig. 5-18(b), Fig. 5-19(b) and Fig. 5-20(b) for 2×2 , 3×3 and 4×4 systems, respectively. There is only one labeling for BPSK and the most matched labelings for $2 \times$ BPSK, $3 \times$ BPSK, $4 \times$ BPSK are Anti-Gray, 3DA2, 4DB2, respectively. In each figure, the multi-dimensional labeling can provide lower BER floor than the conventional one because the demapper and the decoder curve can intersect at farther point in the respective EXIT-chart in Fig. 5-18(a), Fig. 5-19(a) and Fig. 5-20(a). Note that the performance gain can be achieved without increasing receiver complexity. In addition, we can observe from Fig. 5-18(a), Fig. 5-19(a) and Fig. 5-20(a) that with higher dimensional mapper, the labeling with better EXIT-chart characteristics can be chosen and therefore it can make tunnel open at lower threshold and achieve better BER floor, which can be verified by the performance plots. Similar observations can be also obtained from Fig. 5-21 and Fig. 5-22 for $N \times N$ QPSK, from

Fig. 5-23 for $N \times 8$ -PSK and from Fig. 5-24 for $N \times 16$ -QAM to conform the advantages of our multi-dimensional labelings.

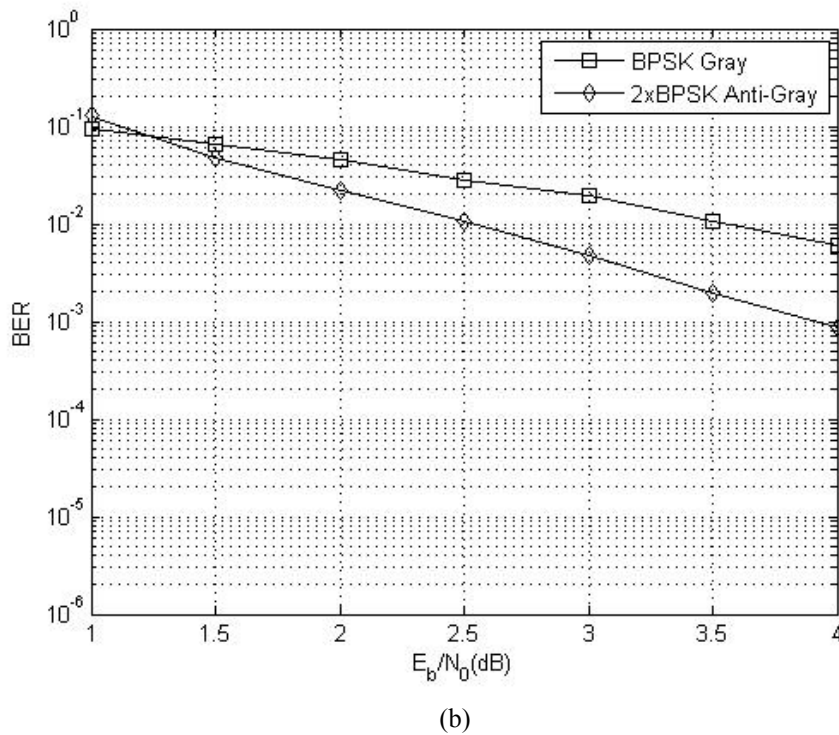
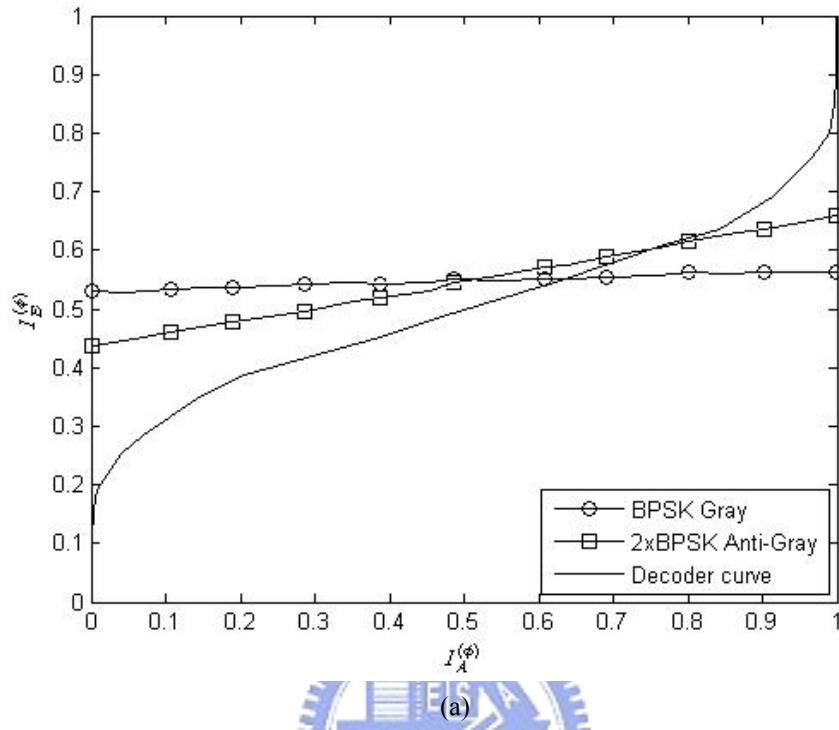
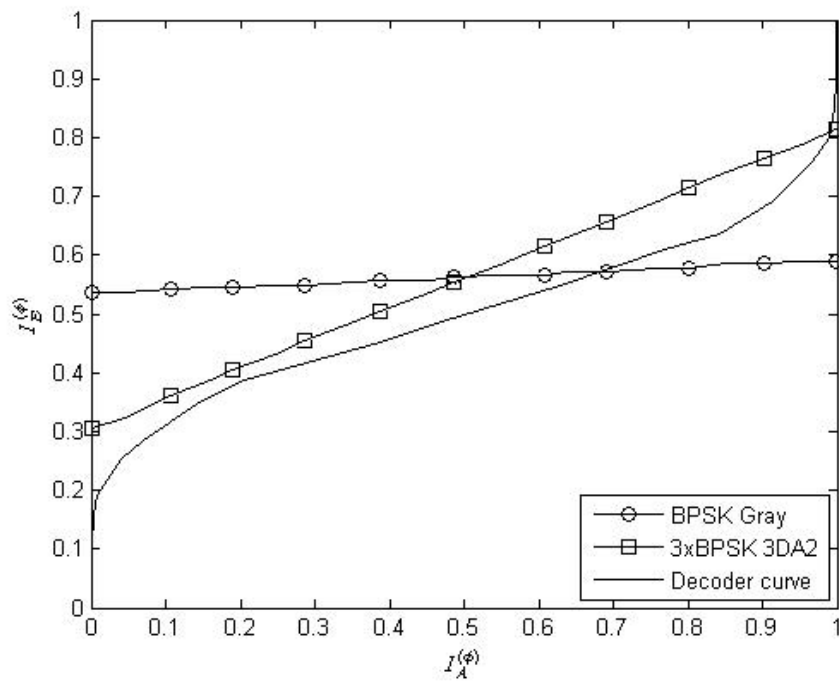
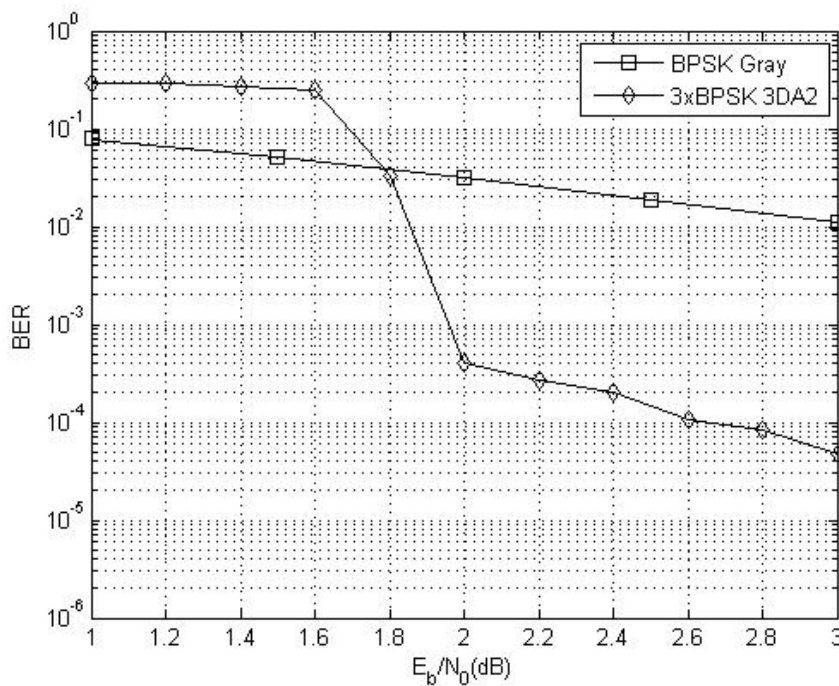


Fig. 5-18 (a) EXIT-chart at $E_b / N_0 = 2\text{dB}$ and (b) performance plots of the BICM-ID system with (5, 7) convolutional code in 2x2 fast Rayleigh fading channel

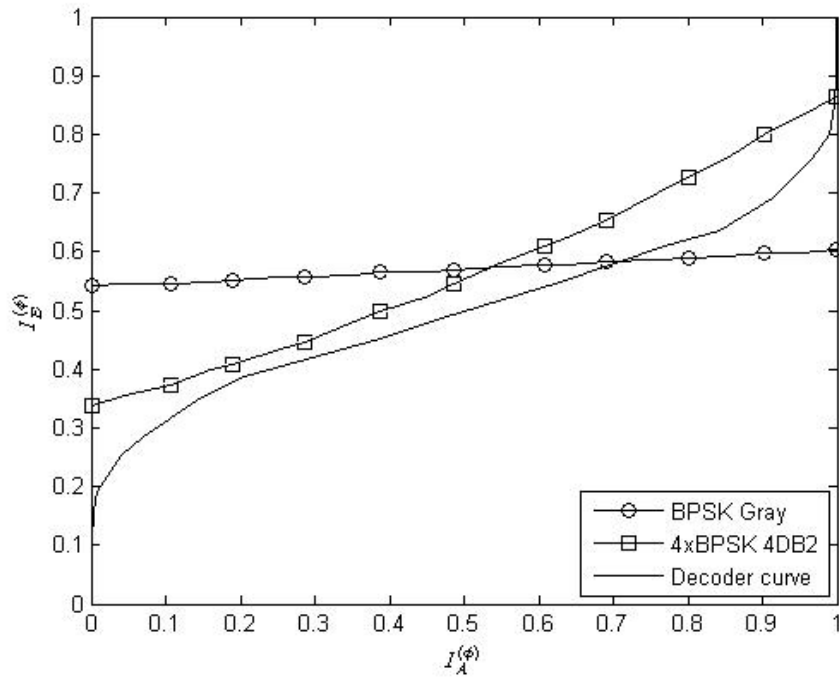


(a)

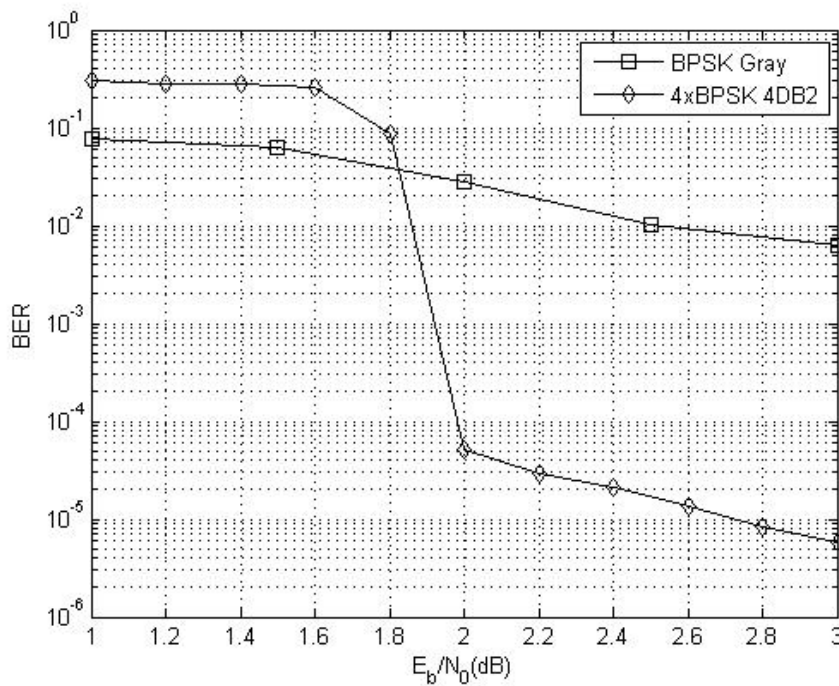


(b)

Fig. 5-19 (a) EXIT-chart at $E_b / N_0 = 2\text{dB}$ and (b) performance plots of the BICM-ID system with (5, 7) convolutional code in 3x3 fast Rayleigh fading channel



(a)



(b)

Fig. 5-20 (a) EXIT-chart at $E_b / N_0 = 2\text{dB}$ and (b) performance plots of the BICM-ID system with (5, 7) convolutional code in 4x4 fast Rayleigh fading channel

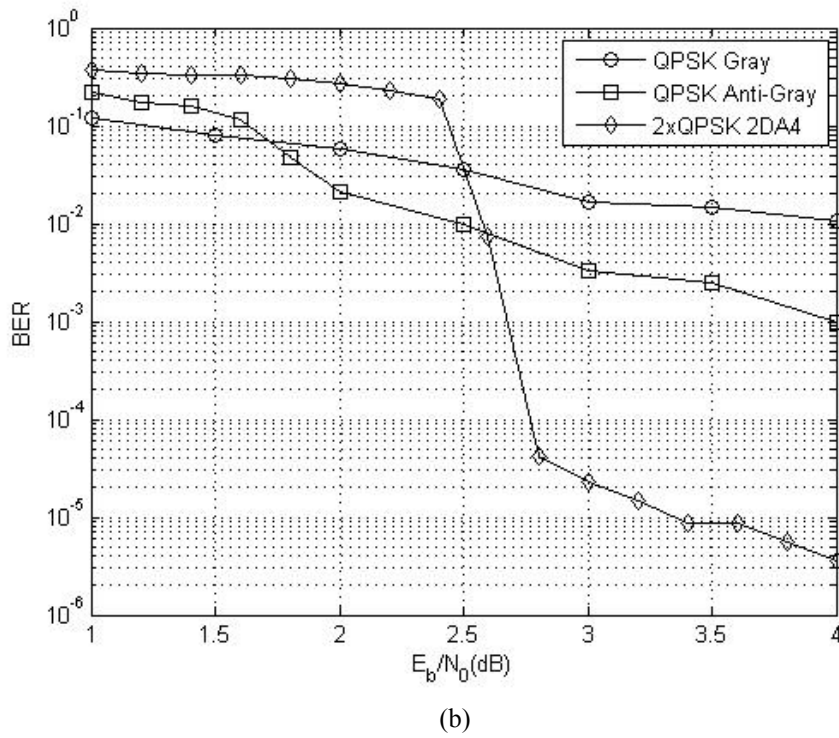
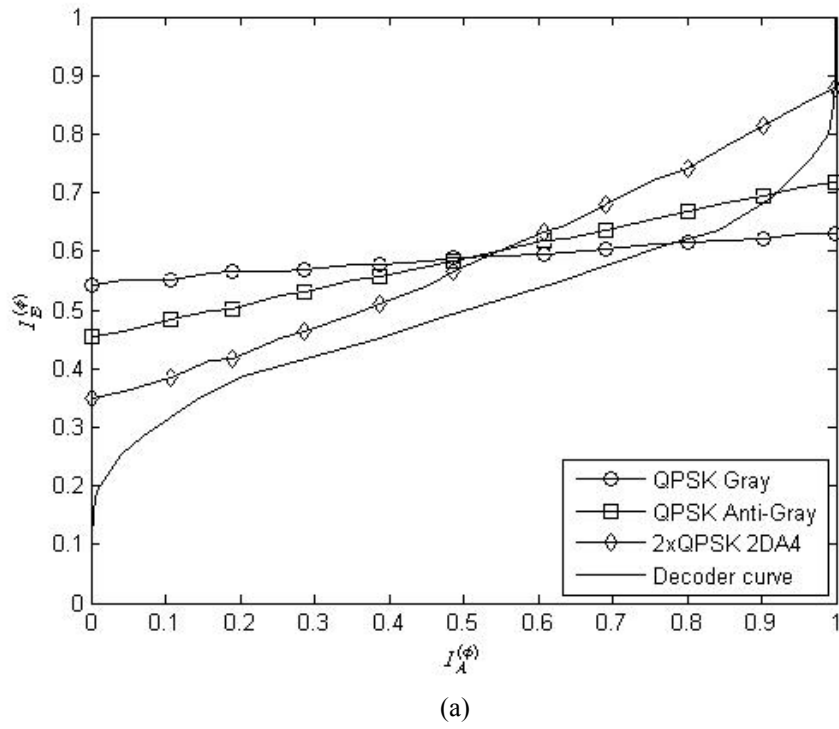
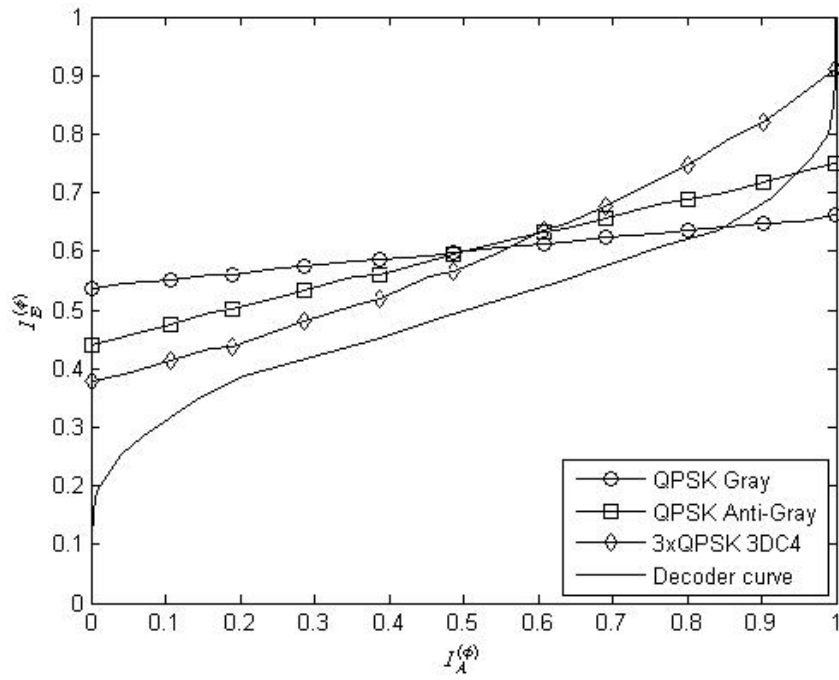
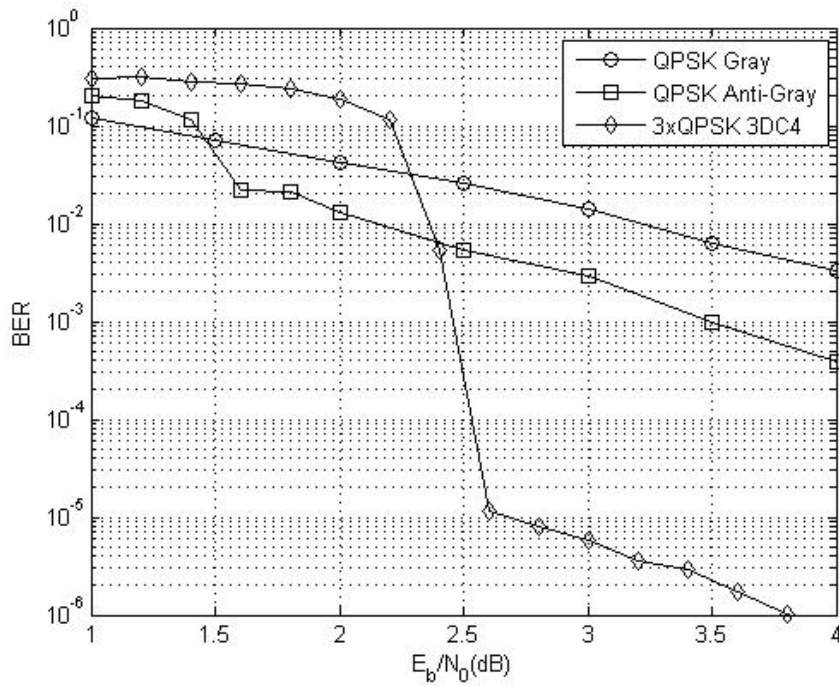


Fig. 5-21 (a) EXIT-chart at $E_b / N_0 = 3\text{dB}$ and (b) performance plots of the BICM-ID system with (5, 7) convolutional code in 2x2 fast Rayleigh fading channel



(a)



(b)

Fig. 5-22 (a) EXIT-chart at $E_b/N_0 = 3$ dB and (b) performance plots of the BICM-ID system with (5, 7) convolutional code in 3x3 fast Rayleigh fading channel

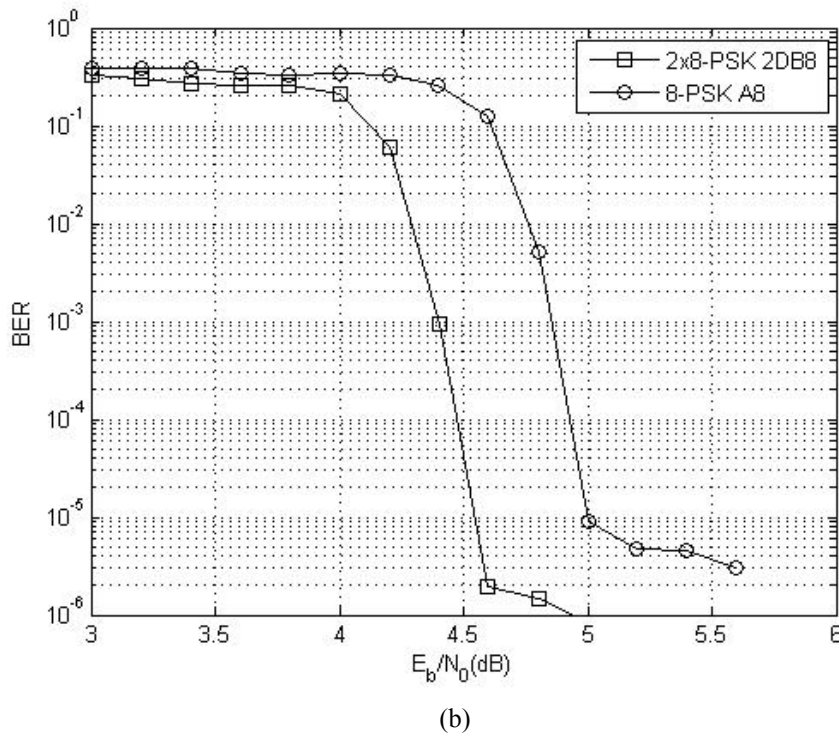
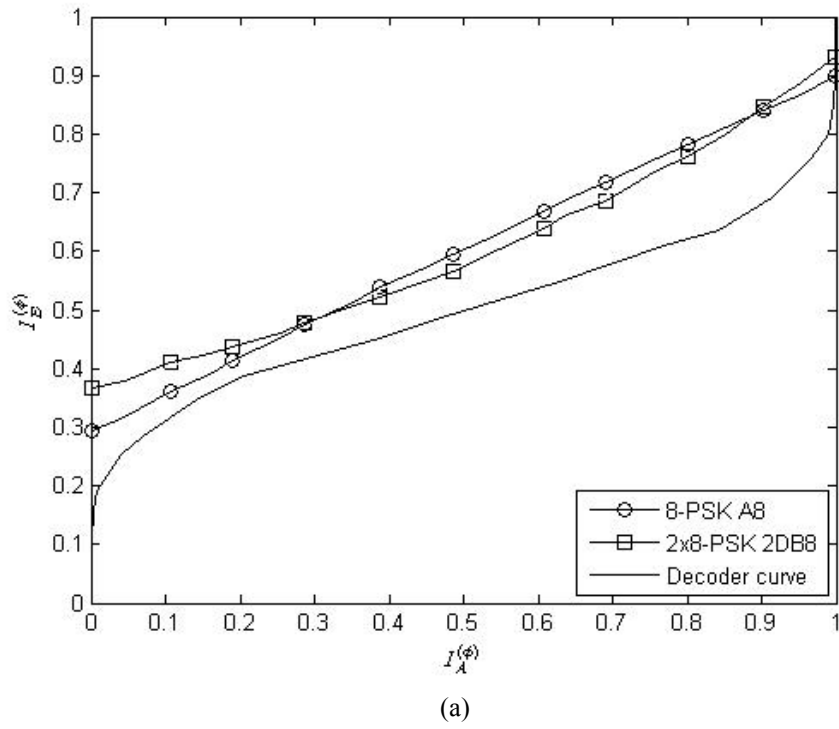
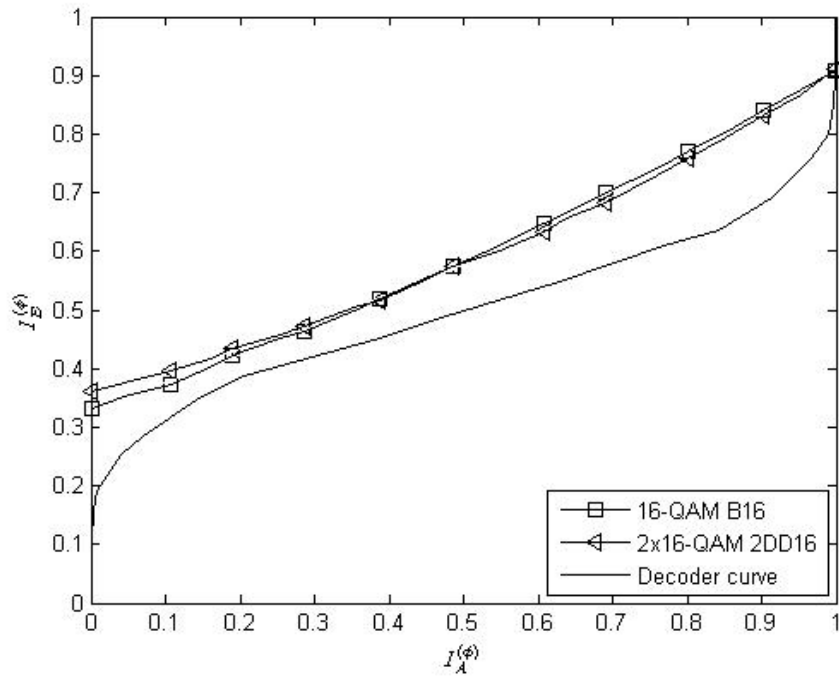
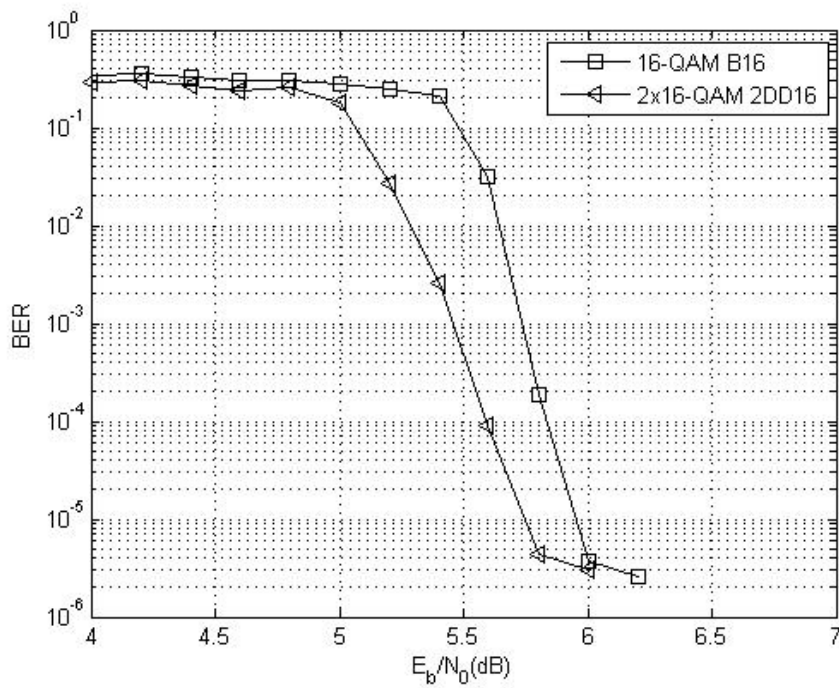


Fig. 5-23 (a) EXIT-chart at $E_b / N_0 = 5$ dB and (b) performance plots of the BICM-ID system with (5, 7) convolutional code in 2x2 fast Rayleigh fading channel



(a)



(b)

Fig. 5-24 (a) EXIT-chart at $E_b / N_0 = 6\text{dB}$ and (b) performance plots of the BICM-ID system with (5, 7) convolutional code in 2x2 fast Rayleigh fading channel

5-4-2 Multi-dimensional Mapping over Time Domain

In a SISO system, we compare the performance with a multi-dimensional mapper and with a conventional multi-dimensional mapper in AWGN and block Rayleigh fading channels. For $N \times$ BPSK and BPSK modulation, we simulate the performance in Fig. 5-25(b) and Fig. 5-26(b). In AWGN channels, Fig. 5-25(b), there is only one labeling for BPSK and the most matched labelings for $2 \times$ BPSK, $3 \times$ BPSK, $4 \times$ BPSK are Anti-Gray, 3DA2, 4DB2, respectively. With higher dimensional labeling, the BER floor can be made lower and SNR gain can be obtained at BER 10^{-5} . It can also be observed from Fig. 5-25(a) that higher dimensional labeling has better EXIT-chart characteristics. Similar observations can be also obtained from Fig. 5-27 and Fig. 5-28 for $N \times$ QPSK, Fig. 5-29 and Fig. 5-30 for $N \times$ 8-PSK and Fig. 5-31 and Fig. 5-32 for $N \times$ 16-QAM. Especially, it can be seen from Fig. 5-29 and Fig. 5-31 that the BER floor of the most matched labelings for 8-PSK and 16-QAM in AWGN channel as already observed in Fig. 4-5 and Fig. 4-8 can be made lower with multi-dimensional labelings. These simulation results conform the advantages of our multi-dimensional labelings.

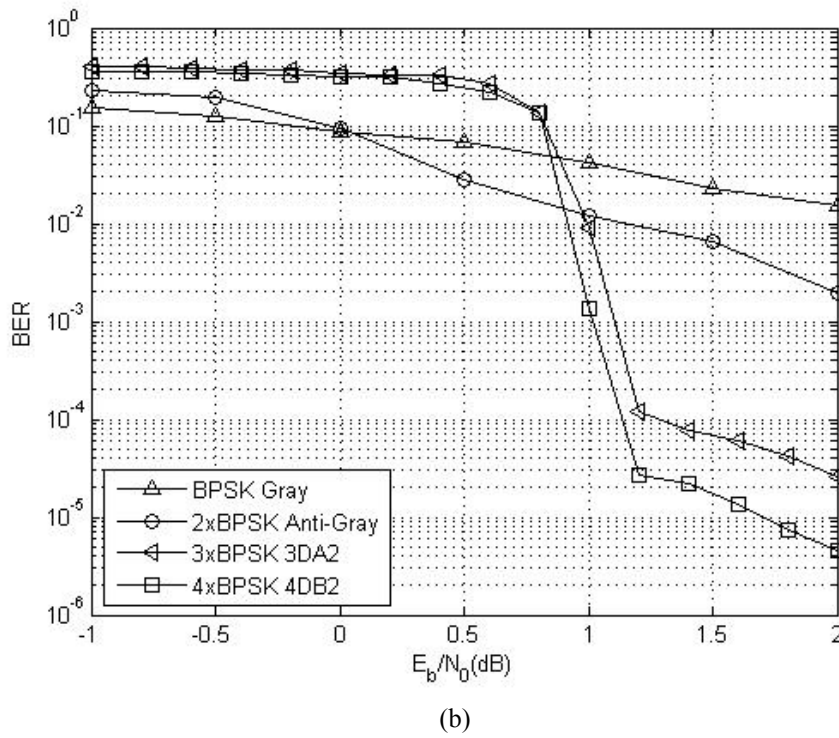
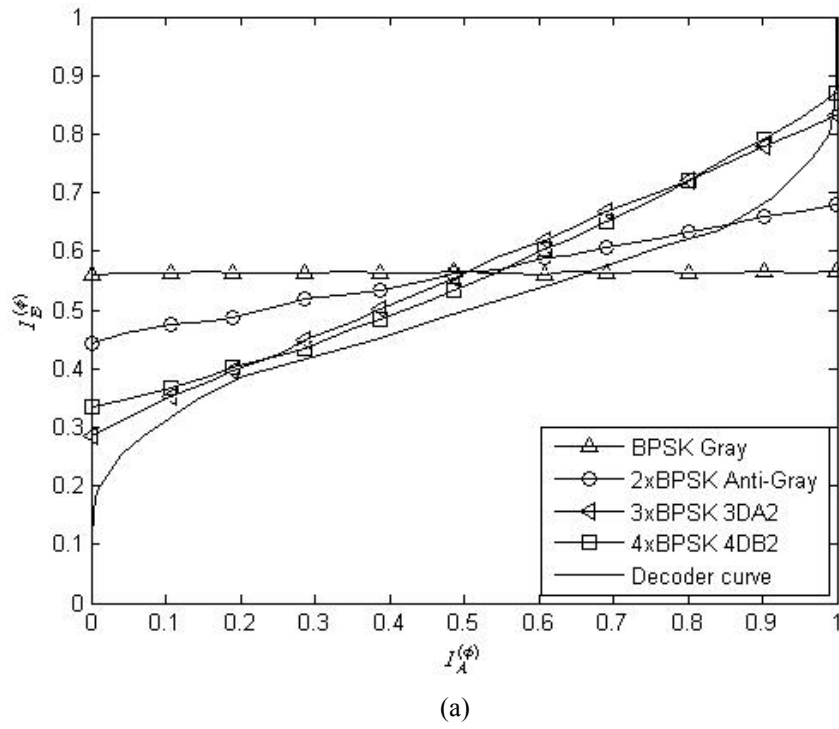
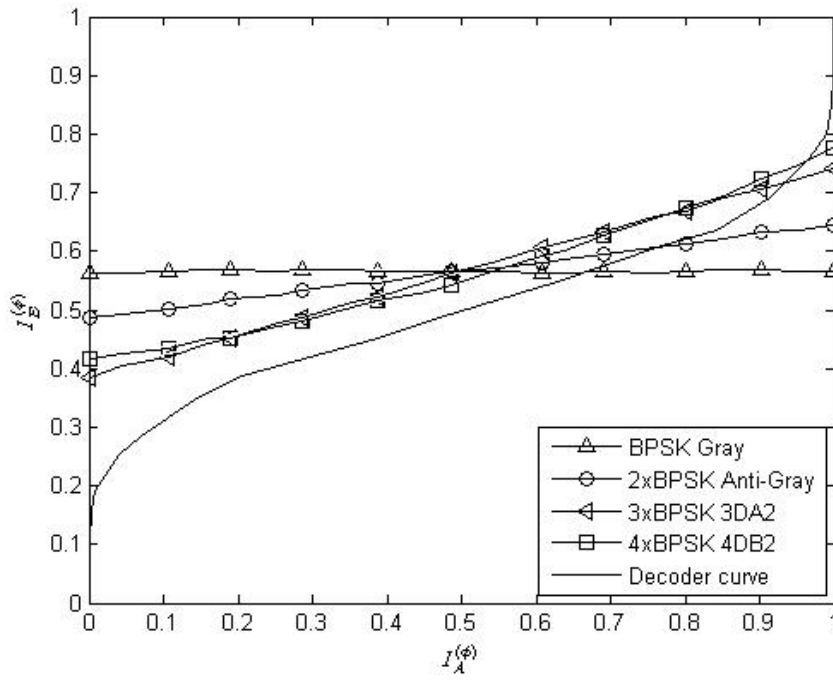
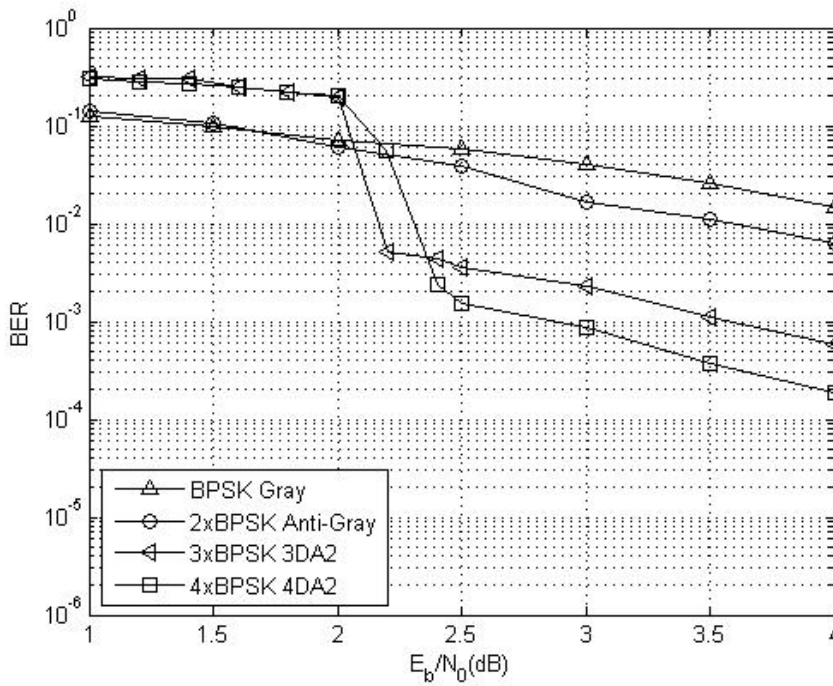


Fig. 5-25 (a) EXIT-chart at $E_b/N_0 = 1\text{dB}$ and (b) performance plots of the BICM-ID system with (5, 7) convolutional code in 1x1 AWGN channel



(a)



(b)

Fig. 5-26 (a) EXIT-chart at $E_b / N_0 = 3\text{dB}$ and (b) performance plots of the BICM-ID system with (5, 7) convolutional code in 1x1 block Rayleigh fading channel

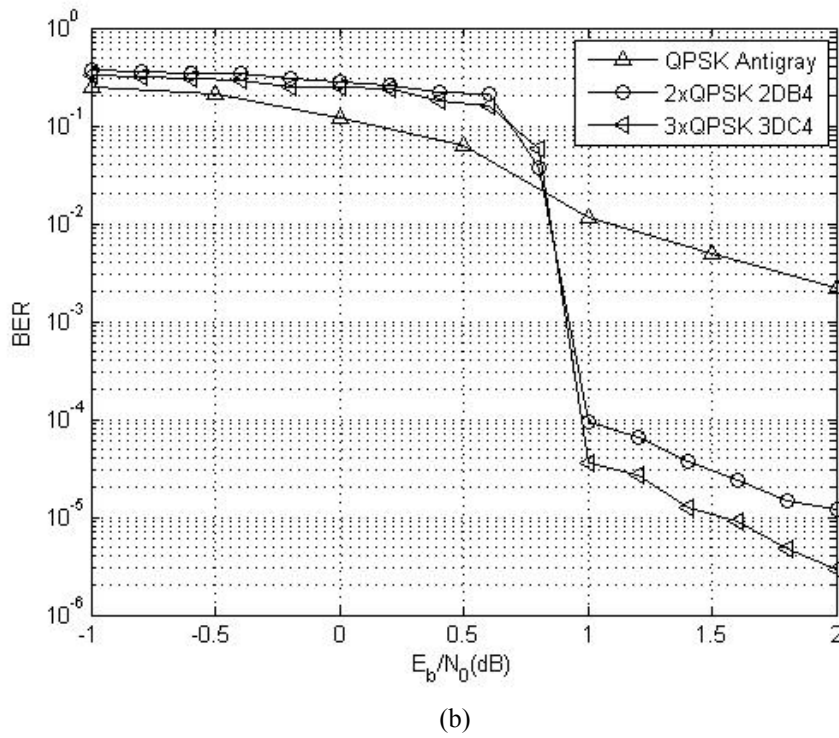
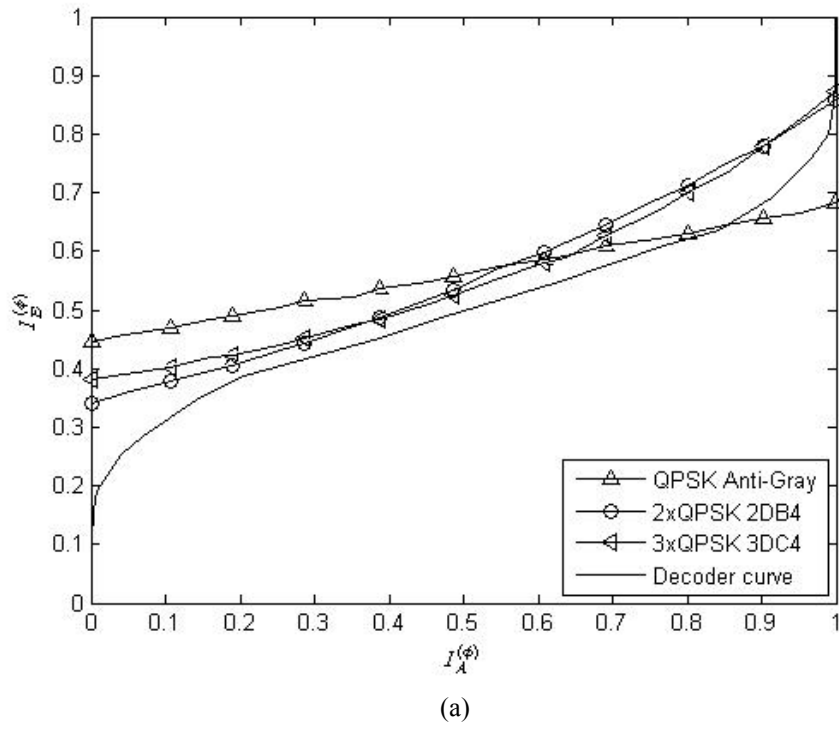
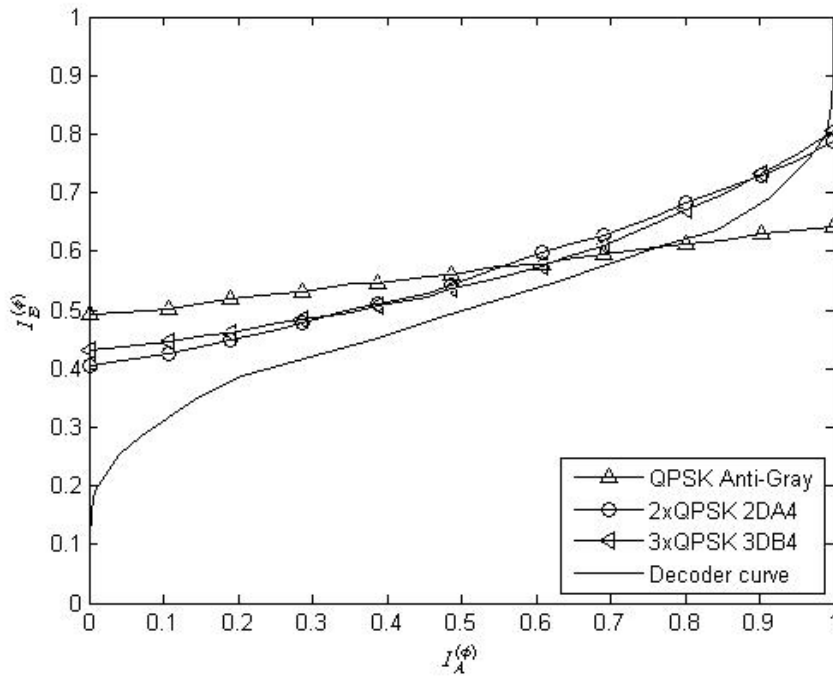
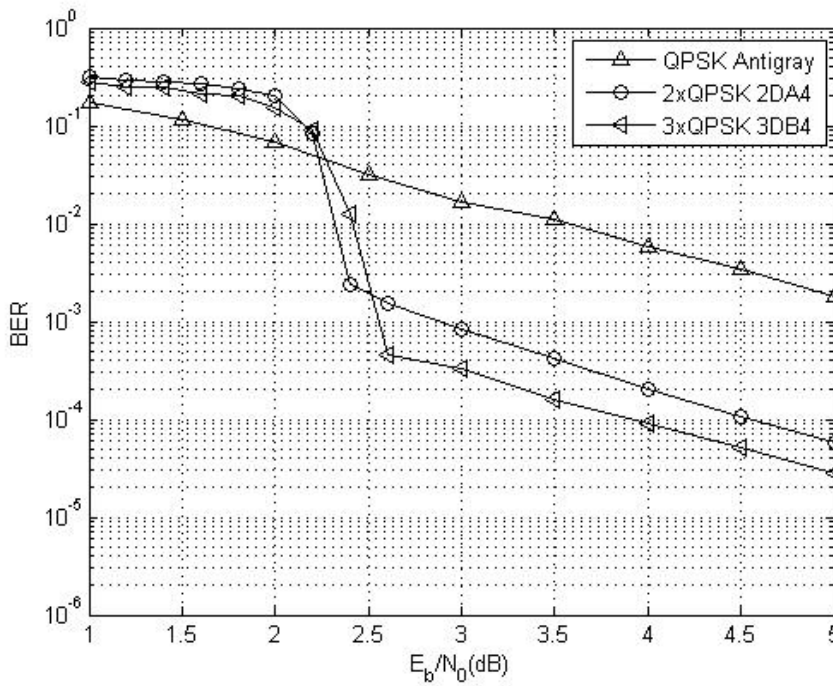


Fig. 5-27 (a) EXIT-chart at $E_b / N_0 = 1$ dB and (b) performance plots of the BICM-ID system with (5, 7) convolutional code in 1x1 AWGN channel



(a)



(b)

Fig. 5-28 (a) EXIT-chart at $E_b / N_0 = 3$ dB and (b) performance plots of the BICM-ID system with (5, 7) convolutional code in 1x1 block Rayleigh fading channel

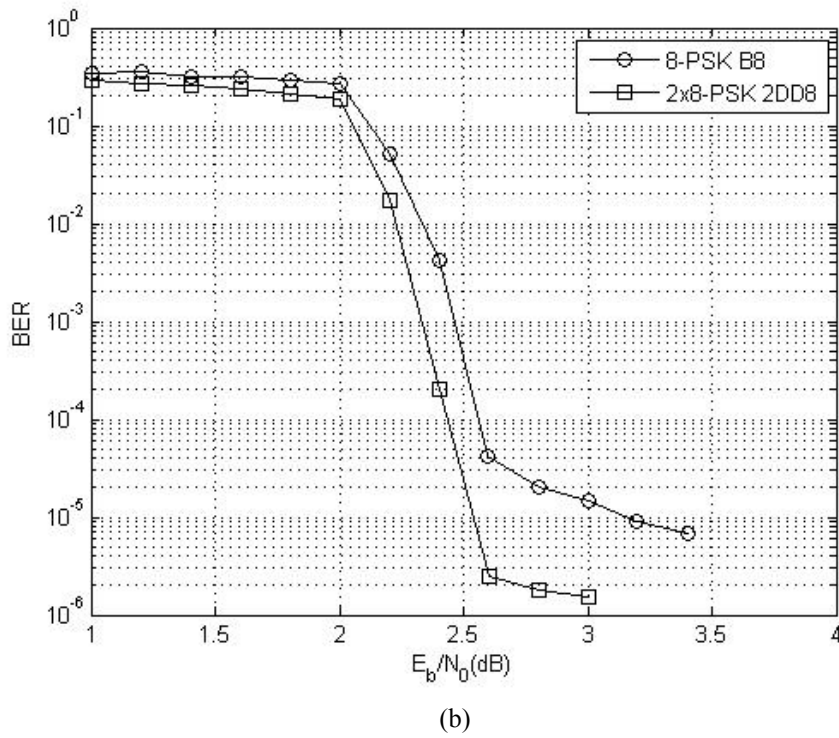
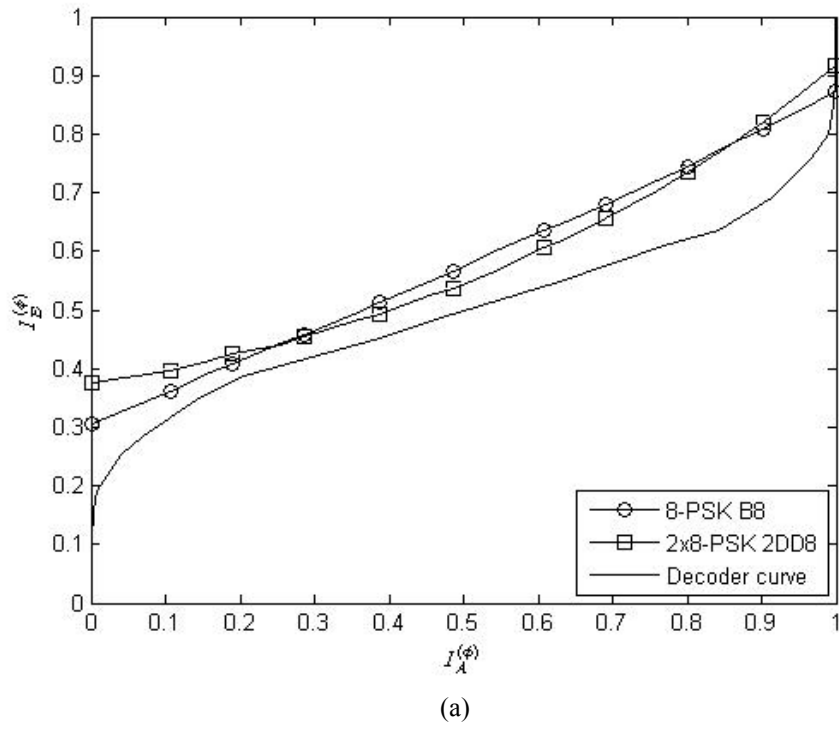


Fig. 5-29 (a) EXIT-chart at $E_b / N_0 = 2.6\text{dB}$ and (b) performance plots of the BICM-ID system with (5, 7) convolutional code in 1x1 AWGN channel

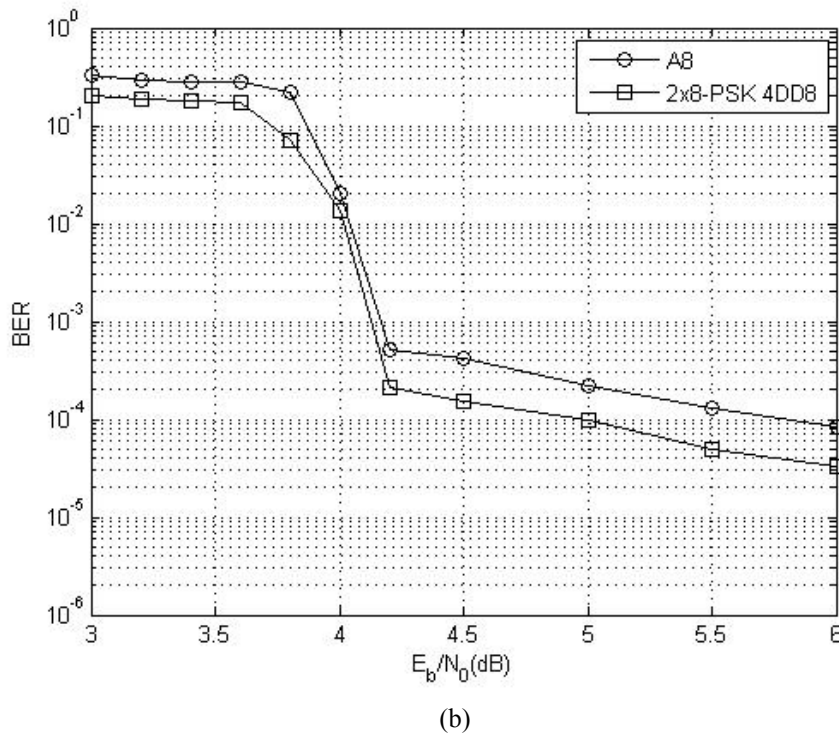
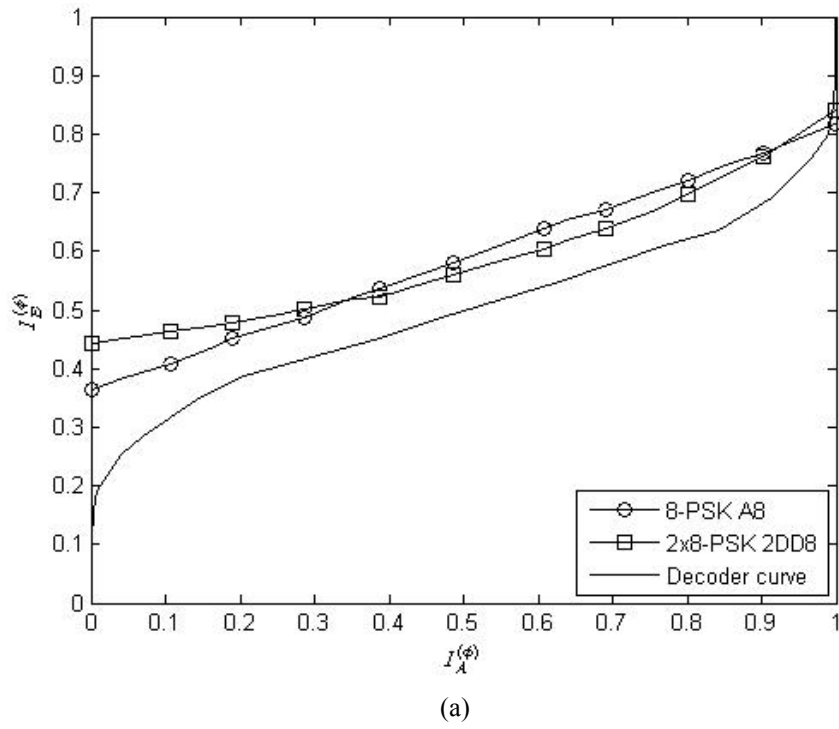


Fig. 5-30 (a) EXIT-chart at $E_b / N_0 = 5$ dB and (b) performance plots of the BICM-ID system with (5, 7) convolutional code in 1x1 block Rayleigh fading channel

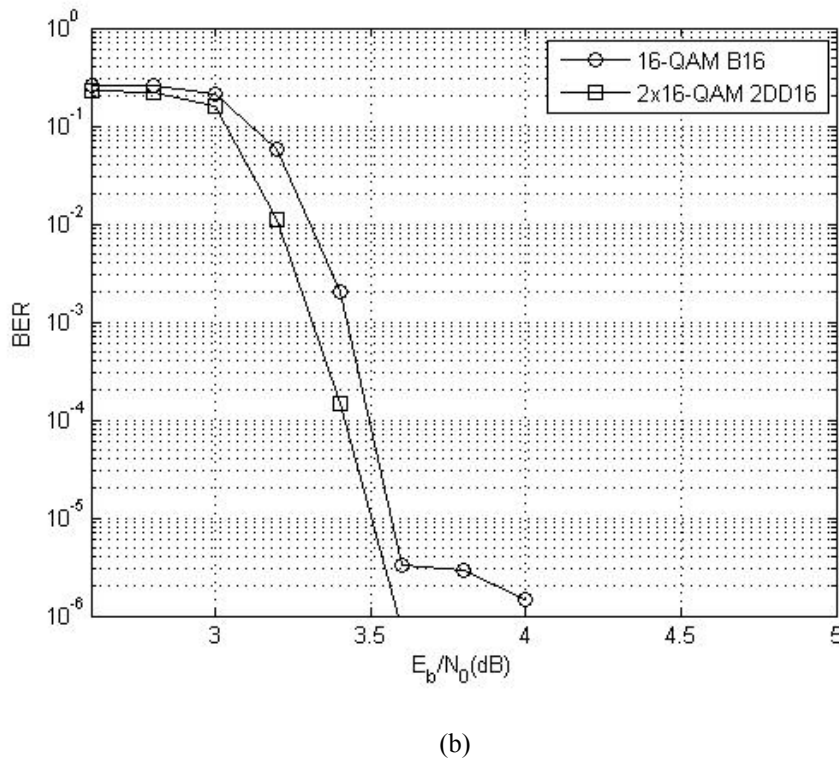
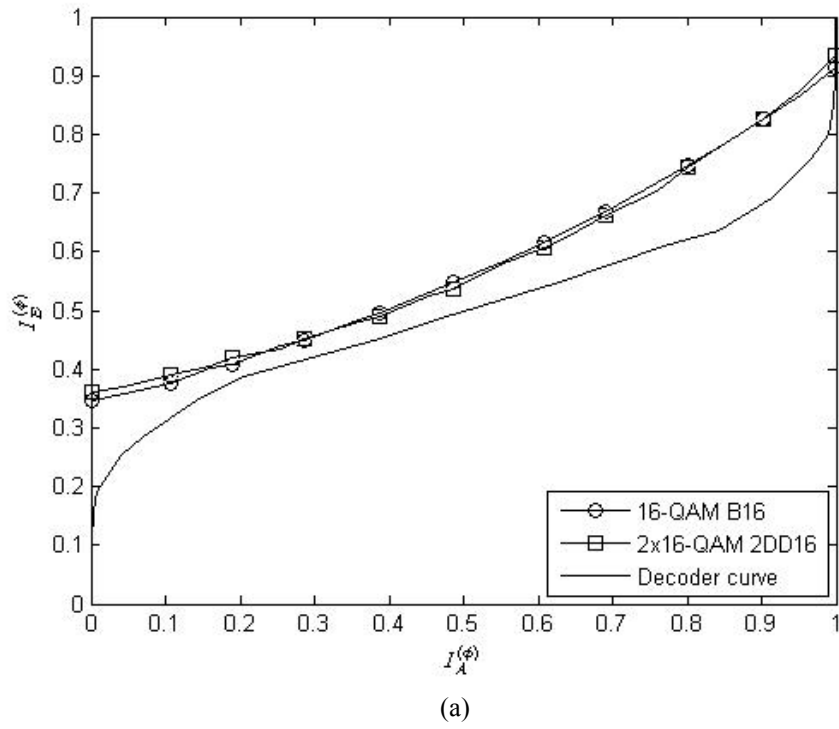
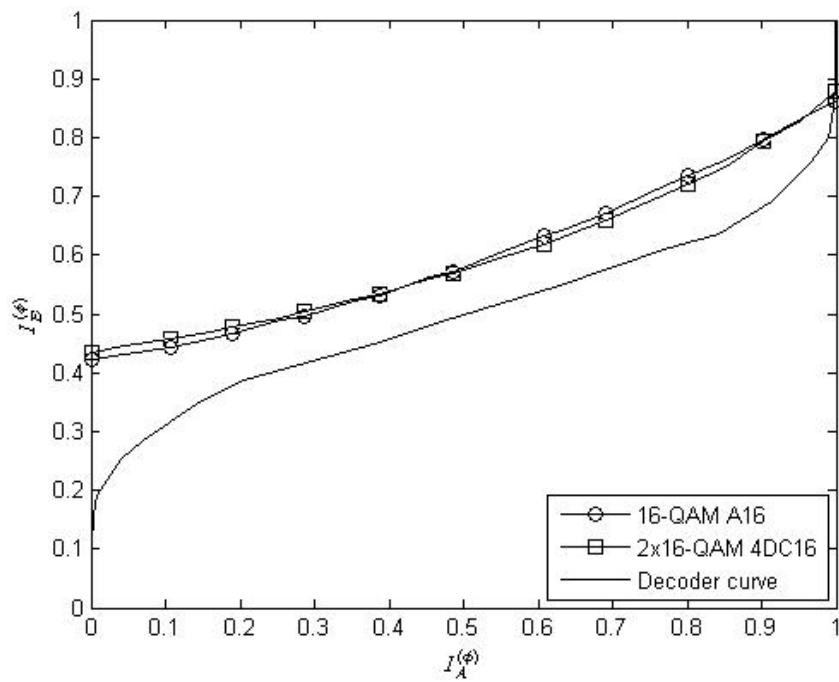
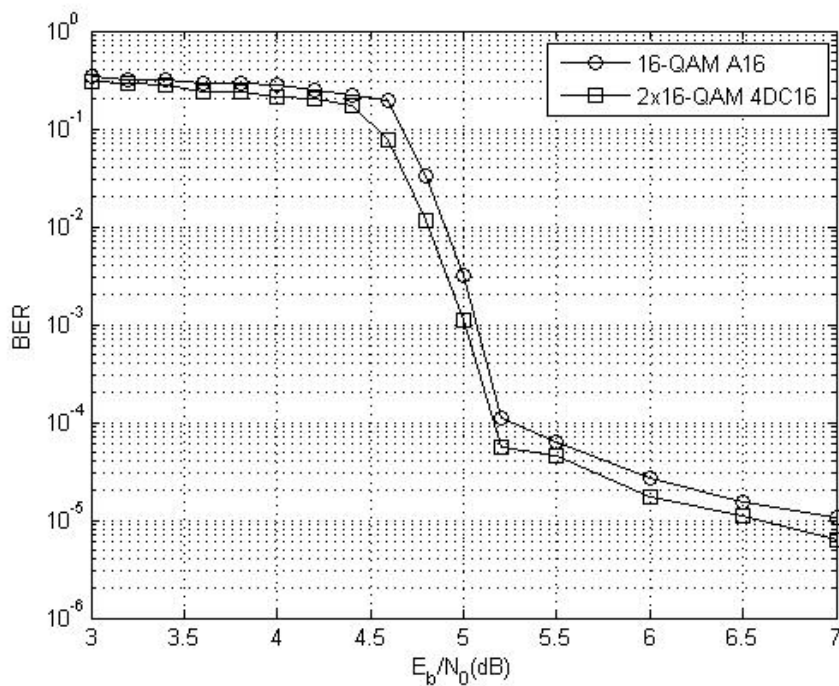


Fig. 5-31 (a) EXIT-chart at $E_b / N_0 = 3.5\text{dB}$ and (b) performance plots of the BICM-ID system with (5, 7) convolutional code in 1x1 AWGN channel



(a)



(b)

Fig. 5-32 (a) EXIT-chart at $E_b / N_0 = 6\text{dB}$ and (b) performance plots of the BICM-ID system with (5, 7) convolutional code in 1x1 block Rayleigh fading channel

Chapter 6

Conclusions

A new design of labeling for BICM-ID is presented in this thesis by the EXIT-chart based analysis. We propose a systematic design method for regular one-dimensional complex constellation which can obtain a set of labelings with good EXIT-chart characteristics. Given an outer code, the optimal labeling which makes the demapper and decoder transfer curve intersect at a point as far as possible while still makes the tunnel open can be chosen to obtain acceptable BER performance. We also extend the design method to multi-dimension modulation schemes to take advantage of flexibility provided by multi-dimension space. Verified by the simulation results, our design can provide remarkable SNR gain over the conventional ones.



Reference

- [1] G. Ungerboeck, "Channel coding with multilevel/phase signals," *IEEE Trans. Inform. Theory*, vol. 28, pp. 55–67, Jan. 1982.
- [2] Divsalar D and Simon M K., "The design of trellis coded MPSK for fading channel: Performance criteria," *IEEE Trans. Commun.*, vol. 36, Issue: 9, pp.1004-1012, Sep. 1988
- [3] E. Zehavi, "Eight-PSK trellis codes for a Rayleigh channel," *IEEE Trans. Commun.*, vol. 40, pp. 873-884, May 1992.
- [4] G. Caire, G. Taricco, and E. Biglieri, "Bit-interleaved coded modulation," *IEEE Trans. Inform. Theory*, vol. 44, pp. 927-945, May 1998.
- [5] X. Li and J. A. Ritcey, "Trellis coded modulation with bit interleaving and iterative decoding," *IEEE J. Select. Areas Commun.*, vol. 17, pp.715-724,1999.
- [6] A. Chindapol and J. A. Ritcey, "Design, analysis, and performance evaluation for BICM-ID with square QAM constellations in Rayleigh fading channels," *IEEE J. Select. Areas Commun.*, vol. 19, pp. 944-957, May 2001.
- [7] X. Li, A. Chindapol, and J.A. Ritcey, "Bit-interleaved coded modulation with iterative decoding and 8PSK signaling," *IEEE Trans. Commun.*, vol.50, no.8, pp.1250–1257, Aug. 2002.
- [8] S. ten Brink, "Convergence of iterative decoding," *Electron. Lett.*, vol. 35, pp. 806-808, May 1999.
- [9] S. ten Brink, "Designing iterative decoding schemes with the extrinsic information transfer chart", *AEU Int. J. Electron Commun.*, vol. 54, no. 6, pp. 389-398, Dec. 2000.
- [10] A. Sezgin and E. A. Jorswieck, "Impact of the mapping strategy on the performance of APP decoded space-time block codes," *IEEE Trans. Signal Process.*, vol. 53, pp. 4685-4690, Dec. 2005.
- [11] F. Schreckenbach, N. Gortz, J. Hagenauer, and G. Bauch, "Optimization of symbol mappings for bit-interleaved coded modulation with iterative decoding," *IEEE Commun. Lett.*, vol 7, no 12, pp. 593-595, Dec. 2003
- [12] Y. Huang, J.A. Ritcey, "Optimal constellation labeling for iteratively decoded bit-interleaved space-time coded modulation," *IEEE Trans. Inform. Theory*, vol. 51, no. 5, pp. 1865–1871, May 2005.
- [13] Qi Xin, Zhao Ming, Zhou Shidong, Wang Jing, "Multi-dimensional MPSK for iterative demapping over AWGN and Rayleigh fading channels", *VTC 2005-Spring. 2005 IEEE 61st*, pp. 581-586, May 2005.

- [14] Qi X, Zhao M, Zhou S, Wang J , “Multidimensional modulation used in BICM-ID,” *ELECTRONICS LETTERS*, vol. 41, no. 3, pp. 140-142, FEB 3 2005
- [15] F. Simoens, H. Wymeersch, H. Bruneel, M. Moeneclaey, “Multi-dimension Mapping for Bit-Interleaved Coded Modulation with BPSK/QPSK signaling,” *IEEE Commun. Lett.*, Vol. 9, No. 5, pp. 453-455, May 2005
- [16] N.H. Tran and H.H. Nguyen, “Design and performance of BICM-ID systems with hypercube constellations,” *IEEE Trans. Wireless Commun.*, vol.5, no.5, pp.1169–1179, May 2006.
- [17] F. Simoens, H. Wymeersch and M. Moeneclaey, “Spatial Mapping for MIMO systems,” in *IEEE Information Theory Workshop proceedings*, Oct. 2004.
- [18] N. Gresset, J.J. Boutros and L. Brunel, “Multi-Dimensional Mappings for Iteratively Decoded BICM on Multiple Antenna Channels,” *IEEE Trans. Inform. Theory*, vol. 51, no. 9, pp. 3337–3346, Sept. 2005.
- [19] L. R. Bahl, J. Cocke, F. Jelinek, and J. Raviv, “Optimal decoding of linear codes for minimizing symbol error rate,” *IEEE Trans. Inform. Theory*, vol. 20, pp.284-287, Mar. 1974.
- [20] S. ten Brink, “Convergence Behavior of Iterative Decoded Parallel Concatenated Codes,” *IEEE Trans. Comm.*, vol. 49, no. 10, pp. 1727-1737, Oct. 2001.
- [21] A. Boronka, J. Speidel, “A low complexity MIMO system based on BLAST and iterative anti-gray-demapping,” *IEEE International Symposium on Personal, Indoor and Mobile Radio Communications (PIMRC)*, Sept. 2003.
- [22] C. Berrou, A. Glavieux and P. Thitimajshima, “Near Shannon limit error-correcting coding and decoding: turbo-codes (1),” *Proc. IEEE ICC*, Geneva, Switzerland, pp. 1064-1070, May 1993.
- [23] C. Berrou and A. Glavieux, “Near optimum error correcting coding and decoding : turbo-codes,” *IEEE Trans. Commun.*, vol. 44, no. 10, pp. 1261–1271, 1996.
- [24] J. Tan and G. L. Stuber, “Analysis and design of symbol mappers for iteratively decoded BICM,” *IEEE Trans. Wireless Commu*, vol 4, pp.662-672, Mar. 2005
- [25] N.S Muhammad., J.Speidel, “Joint optimization of signal constellation and bit labeling for bit-interleaved coded modulation with iterative decoding,” *IEEE Commun. Lett.*, vol. 9, no. 9, pp. 775~777, Sept. 2005.
- [26] S.S. Pietrobon, R.H. Deng, A. Lafanechere, G. Ungerboeck and D.J. Costello, “Trellis-Coded Multidimensional Phase Modulation,” *IEEE Trans. Inform. Theory*, vol. 36, no. 1, pp. 63~89, Jan. 1990.
- [27] Y. Huang, J.A. Ritcey, “Tight BER Bounds for Iteratively Decoded Bit-Interleaved Space-Time Coded Modulation,” *IEEE Commun. Lett.*, vol. 8, no. 3, pp. 153~155, Mar. 2004.